

Electronic Theses and Dissertations, 2004-2019

2018

Analytical and Numerical Investigations of the Kudryashov Generalized KdV Equation

William Hilton
University of Central Florida

 Part of the [Mathematics Commons](#)
Find similar works at: <https://stars.library.ucf.edu/etd>
University of Central Florida Libraries <http://library.ucf.edu>

This Masters Thesis (Open Access) is brought to you for free and open access by STARS. It has been accepted for inclusion in Electronic Theses and Dissertations, 2004-2019 by an authorized administrator of STARS. For more information, please contact STARS@ucf.edu.

STARS Citation

Hilton, William, "Analytical and Numerical Investigations of the Kudryashov Generalized KdV Equation" (2018). *Electronic Theses and Dissertations, 2004-2019*. 6606.
<https://stars.library.ucf.edu/etd/6606>

ANALYTICAL AND NUMERICAL INVESTIGATIONS OF THE KUDRYASHOV
GENERALIZED KDV EQUATION

by

WILLIAM STUART HILTON
B.S. University of Florida, 2015

A thesis submitted in partial fulfillment of the requirements
for the degree of Master of Science
in the Department of Mathematics
in the College of Sciences
at the University of Central Florida
Orlando, Florida

Fall Term
2018

© 2018 William Stuart Hilton

ABSTRACT

This thesis concerns an analytical and numerical study of the Kudryashov Generalized Korteweg-de Vries (KG KdV) equation. Using a refined perturbation expansion of the Fermi-Pasta-Ulam (FPU) equations of motion, the KG KdV equation, which arises at sixth order, and general higher order KdV equations are derived. Special solutions of the KG KdV equation are derived using the tanh method. A pseudospectral integrator, which can handle stiff equations, is developed for the higher order KdV equations. The numerical experiments indicate that although the higher order equations exhibit complex dynamics, they fail to reach energy equipartition on the time scale considered.

To my mother, Samantha

ACKNOWLEDGMENTS

I thank my adviser, Dr. C. Schober, for her outstanding and tireless mentorship. I also thank Drs. A. Islas and B. Moore for their generosity in entertaining many questions.

TABLE OF CONTENTS

LIST OF FIGURES	vii
LIST OF TABLES	x
CHAPTER 1: INTRODUCTION	1
CHAPTER 2: THE FERMI PASTA ULAM PROBLEM	1
2.1 Formulation	1
2.2 Diagonalization of the Linear Regime	5
2.3 Numerics	8
2.4 Results and Discussion	8
CHAPTER 3: ON A CONTINUUM LIMIT OF THE FPU LATTICE	16
3.1 Introduction	16
3.2 From FPU to KdV	16
3.2.1 Order Four Expansion: Korteweg-de Vries Equation	17
3.2.2 Order Six Expansion: Kudryashov Generalized Korteweg-de Vries Equation	20
3.3 Tanh Method Solutions	22
3.3.1 KdV Equation	24
3.3.2 KG KdV Equation	26
3.4 Sech Solutions	28
CHAPTER 4: ANALYSIS OF GENERALIZED MODIFIED KDV EQUATIONS	30
4.1 Zabusky and Kruskal's Scheme for the KdV Equation	30
4.1.1 Results	30
4.2 Numerical Experiments	34
4.2.1 Indicators of Equipartition	34
4.2.2 Remarks on Error	36
4.2.3 Results on Equipartition	41
CHAPTER 5: CONCLUSION	61
APPENDIX A: ALTERNATIVE PROJECTIONS OF DISPLACEMENT	62
APPENDIX B: MTH ORDER KUDRYASHOV GENERALIZED KDV EQUATION	67
INDEX	74
REFERENCES	75

LIST OF FIGURES

2.1	In the upper frame, the equilibrium FPU lattice is illustrated with monatomic circular nodes connected by a (nonlinear) spring force. In the lower frame, a non-equilibrium FPU lattice is illustrated, wherein the displacement of the j th node, q_j is nonzero.	1
2.2	The quantity plotted is the energy, E_j , in the first five modes. $N = 32, \alpha = \frac{1}{4}, \Delta t = 1/16$. The initial form of the string was a $q_j = \sin\left(\frac{j\pi}{N}\right)$	10
2.3	This drawing shows not the energy but the actual shapes, i.e., the displacement of the string at various times as indicated in the legend. The conditions are $N = 32, \alpha = \frac{1}{4}, \Delta t = 1/16$. The initial form of the string was a $q_j = \sin\left(\frac{j\pi}{N}\right)$	11
2.4	Same conditions as Figure 2.2 but the quadratic term in the force was stronger. $\alpha = 1$	12
2.5	The quantity plotted is the energy, E_j , in the first five modes. $N = 32, \beta = 8, \Delta t = 1/16$. The initial form of the string was $q_j = \sin\left(\frac{j\pi}{N}\right)$	13
2.6	The quantity plotted is the energy, E_j , in the first five modes. $N = 32, \beta = \frac{1}{16}, \Delta t = 1/64$. The initial form of the string was determined by placing two thirds of the energy in mode five and one third in mode seven.	14
2.7	The quantity plotted is the energy, E_j , in the first two modes. $N = 32, \alpha = \frac{1}{4}, \Delta t = 1/16$. The initial form of the string was a $q_j = \sin\left(\frac{j\pi}{N}\right)$	15
4.1	Projection of solution of the finite difference scheme, (4.2), with $\delta = .022, N = 2^6, h = N^{-1}, k = N^{-2}$, and $u(jh, 0) = \cos(\pi jh)$. Solitary waves are identified as the eight wave forms all having appeared by $t = 1.14$	31
4.2	Solution of the finite difference scheme, (4.2), with $\delta = .022, N = 2^6, h = N^{-1}, k = N^{-2}$, and $u(jh, 0) = \cos(\pi jh)$. Points, $(x, t, u(x, t))$, are colored corresponding to a logarithmic scaling of ∇u	32
4.3	Projection of solution of the finite difference scheme, (4.2), with $\delta = .022, N = 2^6, h = N^{-1}$, and $k = N^{-2}$, and $u(jh, 0) = \cos(\pi jh)$. Neighborhoods where $0 < \nabla u \ll 1$ are colored corresponding to ∇u . Solitons are identified as the nine the wave forms appearing near $t = 1$, each propagating with an approximately constant velocity.	33
4.4	KdV equation, $\delta = 1$: Comparison of the exact traveling wave solution, (3.71), and the PS-RK4 solution obtained with $h = .1 \cdot N^{-2}$ and $N = 128$. The lower right graph plots $E_{\max}(t)$	37

4.5	KG KdV equation, $\delta = 1$: Comparison of the exact traveling wave solution, (3.71), and the PS-RK4 solution obtained with $h = .1 \cdot N^{-2}$ and $N = 128$. The lower right graph plots $E_{\max}(t)$	38
4.6	KdV equation, $\delta = 0.022$: Comparison of the exact traveling wave solution, (3.71), and the PS-RK4 solution obtained with $h = .1 \cdot N^{-2}$ and $N = 128$. The lower right graph plots $E_{\max}(t)$	39
4.7	KG KdV equation, $\delta = 0.022$: Comparison of the exact traveling wave solution, (3.71), and the PS-RK4 solution obtained with $h = .1 \cdot N^{-2}$ and $N = 128$. The lower right graph plots $E_{\max}(t)$	40
4.8	Projection of solutions of PS-RK4, with $N = 2^7$, $h = .1 \cdot N^{-2}$, $\delta = 0.018$, $u(x, 0) = \cos(\pi x)$	43
4.9	Projection of solutions of PS-RK4, with $N = 2^7$, $h = .1 \cdot N^{-2}$, $\delta = 0.021$, $u(x, 0) = \cos(\pi x)$	44
4.10	Projection of solutions of PS-RK4, with $N = 2^7$, $h = .1 \cdot N^{-2}$, $\delta = 0.022$, $u(x, 0) = \cos(\pi x)$	45
4.11	Projection of solutions of PS-RK4, with $N = 2^7$, $h = .1 \cdot N^{-2}$, $\delta = 0.023$, $u(x, 0) = \cos(\pi x)$	46
4.12	Plot of the power, $P(j, 10)$, of the solutions of PS-RK4, with $N = 2^7$, $h = .1 \cdot N^{-2}$, $u(x, 0) = \cos(\pi x)$, and $\delta = 0.018$	48
4.13	Plot of the power, $P(j, 10)$, of the solutions of PS-RK4, with $N = 2^7$, $h = .1 \cdot N^{-2}$, $u(x, 0) = \cos(\pi x)$, and $\delta = 0.021$	49
4.14	Plot of the power, $P(j, 10)$, of the solutions of PS-RK4, with $N = 2^7$, $h = .1 \cdot N^{-2}$, $u(x, 0) = \cos(\pi x)$, and $\delta = 0.022$	50
4.15	Plot of the power, $P(j, 10)$, of the solutions of PS-RK4, with $N = 2^7$, $h = .1 \cdot N^{-2}$, $u(x, 0) = \cos(\pi x)$, and $\delta = 0.023$	51
4.16	Projection of the power, $P(j, t)$, of the solutions of PS-RK4, with $N = 2^7$, $h = .1 \cdot N^{-2}$, $u(x, 0) = \cos(\pi x)$, and $\delta = 0.018$	52
4.17	Projection of the power, $P(j, t)$, of the solutions of PS-RK4, with $N = 2^7$, $h = .1 \cdot N^{-2}$, $u(x, 0) = \cos(\pi x)$, and $\delta = 0.021$	53
4.18	Projection of the power, $P(j, t)$, of the solutions of PS-RK4, with $N = 2^7$, $h = .1 \cdot N^{-2}$, $u(x, 0) = \cos(\pi x)$, and $\delta = 0.022$	54
4.19	Projection of the power, $P(j, t)$, of the solutions of PS-RK4, with $N = 2^7$, $h = .1 \cdot N^{-2}$, $u(x, 0) = \cos(\pi x)$, and $\delta = 0.023$	55
4.20	Plot of the spectral entropy, $S(t)$, of the solutions of PS-RK4, with $N = 2^7$, $h = .1 \cdot N^{-2}$, $u(x, 0) = \cos(\pi x)$	57

4.21	KG KdV-1 equation: Plots of the solution, power spectrum, and spectral entropy with $N = 2^{11}$, $h = N^{-2}$, $\delta = 0.001$, $u(x, 0) = \cos(\pi x)$, using PS-RK4.	60
A.1	Projection of solutions of PS-RK4, with $N = 2^7$, $h = .1 \cdot N^{-2}$, $\delta = 0.018$, $u(x, 0) = \cos(\pi x)$. Points, $u(x, t) \in \mathbb{R}$, are colored with a linear mapping.	63
A.2	Projection of solutions of PS-RK4, with $N = 2^7$, $h = .1 \cdot N^{-2}$, $\delta = 0.021$, $u(x, 0) = \cos(\pi x)$. Points, $u(x, t) \in \mathbb{R}$, are colored with a linear mapping.	64
A.3	Projection of solutions of PS-RK4, with $N = 2^7$, $h = .1 \cdot N^{-2}$, $\delta = 0.022$, $u(x, 0) = \cos(\pi x)$. Points, $u(x, t) \in \mathbb{R}$, are colored with a linear mapping.	65
A.4	Projection of solutions of PS-RK4, with $N = 2^7$, $h = .1 \cdot N^{-2}$, $\delta = 0.023$, $u(x, 0) = \cos(\pi x)$. Points, $u(x, t) \in \mathbb{R}$, are colored with a linear mapping.	66

LIST OF TABLES

4.1 The quantity $\tilde{S}_{\text{normal}}$ for the solutions of PS-RK4, with $N = 2^7$, $h = .1 \cdot N^{-2}$,
 $u(x, 0) = \cos(\pi x)$ 58

CHAPTER 1: INTRODUCTION

Classification of systems as ergodic is of significant mathematical and scientific interest. While ergodic theory is well-established, analytic results tend to handle only very special cases. Indeed, it was this kind of difficulty from which the Fermi-Pasta-Ulam (FPU) problem came about.

During Summer 1952 at the Los Alamos National Laboratory, discussions between E. Fermi and S. Ulam led to an exploration of the long time-scale evolution of a perturbed Hamiltonian system in order to examine equipartition of energy, in which energy is approximately uniformly distributed among the modes. The pair of researchers ultimately settled on modeling the (1+1)-dimensional nonlinear wave equation with Dirichlet boundary conditions. In the corresponding linear problem with appropriate initial data, the solution is certainly known to oscillate uniformly in time, i.e. there is a single nonzero constant mode. In the nonlinear problem, small time-scale computations revealed that energy in the initial mode decreased and energy in neighboring modes increased. Fermi generalized results by Poincaré and conjectured that the system would soon become ergodic, i.e. that the system would reach a state of equipartition of energy.

The following summer, with the aid of J. Pasta and M. Tsingou, a numerical scheme was implemented on an early digital computer. The results, which have continued to generate significant interest, experimentation, and analysis, indicated that the ergodic hypothesis did not hold for small perturbations on computed time scales. Instead, in what is now dubbed the FPU paradox, periodic recurrence of energy in the modes was observed.

Stimulated by ten years of lingering questions about the FPU problem, work by N. Zabusky and M. Kruskal in 1965 had a substantial impact by relating the FPU problem with solitary wave phenomenon in the continuum [22]. Kruskal, in particular, hypothesized a method of transforming certain features of the FPU problem dynamics into a problem entirely in the continuum. What resulted was the Korteweg-de Vries (KdV) equation, which provided a so-called long wavelength model of the FPU lattice. This

motivated intense interest in infinite-dimensional integrable systems and soliton theory, which is as related to the original FPU problem as it is intriguing in its own right. The following year, in work by F. Izrailev and B. Chirikov [8], it was found that equipartition was achieved in the same problem when energy initially placed in a mode was sufficiently large. This motivated the conjecture of an energy threshold for the ergodic hypothesis.

In 1982, F. Fucito [7] conjectured that near recurrence of energy in the modes would eventually transition into exact recurrence of energy in the modes for every perturbation, although achieved in a time that increases exponentially as energy decreases down toward the energy threshold.

Within the last decade, N. Kudryashov has considered a higher order expansion of certain cases of a continuum limit of the FPU problem, using the usual refined perturbation expansion due to Kruskal [9–11]. Kudryashov found that these equations fail the Painleve test. A. Volkov also noted some special solutions to these equations [19].

In Chapter 2, we begin this thesis with a review of the Fermi-Pasta-Ulam (FPU) problem. Although a handful of analytic results have appeared since, we focus primarily on the original numerical experiment, its interpretation, and its limitations. We also briefly remark on the formulation of the problem and provide some analysis of the system and the numerics.

In Chapter 3, a means of passing from the FPU equations of motion to a continuum limit is provided, using Kruskal’s classic long wavelength assumption. We give a similar treatment to an expansion of arbitrary order in the appendix. Some analytic results are then derived from the resulting systems – namely, traveling wave solutions via the tanh method.

Kudryashov and Volkov elaborated briefly on the numerical methods used for their higher order equations, noting that a pseudospectral method with mode filtering was used [9–11, 19]. Numerical results suggesting chaos were demonstrated. In Chapter 4, we repeat a classic experiment that followed Kruskal’s derivation of the KdV equation

from the FPU lattice. With this in hand, a pseudospectral method that does not involve filtering of modes is implemented. Some indicators of ergodicity are then proposed and discussed, followed by analysis and interpretation of the results. The numerics suggest that equipartition is achieved on a long time scale for the higher order equations and some of its variants.

CHAPTER 2: THE FERMI PASTA ULAM PROBLEM

2.1 Formulation

Fermi, Pasta, and Ulam [2] considered a chain of $N + 2$ particles where neighboring masses are connected by a nonlinear spring, as illustrated in Figure 2.1.

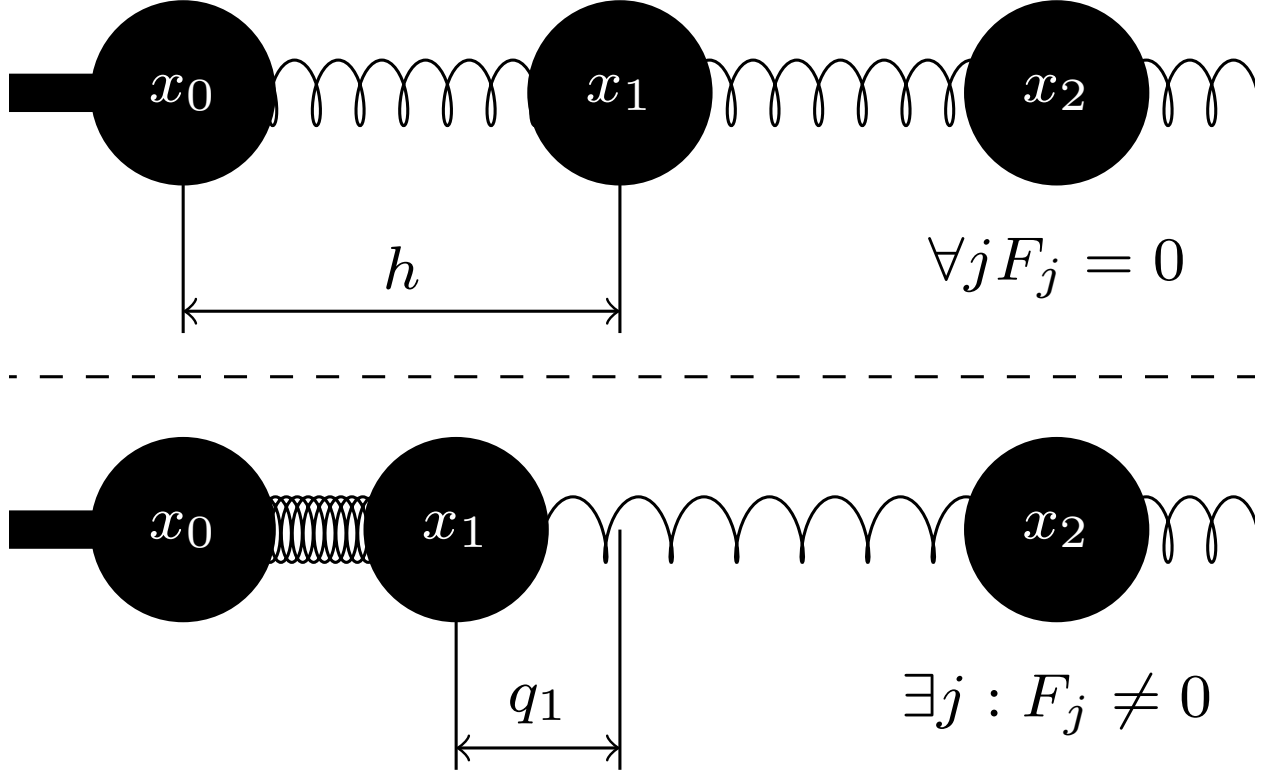


Figure 2.1. In the upper frame, the equilibrium FPU lattice is illustrated with monatomic circular nodes connected by a (nonlinear) spring force. In the lower frame, a non-equilibrium FPU lattice is illustrated, wherein the displacement of the j th node, q_j is nonzero.

The particles, restoring forces, and resting spring lengths are assumed to be identical. The force, F , is assumed to be the sum of forces imposed by the nearest neighbors, i.e.,

$$F_j = F(x_{j+1} - x_j) - F(x_j - x_{j-1}) \quad (2.1)$$

for the j th mass, with x_j being displacement from the mass's equilibrium position. The force, F , is weakly nonlinear, dependent upon the relative displacements, $\delta_+ x_j = x_{j+1} - x_j$

and $\delta_-x_j = x_j - x_{j-1}$, so that

$$F_j = \frac{1}{h} \sum_{i=1}^M K_i \frac{(\delta_+x_j)^i - (\delta_-x_j)^i}{i!}, \quad \forall j : 1 \leq j \leq N, \quad (2.2)$$

where K_i is the i th order spring constant component. Imposing Dirichlet boundary conditions, we have the Initial Boundary Value Problem,

$$\left\{ \begin{array}{ll} \ddot{x}_j = \frac{1}{mh} \sum_{i=1}^M K_i \frac{(\delta_+x_j)^i - (\delta_-x_j)^i}{i!}, & \forall j \in \{1, 2, \dots, N\}, \quad (2.3) \\ x_j(0) = f_j(0), & \forall j \in \{1, 2, \dots, N\}, \quad (2.4) \\ \dot{x}_j(0) = 0, & \forall j \in \{1, 2, \dots, N\}, \quad (2.5) \\ x_0(t) = x_{N+1}(t) = 0, & \forall t \geq 0. \quad (2.6) \end{array} \right.$$

In the original FPU experiments, $M = 3$ and the restoring force, F , is dependent on only linear, quadratic, and cubic terms. Recasting the spring constants as in [2], one obtains

$$F_j = \frac{k}{h} [\gamma(x_{j+1} - x_j) + \alpha(x_{j+1} - x_j)^2 + \beta(x_{j+1} - x_j)^3 - \quad (2.7)$$

$$(\gamma(x_j - x_{j-1}) + \alpha(x_j - x_{j-1})^2 + \beta(x_j - x_{j-1})^3)]$$

$$= \frac{k}{h} [\gamma(x_{j+1} + x_{j-1} - 2x_j) + \alpha((x_{j+1} - x_j)^2 - (x_j - x_{j-1})^2) + \quad (2.8)$$

$$\beta((x_{j+1} - x_j)^3 - (x_j - x_{j-1})^3).]$$

For $M = 3$ and $\gamma = k = h = m = 1$, Equations (2.3)—(2.6) become

$$\left\{ \begin{array}{ll} \ddot{x}_j = x_{j+1} - 2x_j + x_{j-1} + & (2.9) \\ \alpha((x_{j+1} - x_j)^2 - (x_j - x_{j-1})^2) + & \\ \beta((x_{j+1} - x_j)^3 - (x_j - x_{j-1})^3), & \forall j \in \{1, 2, \dots, N\}, \end{array} \right.$$

$$x_j(0) = f_j(0), \quad \forall j \in \{1, 2, \dots, N\}, \quad (2.10)$$

$$\dot{x}_j(0) = 0, \quad \forall j \in \{1, 2, \dots, N\}, \quad (2.11)$$

$$x_0(t) = x_{N+1}(t) = 0, \quad \forall t \geq 0. \quad (2.12)$$

To simplify the analysis of the nonlinear dynamics, we consider two cases. In particular, the system that arises when α is nonzero and $\beta = 0$ is referred to as the FPU- α problem.

Similarly, $\alpha = 0$ and β nonzero gives the FPU- β problem. To formulate the problem in Equations (2.9)—(2.12) as a $2N$ dimensional system of first order ordinary differential equations, we define the new variables $q_j(t) = x_j(t)$ and $p_j(t) = \dot{x}_j(t)$, yielding

$$\begin{cases} \dot{q}_j = p_j, & \forall j \in \{1, 2, \dots, N\}, \end{cases} \quad (2.13)$$

$$\begin{cases} \dot{p}_j = (q_{j+1} + q_{j-1} - 2q_j) + \end{cases} \quad (2.14)$$

$$\begin{cases} \alpha((q_{j+1} - q_j)^2 - (q_j - q_{j-1})^2) + \\ \beta((q_{j+1} - q_j)^3 - (q_j - q_{j-1})^3), & \forall j \in \{1, 2, \dots, N\}, \end{cases}$$

$$\begin{cases} q_j(0) = f_j(0), & \forall j \in \{1, 2, \dots, N\}, \end{cases} \quad (2.15)$$

$$\begin{cases} p_j(0) = 0, & \forall j \in \{1, 2, \dots, N\}, \end{cases} \quad (2.16)$$

$$\begin{cases} q_0(t) = q_{N+1}(t) = 0, & \forall t \geq 0. \end{cases} \quad (2.17)$$

Letting $\mathbf{q} = (q_1, \dots, q_N)^T$, $\mathbf{p} = (p_1, \dots, p_N)^T$, and $\mathbf{z} = (\mathbf{q}, \mathbf{p})^T$, Equations (2.13)—(2.17) can be written in Hamiltonian form,

$$\begin{cases} \dot{\mathbf{z}} = \mathbf{J}\nabla H, \end{cases} \quad (2.18)$$

$$\begin{cases} \mathbf{z}(0) = (\mathbf{f}(0), \mathbf{0})^T \in \mathbb{R}^{2N}, \end{cases} \quad (2.19)$$

where $\mathbf{J} = \begin{pmatrix} 0 & \mathcal{I}_{N \times N} \\ -\mathcal{I}_{N \times N} & 0 \end{pmatrix}$ and $H : \mathbb{R}^{2N} \rightarrow \mathbb{R}$ by

$$H(\mathbf{q}, \mathbf{p}) = \sum_{i=1}^N \frac{p_i^2}{2} + \sum_{i=1}^N \frac{(q_{i+1} - q_i)^2}{2} + \alpha \frac{(q_{i+1} - q_i)^3}{3} + \beta \frac{(q_{i+1} - q_i)^4}{4}. \quad (2.20)$$

Note that Equations (2.18)—(2.19) imply Equation (2.17) due to the linear dependence of the boundary conditions. This Hamiltonian is readily verified:

$$\frac{\partial H}{\partial p_j} = \frac{\partial}{\partial p_j} \sum_{i=1}^N \frac{p_i^2}{2} + \frac{\partial}{\partial p_j} \sum_{i=1}^N \frac{(q_{i+1} - q_i)^2}{2} + \alpha \frac{(q_{i+1} - q_i)^3}{3} + \beta \frac{(q_{i+1} - q_i)^4}{4}, \quad (2.21)$$

$$= \frac{\partial}{\partial p_j} \sum_{i=1}^N \frac{p_i^2}{2} + 0, \quad (2.22)$$

$$= \frac{2p_i}{2} \delta_{i,j}, \quad (2.23)$$

$$= p_j, \quad (2.24)$$

$$= \dot{q}_j, \quad (2.25)$$

and

$$\frac{\partial H}{\partial q_j} = \frac{\partial}{\partial q_j} \sum_{i=1}^N \frac{p_i^2}{2} + \frac{\partial}{\partial q_j} \sum_{i=1}^N \frac{(q_{i+1} - q_i)^2}{2} + \alpha \frac{(q_{i+1} - q_i)^3}{3} + \beta \frac{(q_{i+1} - q_i)^4}{4}, \quad (2.26)$$

$$= 0 + \frac{\partial}{\partial q_j} \sum_{i=1}^N \frac{(q_{i+1} - q_i)^2}{2} + \alpha \frac{(q_{i+1} - q_i)^3}{3} + \beta \frac{(q_{i+1} - q_i)^4}{4}, \quad (2.27)$$

$$= \frac{\partial}{\partial q_j} \sum_{i=1}^N \frac{q_{i+1}^2 - 2q_{i+1}q_i + q_i^2}{2} + \alpha \frac{q_{i+1}^3 - 3q_{i+1}^2q_i + 3q_{i+1}q_i^2 - q_i^3}{3} + \quad (2.28)$$

$$\beta \frac{q_{i+1}^4 - 4q_{i+1}^3q_i + 6q_{i+1}^2q_i^2 - 4q_{i+1}q_i^3 + q_i^4}{4},$$

$$= -q_{j+1} + 2q_j - q_{j-1} - \alpha(q_{j+1}^2 - 2q_{j+1}q_j + 2q_jq_{j-1} - q_{j-1}^2) - \quad (2.29)$$

$$\beta(q_{i+1}^3 - 3q_{i+1}^2q_i + 3q_{i+1}q_i^2 - 2q_i^3 + 3q_i^2q_{i-1} - 3q_iq_{i-1}^2 + q_{i-1}^3), \quad (2.30)$$

$$= -(q_{j+1} + q_{j-1} - 2q_j) - \alpha((q_{j+1} - q_j)^2 - (q_j - q_{j-1})^2) \quad (2.31)$$

$$- \beta((q_{j+1} - q_j)^3 - (q_j - q_{j-1})^3),$$

$$= -\dot{p}_j. \quad (2.32)$$

2.2 Diagonalization of the Linear Regime

In Equations (2.13)—(2.17), the linear regime is governed by $\ddot{\mathbf{q}} = \mathbf{L}\mathbf{q}$ where

$$\mathbf{L} = \begin{pmatrix} -2 & 1 & 0 & 0 & 0 & \cdots & 0 & 0 \\ 1 & -2 & 1 & 0 & 0 & \cdots & 0 & 0 \\ 0 & 1 & -2 & 1 & 0 & \cdots & 0 & 0 \\ & & \ddots & \ddots & \ddots & & & \\ 0 & 0 & 0 & 0 & \cdots & 0 & 1 & -2 \end{pmatrix}_{N \times N}. \quad (2.33)$$

Notice that \mathbf{L} is a 1-bandwidth symmetric Topelitz matrix (with a main diagonal of -2 and an off-diagonal of 1.) To address the question of the partitioning of the ‘energy’, H , we introduce the Fourier normal modes by seeking $\mathbf{x} \in \mathbb{C}^N$, dependent upon λ , such that

$$(\mathbf{L} - \lambda \mathcal{I}_{N \times N})\mathbf{x} = \mathbf{0}. \quad (2.34)$$

This produces the system of equations

$$x_{j+1} + (-2 - \lambda)x_j + x_{j-1} = 0, \quad 1 \leq j \leq N \quad (2.35)$$

where $x_0 = x_{N+1} = 0$. Using finite difference methods, suppose $x_j = z^j$. Then the characteristic polynomial is of the form $z^2 + (-2 - \lambda)z + 1$ whose zeros are given by z_{\pm} . But this requires $z_+z_- = 1$, so we define $z_0 = z_+ = \frac{1}{z_-}$. The general solution to Equation (2.35) is an arbitrary linear combination of z_{\pm} , i.e. $x_j = c_1 z_0^j + c_2 z_0^{-j}$. The first boundary condition, $x_0 = 0$, implies $0 = c_1 + c_2$. So we let $c = c_1 = -c_2$. The second boundary condition, $x_{N+1} = 0$, implies $z_0^{2(N+1)} = 1$. So, in fact, z_0 are the $2(N+1)$ th roots of unity. Namely,

$$z_0(\lambda) = e^{\frac{2k\pi i}{2(N+1)}} = e^{\frac{k\pi i}{N+1}}, \quad 1 \leq k \leq 2(N+1). \quad (2.36)$$

Using the characteristic polynomial and Equation (2.36),

$$1 + (-2 - \lambda)z + z^2 = (z - z_0(\lambda))(z - z_0^{-1}(\lambda)), \quad (2.37)$$

$$= \left(z - e^{\frac{k\pi i}{N+1}} \right) \left(z - e^{-\frac{k\pi i}{N+1}} \right), \quad (2.38)$$

$$= z^2 - 2z \cos \left(\frac{k\pi}{N+1} \right) + 1. \quad (2.39)$$

By equating coefficients of the left hand side of (2.37) and the right hand side of (2.39),

$$\lambda = 2 \cos \left(\frac{k\pi}{N+1} \right) - 2 = - \left(2 \sin \left(\frac{k\pi}{2N+2} \right) \right)^2. \quad (2.40)$$

Define λ_k to be the k th λ satisfying Equation (2.40) and let $\mathbf{x}_{jk} \in \mathbb{C}$ be the j th element of the k th vector, \mathbf{x}_k , satisfying Equation (2.34). Then

$$\mathbf{x}_{jk} = cz_0(\lambda_k) - cz_0^{-1}(\lambda_k) \quad (2.41)$$

$$= ce^{\frac{jk\pi i}{N+1}} - ce^{-\frac{jk\pi i}{N+1}} \quad (2.42)$$

$$= -2ic \sin \left(\frac{jk\pi}{N+1} \right). \quad (2.43)$$

Since c is arbitrary, we let $c = -\frac{\sqrt{\frac{2}{N+1}}}{2i}$ so that

$$\mathbf{x}_{jk} = \sqrt{\frac{2}{N+1}} \sin \left(\frac{jk\pi}{N+1} \right). \quad (2.44)$$

Consequently, we define a transformation to normal modes $(\mathbf{q}, \mathbf{p}) \mapsto (\mathbf{u}, \mathbf{v})$ by

$$u_j = \sqrt{\frac{2}{N+1}} \sum_{k=1}^N q_k \sin \left(\frac{\pi jk}{N+1} \right), \quad (2.45)$$

$$v_j = \sqrt{\frac{2}{N+1}} \sum_{k=1}^N p_k \sin \left(\frac{\pi jk}{N+1} \right). \quad (2.46)$$

The closed form Hamiltonian in normal mode coordinates has been derived [15], in which

$$\begin{aligned}
H(\mathbf{u}, \mathbf{v}) &= \sum_{j=1}^N \frac{1}{2} (v_j^2 + \lambda_j u_j^2) + \frac{\alpha}{3\sqrt{2N+2}} \sum_{j,k,l=1}^N S_3(j, k, l) \sqrt{\lambda_j \lambda_k \lambda_l} u_j u_k u_l \\
&\quad + \frac{\beta}{8(N+1)} \sum_{j,k,l,m=1}^N S_4(j, k, l, m) \sqrt{\lambda_j \lambda_k \lambda_l \lambda_m} u_j u_k u_l u_m.
\end{aligned} \tag{2.47}$$

where

$$S_3(j, k, l) = \delta_{j+k,l} + \delta_{j+l,k} + \delta_{k+l,j} - \delta_{j+k+l, 2N+2}, \tag{2.48}$$

$$S_4(j, k, l) = \delta_{j+k+l,m} + \delta_{k+l+m,j} + \delta_{l+m+j,k} + \delta_{m+j+k,l} + \delta_{j+k,l+m} \tag{2.49}$$

$$\begin{aligned}
&+ \delta_{j+l,k+m} + \delta_{j+m,k+l} - \delta_{j+k+l+m, 2N+2} - \delta_{j+k+l, m+2N+2} - \delta_{k+l+m, j+2N+2} \\
&- \delta_{l+m+j, k+2N+2} - \delta_{m+j+k, l+2N+2},
\end{aligned}$$

$$\delta_{n,m} = \begin{cases} 0, & n \neq m, \\ 1, & \text{otherwise.} \end{cases} \tag{2.50}$$

Fermi and colleagues noted that the nonlinearity is weak by design, rendering small the normed difference between the normalized Hamiltonian of the system (2.13)—(2.17) and its linear counterpart. Consequently, in the numerical experiments, we track $\bar{H} : \mathbb{R}^{2N} \rightarrow \mathbb{R}$ by

$$\bar{H}(\mathbf{u}, \mathbf{v}) = \frac{1}{2} \sum_{i=1}^N v_i^2 + \left(2 \sin \left(\frac{k\pi}{2N+2} \right) \right)^2 u_i^2 + \mathcal{O}(\alpha + \beta). \tag{2.51}$$

Notice that the j th term of the sum in (2.51) gives the approximate energy in the j th normal mode of the system (2.13)—(2.17). So $\forall j : 1 \leq j \leq N$, we define $E_j : \mathbb{R} \rightarrow \mathbb{R}$ by

$$E_j(t) = \frac{1}{2} v_j^2(t) + 4 \sin^2 \left(\frac{k\pi}{2N+2} \right) u_j^2(t). \tag{2.52}$$

2.3 Numerics

To proceed experimentally, we notice that the ordinary differential equations in (2.13)—(2.14) are of the form

$$\begin{cases} \dot{\mathbf{q}} = \mathbf{p}, \\ \dot{\mathbf{p}} = f(\mathbf{q}). \end{cases} \quad (2.53)$$

$$\quad (2.54)$$

We note the Taylor expansions

$$\mathbf{q}(t + \Delta t) = \mathbf{q}(t) + \Delta t \dot{\mathbf{q}}(t) + \mathcal{O}((\Delta t)^2), \quad (2.55)$$

$$\mathbf{p}(t + \Delta t) = \mathbf{p}(t) + \Delta t \dot{\mathbf{p}}(t) + \mathcal{O}((\Delta t)^2). \quad (2.56)$$

Then by solving Equations (2.55) and (2.56) for the first derivative and substituting the result into (2.53) and (2.54),

$$\mathbf{q}(t + \Delta t) = \mathbf{q}(t) + \Delta t \mathbf{p}(t) + \mathcal{O}((\Delta t)^2), \quad (2.57)$$

$$\mathbf{p}(t + \Delta t) = \mathbf{p}(t) + \Delta t f(\mathbf{q}(t)) + \mathcal{O}((\Delta t)^2). \quad (2.58)$$

We let $t_n = t_0 + n\Delta t = n\Delta t$ and we define

$$\bar{\mathbf{q}}(t_n) = \bar{\mathbf{q}}(t_{n-1}) + \Delta t \bar{\mathbf{p}}(t_{n-1}), \quad (2.59)$$

$$\bar{\mathbf{p}}(t_n) = \bar{\mathbf{p}}(t_{n-1}) + \Delta t f(\bar{\mathbf{q}}(t_n)). \quad (2.60)$$

Hence we have a first order approximation of the system in (2.53)—(2.54). This is the so-called symplectic Euler method. We implement this algorithm by taking f to be the corresponding function in Equations (2.13)—(2.17).

2.4 Results and Discussion

The results of our computations appear to uphold Fermi's original conclusions. Since Fermi's paper did not elaborate on the finite difference scheme employed, the results may differ slightly. In particular, the dynamical system defined by the numerical method

introduces oscillations in the Hamiltonian that were not present in Fermi’s work, as they were likely manually filtered via hand-drawing of the data.

The computation is executed as follows: given initial data, the system was started from rest at time $t = 0$. A time-step, say τ , is used to implement the numerical scheme so that $t = j\tau$. Note that the linear problem, where $\alpha = \beta = 0$, oscillates temporally with approximate period $\delta t := \frac{2N}{\tau}$. So for comparative purposes, we map $t \mapsto \frac{t\tau}{2N}$ to emphasize the relative propagation of the nonlinear string. We refer to this scaled temporal domain as the “computational oscillations.” The distribution of energy in the Fourier modes was computed as a discrete function of time. The graphs show the behavior of the energy, E_j , residing in various modes as a function of scaled time; for example, in Figure 2.2 the energy content of each of the first five modes is plotted. Unless otherwise stated, the abscissa is the discrete scaled time parameter and the ordinate is the modal energy E_j of the approximate solution to the system.

As is illustrated in Figure 2.2, we first consider the quadratic forcing, $\alpha = \frac{1}{4}$ and $\beta = 0$, and a sine wave as the initial position of the string, i.e. $q_j = \sin\left(\frac{j\pi}{N}\right)$. Initially, a gradual increase of energy in the higher modes is shown – mode two starts increasing first, followed by mode three, and so on. After about six-thousand time-steps, however, this gradual sharing of energy among successive modes ceases and a mode dominates. For example, note how mode two is seen to increase quickly at the cost of all other modes, having, at one time, more energy than all the others put together. Then mode three behaves similarly, and so on. Finally, at a later time, mode one comes back to within one per cent of its initial value so that the system appears quasi-periodic. Figure 2.3 illustrates not the energy but the actual shapes, i.e., the displacement of the string at various times. Displacement quantities are mapped onto the second dimension for ease of graphical interpretation, unlike the more intuitive construction in Figure 2.1.

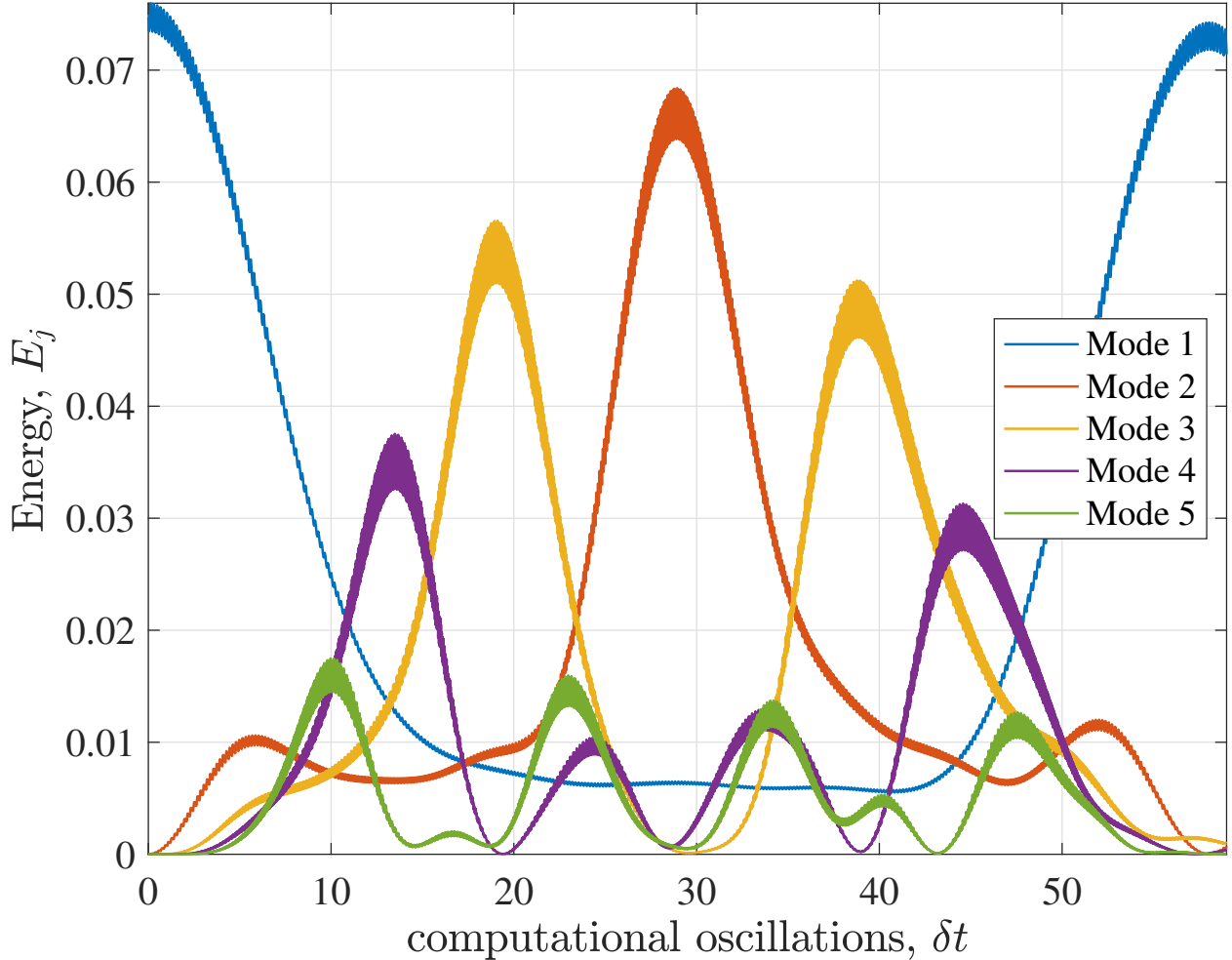


Figure 2.2. The quantity plotted is the energy, E_j , in the first five modes. $N = 32, \alpha = \frac{1}{4}, \Delta t = 1/16$. The initial form of the string was a $q_j = \sin\left(\frac{j\pi}{N}\right)$.

In Figure 2.4, the quadratic force is increased to $\alpha = 1$. Notice that, by $\delta t = 15$, more energy is present in mode five than in the fifth mode of the $\alpha = \frac{1}{4}$ case in Figure 2.2. Several more modes, which are not plotted for clarity, were also excited more than mode one by this time. Moreover, the energy in mode one recovers to within $\frac{1}{10}$ of the energy initially in mode one. While it was not initially clear in the FPU experiment that the case of a larger perturbation would lead to equipartition, extending the computations out roughly ten-fold readily reveals that near recurrence is not achieved again. It should be noted that large perturbations were, in general, expected to lead to equipartition.

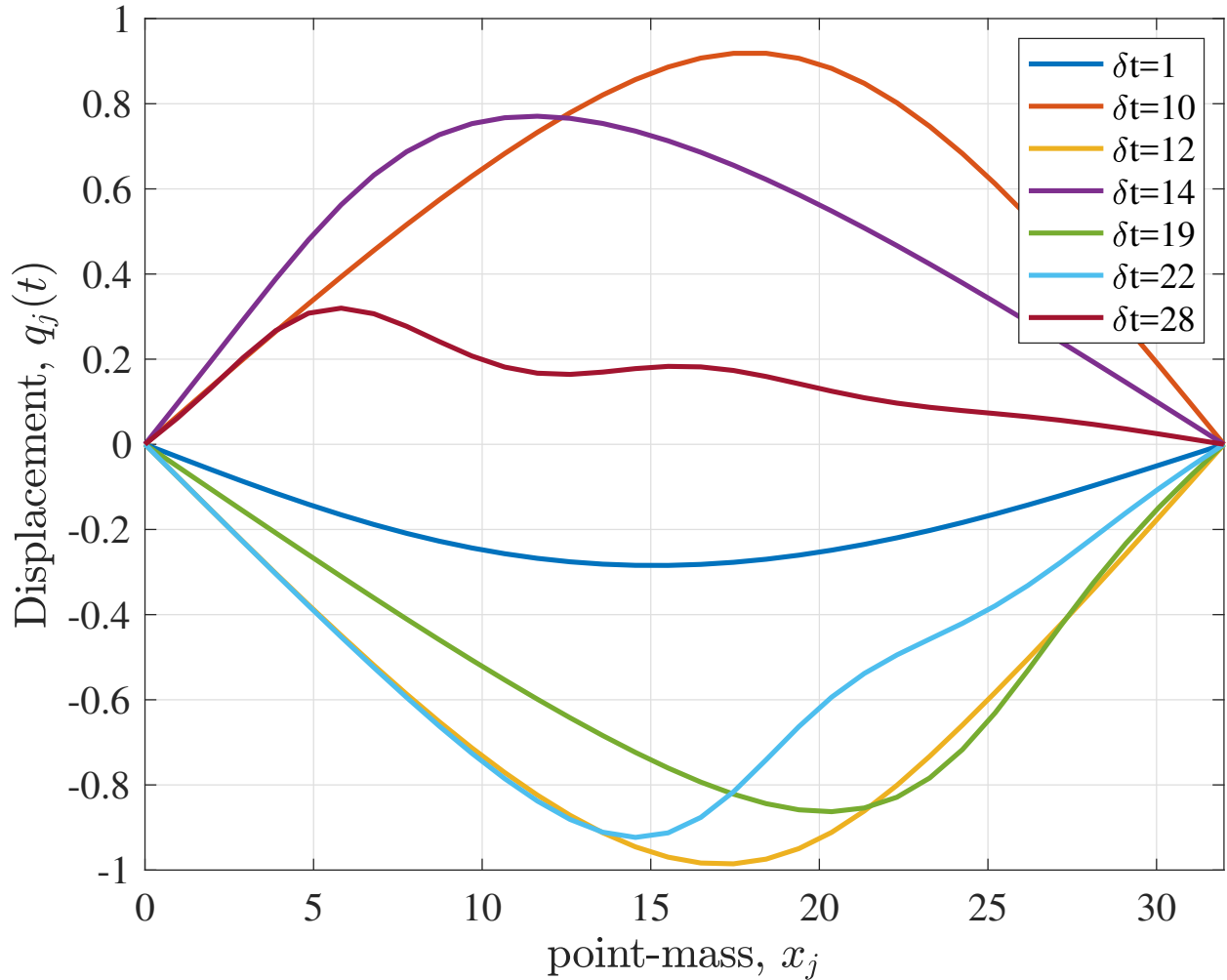


Figure 2.3. This drawing shows not the energy but the actual shapes, i.e., the displacement of the string at various times as indicated in the legend. The conditions are $N = 32$, $\alpha = \frac{1}{4}$, $\Delta t = 1/16$. The initial form of the string was a $q_j = \sin\left(\frac{j\pi}{N}\right)$.

Figure 2.5 provides the results for the same initial data as in the preceding figures, i.e. $q_j = \sin\left(\frac{j\pi}{N}\right)$, but with cubic forcing where $\alpha = 0$ and $\beta \neq 0$. Similar quasi-period dynamics are exhibited. This is unexpected since the perturbation, $\beta = 8$, is large. But the cubic restoring force is acting on symmetric initial data.

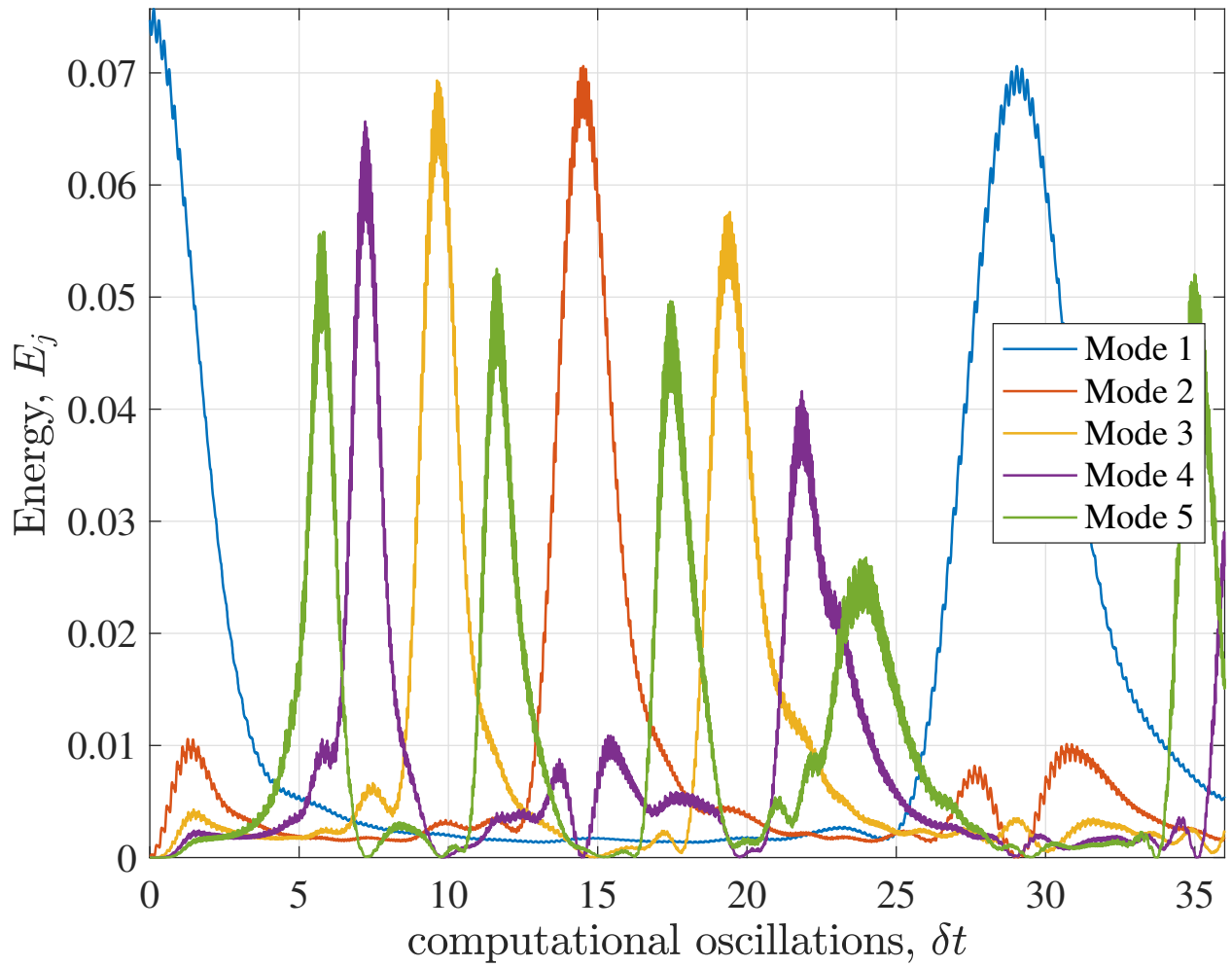


Figure 2.4. Same conditions as Figure 2.2 but the quadratic term in the force was stronger. $\alpha = 1$.

In Figure 2.6, the nature of these special cases is seen more clearly – all the energy is initially placed in two modes, namely two thirds in mode five and one third in mode seven and $\beta = \frac{1}{16}$. We find that $\forall t \leq 10560$

$$\sup_{j:j \neq 5 \vee 7} \|E_j(t)\|_2 \leq 8 \times 10^{-3}. \quad (2.61)$$

Moreover, $E_5(t)$ and $E_7(t)$ are approximately constant. This strongly suggests that energy in modes $j : j \neq 5 \vee 7$ is negligible and that the string oscillates with nearly perfect recurrence.

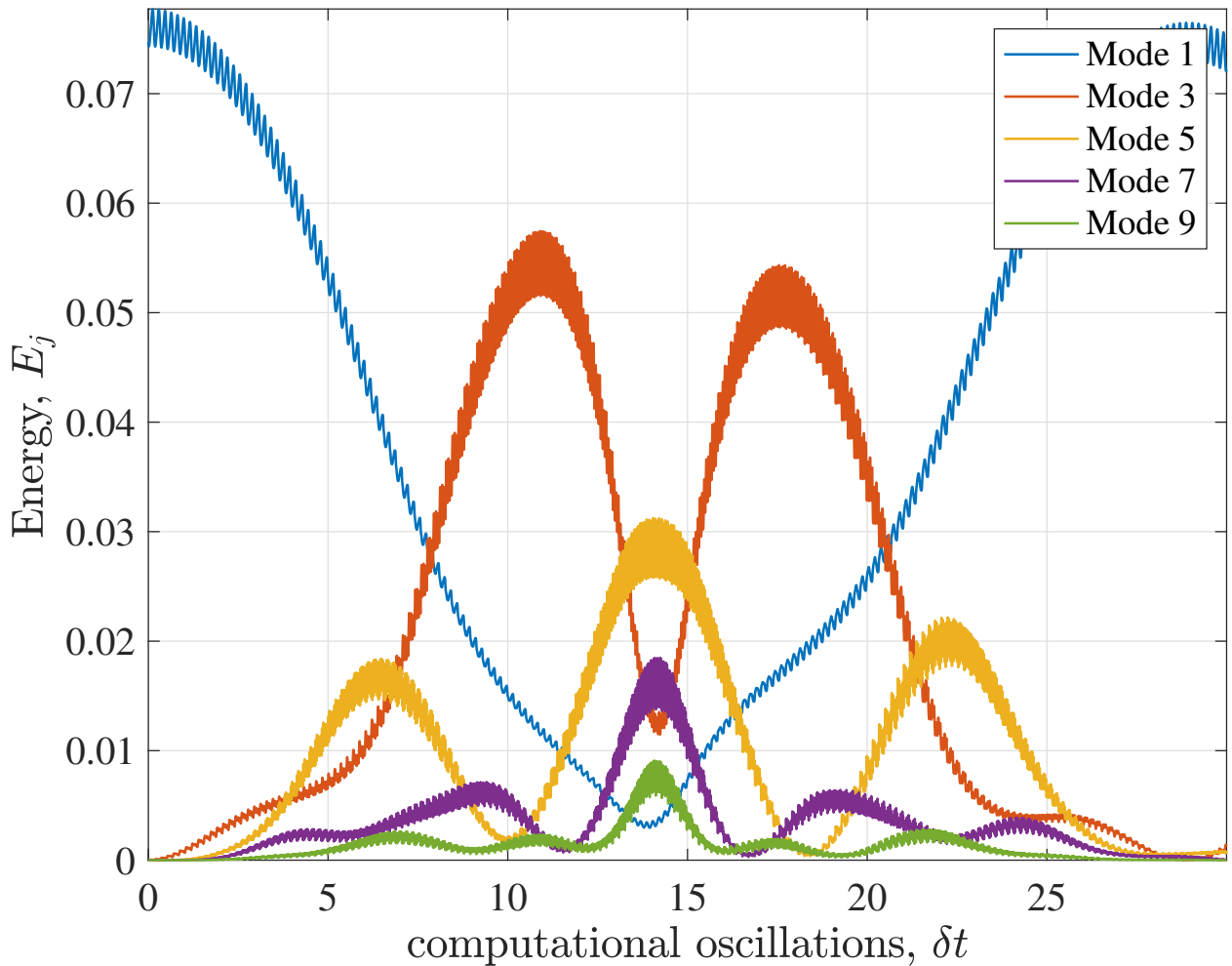


Figure 2.5. The quantity plotted is the energy, E_j , in the first five modes. $N = 32, \beta = 8, \Delta t = 1/16$. The initial form of the string was $q_j = \sin\left(\frac{j\pi}{N}\right)$.

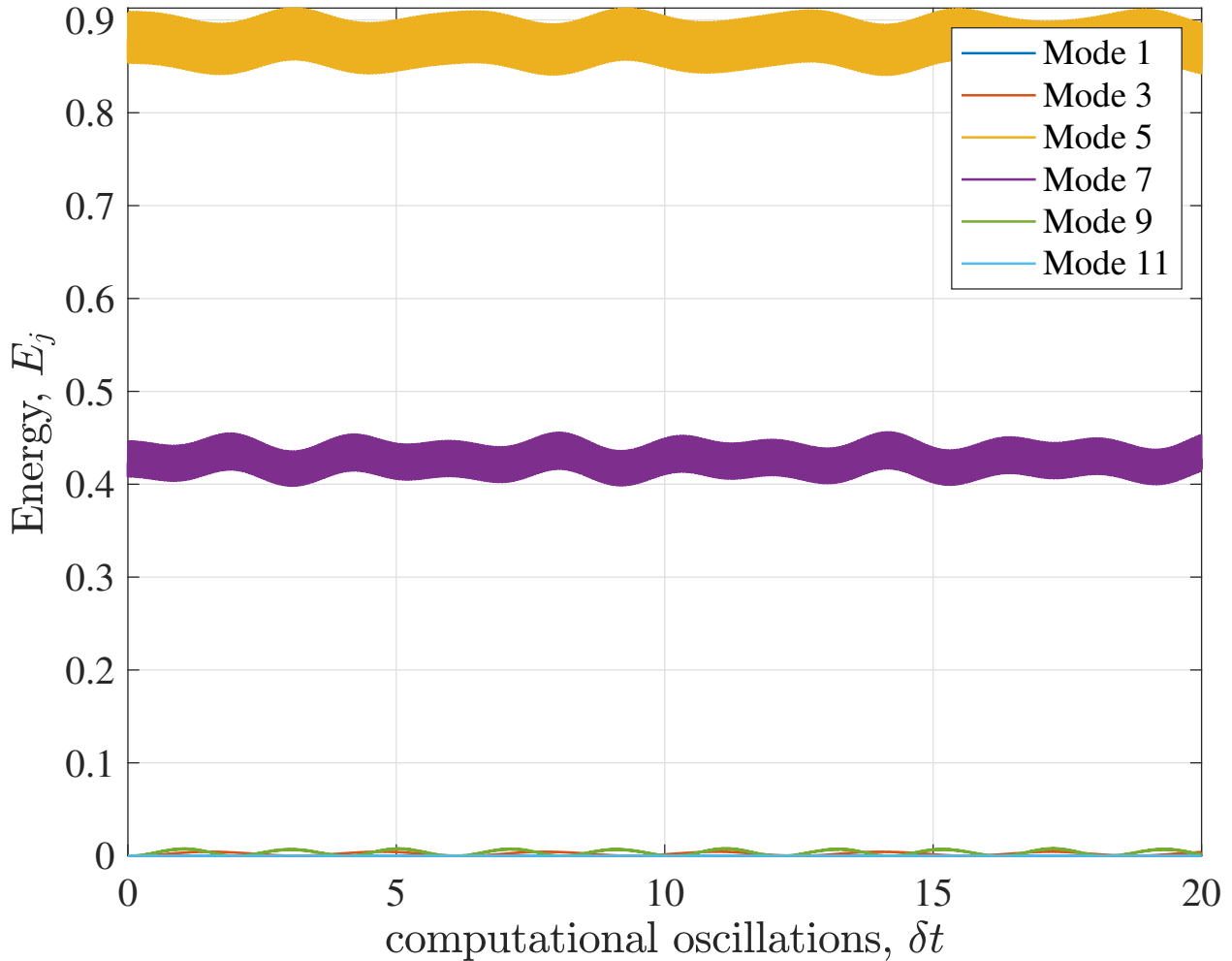


Figure 2.6. The quantity plotted is the energy, E_j , in the first five modes. $N = 32, \beta = \frac{1}{16}, \Delta t = 1/64$. The initial form of the string was determined by placing two thirds of the energy in mode five and one third in mode seven.

For several years following the original FPU experiments, there were concerns about the possibility of numerical artifacts effecting the recurrence phenomenon. In 1972, J. Tuck and M. Menzel [18] reexamined the original FPU experiment, in which they evolved the sine wave initial data over a much longer time frame. In Figure 2.7, we do this by executing the same computation as in Figure 2.2, but for about one hundred times the number of time-steps. The results confirm the original FPU experiment and illustrate further recurrence phenomenon, which Tuck called super-recurrence. It should be noted that this qualitative behavior remains intact even after many tens of thousands of computational oscillations.

On the whole, what is suggested by the numerical experiment is that in certain problems which are nearly linear, there exist quasi-states characterized by, for instance, the recurrence phenomenon seen in the FPU lattice.

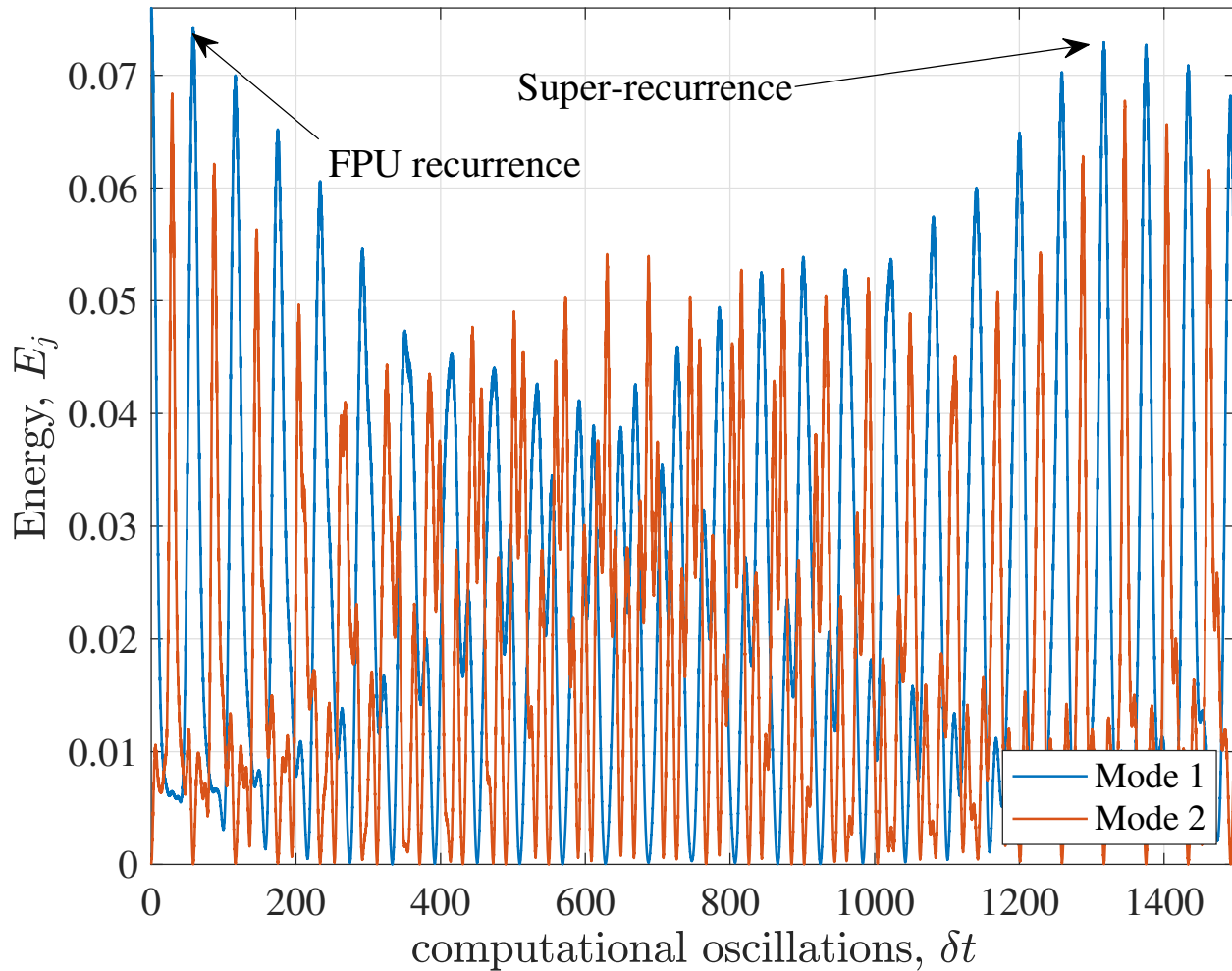


Figure 2.7. The quantity plotted is the energy, E_j , in the first two modes.
 $N = 32, \alpha = \frac{1}{4}, \Delta t = 1/16$. The initial form of the string was a $q_j = \sin\left(\frac{j\pi}{N}\right)$.

CHAPTER 3: ON A CONTINUUM LIMIT OF THE FPU LATTICE

3.1 Introduction

In a celebrated result [22] due to Zabusky and Kruskal, the Korteweg-de Vries equation, which was expected to model long wavelength modes in the FPU- α lattice, revealed via the traveling wave assumption the existence of waves that pass through one another, interact in a nonlinear way, and then remain unchanged after collision. Such structures, which were initially observed by J. Russell as early as 1834 and coined solitary waves, were renamed solitons in the Zabusky paper and, thereafter, gave way to intense interest in soliton theory for several decades. A derivation of the KdV equation and a larger class of related problems was first reported by a collaborators of Zabusky and Kruskal, C. Su and C. Gardner [17]. Shortly thereafter, M. Wadati illustrated a means of passing strictly from the FPU lattice to the Korteweg-de Vries equation and modified Korteweg-de Vries equation [20]. Kruskal appears to have originally proposed the procedure in unpublished conference proceedings shortly before Zabusky and Kruskal's seminal work [22]. The higher order expansion that is derived was first reported by Kudryashov [9].

3.2 From FPU to KdV

Recall from the previous chapter the description of a nearest neighbor force with nonlinear perturbation on a j th particle, say y_j , in an infinite one dimensional monatomic lattice in which

$$\ddot{y}_i = \frac{\kappa}{m} \sum_{j=1}^N K_j ((y_{i+1} - y_i)^j - (y_i - y_{i-1})^j) \quad (3.1)$$

with particle mass m and spring constant κ . The case where $K_1 = \gamma$, $K_2 = \alpha$, $K_3 = \beta$ and $K_n = 0, n \geq 4$ corresponds to the FPU equations of motion. In the interest of adopting a continuum approximation for smooth waves, i.e., waves with a long wavelength

relative to the particle spacing, we define a function $y : D \subset \mathbb{R} \times \mathbb{R} \rightarrow \mathbb{R}$ by

$$y(X, T) := y_j(T) \quad (3.2)$$

where $X = jh$ and $y \in \mathcal{C}^\infty(D)$. Note the M th order Taylor expansion of $y_{i\pm 1}$, wherein

$$y_{i\pm 1} - y_i = \sum_{j=1}^M \frac{(\pm h)^j}{j!} \frac{\partial^j}{\partial X^j} y + \mathcal{O}(h^{M+1}). \quad (3.3)$$

Since y is smooth, its partial derivatives can be interchanged. Therefore, for convenience, we define

$$\partial_{jz} y = \frac{\partial^j y}{\partial z^j}. \quad (3.4)$$

3.2.1 Order Four Expansion: Korteweg-de Vries Equation

Consider the FPU- α case ($\kappa = 1, \beta = 0$) and a 4th order Taylor expansion of y so that Equation (3.1) becomes

$$m\partial_{TT}y = \gamma((y_{i+1} - y_i) - (y_i - y_{i-1})) + \alpha((y_{i+1} - y_i)^2 - (y_i - y_{i-1})^2), \quad (3.5)$$

$$= \gamma((y_{i+1} - y_i) + (y_{i-1} - y_i)) + \alpha((y_{i+1} - y_i)^2 - (y_{i-1} - y_i)^2), \quad (3.6)$$

$$= \gamma \left(\sum_{j=1}^4 \frac{h^j}{j!} \partial_{jX} y + \sum_{j=1}^4 \frac{(-h)^j}{j!} \partial_{jX} y + \mathcal{O}(h^5) \right) \quad (3.7)$$

$$+ \alpha \left(\left(\sum_{j=1}^4 \frac{h^j}{j!} \partial_{jX} y + \mathcal{O}(h^5) \right)^2 - \left(\sum_{j=1}^4 \frac{(-h)^j}{j!} \partial_{jX} y + \mathcal{O}(h^5) \right)^2 \right),$$

$$= \gamma \left(h^2 y_{XX} + \frac{1}{12} h^4 y_{XXXX} \right) \quad (3.8)$$

$$+ \alpha \left(h^2 y_X^2 + h^3 y_X y_{XX} + \frac{h^4}{4} y_{XX}^2 + \frac{h^4}{3} y_X y_{XXX} \right. \\ \left. - \left(h^2 y_X^2 - h^3 y_X y_{XX} + \frac{h^4}{4} y_{XX}^2 + \frac{h^4}{3} y_X y_{XXX} \right) \right) + \mathcal{O}(h^5),$$

$$= \gamma h^2 y_{XX} + 2h^3 \alpha y_X y_{XX} + \gamma \frac{h^4}{12} y_{XXXX} + \mathcal{O}(h^5). \quad (3.9)$$

Therefore,

$$0 = -m\partial_{TT}y + \gamma h^2 y_{XX} + 2h^3 \alpha y_X y_{XX} + \gamma \frac{h^4}{12} y_{XXXX} + \mathcal{O}(h^5). \quad (3.10)$$

In a manner similar to [9], we transform the truncation of Equation (3.10) according to

$$\begin{cases} y(X, T) = \frac{\gamma}{2\alpha h} v(x, \tau), \end{cases} \quad (3.11)$$

$$\begin{cases} x = X - h\sqrt{\frac{\gamma}{m}}T, \end{cases} \quad (3.12)$$

$$\begin{cases} \tau = \frac{\epsilon h}{2}\sqrt{\frac{\gamma}{m}}T. \end{cases} \quad (3.13)$$

Equations (3.11)—(3.13) have frequently been used to transform interpolations of the FPU lattice into KdV-type equations [9, 11, 14, 17, 20, 22]. There are alternative constructions of note, namely in a series of papers [3–6] by G. Friesecke and R. Pego. We now apply Equations (3.11)—(3.13) to Equation (3.10) so that

$$\begin{aligned} 0 &= -m \left(-h\sqrt{\frac{\gamma}{m}} \right)^2 \partial_{xx} \left[\frac{\gamma}{2\alpha h} v \right] + 2 \left(-h\sqrt{\frac{\gamma}{m}} \right) \left(\frac{\epsilon h}{2}\sqrt{\frac{\gamma}{m}} \right) \partial_{x\tau} \left[\frac{\gamma}{2\alpha h} v \right] \\ &\quad + \left(\frac{\epsilon h}{2}\sqrt{\frac{\gamma}{m}} \right)^2 \partial_{\tau\tau} \left[\frac{\gamma}{2\alpha h} v \right] \\ &\quad + \gamma h^2 \partial_{xx} \left[\frac{\gamma}{2\alpha h} v \right] + 2h^3 \alpha \partial_x \left[\frac{\gamma}{2\alpha h} v \right] \partial_{xx} \left[\frac{\gamma}{2\alpha h} v \right] + \gamma \frac{h^4}{12} \partial_{xxxx} \left[\frac{\gamma}{2\alpha h} v \right], \\ &= -\frac{h\gamma^2}{2\alpha} \left(v_{xx} - \epsilon v_{x\tau} + \frac{\epsilon^2}{4} v_{\tau\tau} \right) \\ &\quad + \frac{h\gamma^2}{2\alpha} \left(v_{xx} + v_x v_{xx} + \frac{h^2}{12} v_{xxxx} \right). \end{aligned} \quad (3.14)$$

After multiplying Equation (3.15) by $\frac{2\alpha}{h\gamma^2}$,

$$0 = -v_{xx} + \epsilon v_{x\tau} - \frac{\epsilon^2}{4} v_{\tau\tau} + v_{xx} + 2v_x v_{xx} + \frac{h^2}{12} v_{xxxx}, \quad (3.16)$$

$$= \epsilon v_{x\tau} + v_x v_{xx} + \frac{h^2}{12} v_{xxxx} + \mathcal{O}(\epsilon^2). \quad (3.17)$$

As in [9, 11, 14, 20, 22], the order $\mathcal{O}(\epsilon^2)$ terms in Equation (3.17) are truncated using the assumption that $0 < \epsilon \ll 1$. Thus,

$$0 = \epsilon v_{x\tau} + v_x v_{xx} + \frac{h^2}{12} v_{xxxx}. \quad (3.18)$$

Now transform Equation (3.18) according to

$$\begin{cases} \partial_x v(x, \tau) = u(x, t), & (3.19) \\ t = \frac{\tau}{\epsilon}. & (3.20) \end{cases}$$

Notice that treatment of the Taylor expansion via the previous two transformations and truncations is analogous to the assertion that $|v_{\tau\tau}| \downarrow 0$. It is for this reason that Kruskal's method is referred to as a long wavelength model. So, taking $\delta = \frac{h}{\sqrt{12}}$, we have

$$0 = u_t + uu_x + \delta^2 u_{xxx}. \quad (3.21)$$

Equation (3.21) was considered in [17, 22].

3.2.2 Order Six Expansion: Kudryashov Generalized Korteweg-de Vries Equation

Now consider the FPU- α case ($\kappa = 1, \beta = 0$) and a 6th order Taylor expansion of y so that Equation (3.1) becomes

$$my_{TT} = \gamma((y_{i+1} - y_i) - (y_i - y_{i-1})) + \alpha((y_{i+1} - y_i)^2 - (y_i - y_{i-1})^2), \quad (3.22)$$

$$= \gamma((y_{i+1} - y_i) + (y_{i-1} - y_i)) + \alpha((y_{i+1} - y_i)^2 - (y_{i-1} - y_i)^2), \quad (3.23)$$

$$= \gamma \left(\sum_{j=1}^6 \frac{h^j}{j!} \partial_{jX} y + \sum_{j=1}^6 \frac{(-h)^j}{j!} \partial_{jX} y + \mathcal{O}(h^7) \right) \quad (3.24)$$

$$+ \alpha \left(\left(\sum_{j=1}^6 \frac{h^j}{j!} \partial_{jX} y + \mathcal{O}(h^7) \right)^2 - \left(\sum_{j=1}^6 \frac{(-h)^j}{j!} \partial_{jX} y + \mathcal{O}(h^7) \right)^2 \right),$$

$$= \gamma \left(h^2 y_{XX} + \frac{1}{12} h^4 y_{XXXX} + \frac{1}{360} h^6 y_{6X} \right) \quad (3.25)$$

$$+ \alpha \left(h^2 y_X^2 + h^3 y_X y_{XX} + \frac{h^4}{4} y_{XX}^2 + \frac{h^4}{3} y_X y_{XXX} + \frac{h^5}{6} y_{XX} y_{XXX} + \frac{h^5}{12} y_X y_{XXXX} \right. \\ \left. + \frac{h^6}{36} y_{XXX}^2 + \frac{h^6}{24} y_{XX} y_{XXXX} + \frac{h^6}{60} y_X y_{XXXXX} \right. \\ \left. - \left(h^2 y_X^2 - h^3 y_X y_{XX} + \frac{h^4}{4} y_{XX}^2 + \frac{h^4}{3} y_X y_{XXX} - \frac{h^5}{6} y_{XX} y_{XXX} - \frac{h^5}{12} y_X y_{XXXX} \right. \right. \\ \left. \left. + \frac{h^6}{36} y_{XXX}^2 + \frac{h^6}{24} y_{XX} y_{XXXX} + \frac{h^6}{60} y_X y_{XXXXX} \right) \right) + \mathcal{O}(h^7),$$

$$= \gamma \left(h^2 y_{XX} + \frac{1}{12} h^4 y_{XXXX} + \frac{1}{360} h^6 y_{6X} \right) \quad (3.26)$$

$$+ \alpha \left(2h^3 y_X y_{XX} + \frac{h^5}{3} y_{XX} y_{XXX} + \frac{h^5}{6} y_X y_{XXXX} \right) + \mathcal{O}(h^7).$$

Therefore, upon truncation of higher order terms,

$$0 = -my_{TT} + \gamma h^2 y_{XX} + 2h^3 \alpha y_X y_{XX} + \gamma \frac{h^4}{12} y_{XXXX} \quad (3.27) \\ + \frac{h^5}{3} \alpha y_{XX} y_{XXX} + \frac{h^5}{6} \alpha y_X y_{XXXX} + \frac{h^6}{360} \gamma y_{6X}.$$

We use Equations (3.11)—(3.13), namely

$$\begin{cases} y(X, T) = \frac{\gamma}{2\alpha h} v(x, \tau), \end{cases} \quad (3.28)$$

$$\begin{cases} x = X - h\sqrt{\frac{\gamma}{m}} T, \end{cases} \quad (3.29)$$

$$\begin{cases} \tau = \frac{\epsilon h}{2} \sqrt{\frac{\gamma}{m}} T. \end{cases} \quad (3.30)$$

to transform Equation (3.27). Equation (3.10) is identical to Equation (3.27), save for the higher order terms. Thus, the transformation yields

$$0 = -\frac{h\gamma^2}{2\alpha} \left(v_{xx} - \epsilon v_{x\tau} + \frac{\epsilon^2}{4} v_{\tau\tau} \right) \quad (3.31)$$

$$\begin{aligned} & + \frac{h\gamma^2}{2\alpha} \left(v_{xx} + v_x v_{xx} + \frac{h^2}{12} v_{xxxx} \right) \\ & + \frac{h^5}{3} \alpha \partial_{xx} \left[\frac{\gamma}{2\alpha h} v \right] \partial_{xxx} \left[\frac{\gamma}{2\alpha h} v \right] + \frac{h^5}{6} \alpha \partial_x \left[\frac{\gamma}{2\alpha h} v \right] \partial_{xxxx} \left[\frac{\gamma}{2\alpha h} v \right] + \frac{h^6}{360} \gamma \partial_{6x} \left[\frac{\gamma}{2\alpha h} v \right], \\ & = -\frac{h\gamma^2}{2\alpha} \left(v_{xx} - \epsilon v_{x\tau} + \frac{\epsilon^2}{4} v_{\tau\tau} \right) \quad (3.32) \\ & + \frac{h\gamma^2}{2\alpha} \left(v_{xx} + v_x v_{xx} + \frac{h^2}{12} v_{xxxx} + \frac{h^2}{6} v_{xx} v_{xxx} + \frac{h^2}{12} v_x v_{xxxx} + \frac{h^4}{360} v_{6x} \right). \end{aligned}$$

After multiplying Equation (3.32) by $\frac{2\alpha}{h\gamma^2}$,

$$0 = \epsilon v_{x\tau} + v_x v_{xx} + \frac{h^2}{12} v_{xxxx} + \frac{h^2}{6} v_{xx} v_{xxx} + \frac{h^2}{12} v_x v_{xxxx} + \frac{h^4}{360} v_{6x} + \mathcal{O}(\epsilon^2). \quad (3.33)$$

As in Subsection 3.2.1, the order $\mathcal{O}(\epsilon^2)$ terms in Equation (3.33) are truncated using the assumption that $0 < \epsilon \ll 1$. Thus,

$$0 = \epsilon v_{x\tau} + v_x v_{xx} + \frac{h^2}{12} v_{xxxx} + \frac{h^2}{6} v_{xx} v_{xxx} + \frac{h^2}{12} v_x v_{xxxx} + \frac{h^4}{360} v_{6x}, \quad (3.34)$$

which is then transformed according to

$$\begin{cases} \partial_x v(x, \tau) = u(x, t), \end{cases} \quad (3.35)$$

$$\begin{cases} t = \frac{\tau}{\epsilon}. \end{cases} \quad (3.36)$$

So, taking $\delta = \frac{h}{\sqrt{12}}$, we have

$$0 = u_t + uu_x + 2\delta^2 u_x u_{xx} + \delta^2 u_{xxx} + \delta^2 uu_{xxx} + \frac{2}{5}\delta^4 u_{5x}. \quad (3.37)$$

Equation (3.37) was studied in [9, 19] and, with $\beta \neq 0$, in [11]. We will refer to Equation (3.37) as the Kudryashov Generalized KdV (KG KdV) equation. Dissipative modifications to KG KdV have also been investigated [10].

3.3 Tanh Method Solutions

The tanh method, developed by W. Malfliet and W. Hereman [13], provides for a structured means of seeking a solution to a given one-dimensional nonlinear wave equation. In particular, an equation of the form

$$u_t = F(u, u_x, u_{xx}, \dots) \quad (3.38)$$

is transformed according to the traveling wave assumption

$$\begin{cases} u(x, t) = v(\xi), \\ \xi = k(x - ct). \end{cases} \quad (3.39)$$

$$\xi = k(x - ct). \quad (3.40)$$

This transformation renders the nonlinear wave equation as an ordinary differential equation of the form

$$-ckv_\xi = F(v, kv_\xi, k^2v_{\xi\xi}, \dots). \quad (3.41)$$

Then, upon letting $Y = \tanh \xi$, solutions in the form of a finite power series in Y , i.e.

$$S(Y) = \sum_{j=0}^M a_j Y^j, \quad (3.42)$$

are assumed to satisfy Equation (3.41) by computing the change in derivatives. Indeed, all derivatives of \tanh can be represented in terms of \tanh in a closed form [1], yielding a

straightforward method for finding solutions. In particular, notice that

$$\frac{d}{d\xi} = (1 - Y^2) \frac{d}{dY}, \quad (3.43)$$

$$\frac{d^2}{d\xi^2} = (1 - Y^2) \left(-2Y \frac{d}{dY} + (1 - Y^2) \frac{d^2}{dY^2} \right), \quad (3.44)$$

and so on. For problems similar to the KG KdV equation, an extension of the tanh method has been used [21] where the finite power series solution is of the form

$$S(Y) = \sum_{j=-M}^M a_j Y^j. \quad (3.45)$$

The result of the change of derivatives, as in Equations (3.43) (3.44), are substituted in Equation (3.41). This substitution yields an equation of the form

$$0 = G(S, S_Y, S_{YY}, \dots). \quad (3.46)$$

The highest order linear term, say l , and the highest order nonlinear term, say n , are identified and M is fixed by finding the M that satisfies $M + l = nM$. Finally, G is computed, resulting in an equation of the form

$$P(Y) = 0, \quad (3.47)$$

where P is a polynomial in Y with variable coefficients a_j, c , and k . Coefficients of powers of Y in Equation (3.47) are then equated to the RHS, in which a system of nonlinear equations is produced. Solving the system yields

$$v = \sum_{j=-M}^M a_j \tanh^j(k(x - ct)). \quad (3.48)$$

Note that, in the interest of finding one solution of a special type for our problems, we make the assumption that

$$S(Y) = a_0 + a_2 Y^2. \quad (3.49)$$

3.3.1 KdV Equation

Transform

$$0 = u_t + uu_x + \delta^2 u_{3x} \quad (3.50)$$

according to

$$\begin{cases} u(x, t) = v(\xi) \\ \xi = x - ct \end{cases} \quad (3.51)$$

$$\xi = x - ct \quad (3.52)$$

where $c \in \mathbb{R}$. Then,

$$0 = -cv_\xi + vv_\xi + \delta^2 v_{3\xi}. \quad (3.53)$$

Now, we let $u' = v$ and we suppress the apostrophe notation. Then Equation (3.53) is integrated in ξ to obtain

$$C = -cu + \frac{1}{2}u^2 + \delta^2 u_{\xi\xi}, \quad (3.54)$$

where $C \in \mathbb{R}$. Let $k \in \mathbb{R}$ and suppose

$$u(k\xi) = a_1 + a_2 \tanh^2(k\xi). \quad (3.55)$$

Therefore,

$$\frac{du}{d\xi} = 2ka_2Y - 2ka_2Y^3, \quad (3.56)$$

$$\frac{d^2u}{d\xi^2} = 2k^2a_2 - 8k^2a_2Y^2 + 6k^2a_2Y^4, \quad (3.57)$$

where $Y = \tanh(k\xi)$. Substitute Equations (3.55)—(3.57) with $Y = \tanh(k\xi)$ into Equation (3.54) so that

$$C = -c(a_1 + a_2Y^2) + \frac{1}{2}(a_1 + a_2Y^2)^2 + \delta^2(2k^2a_2 - 8k^2a_2Y^2 + 6k^2a_2Y^4), \quad (3.58)$$

$$= -ca_1 + \frac{1}{2}a_1^2 + 2k^2\delta^2a_2 + Y^2(-ca_2 - 8k^2\delta^2a_2 + a_1a_2) + Y^4(6k^2\delta^2a_2 + \frac{1}{2}a_2^2). \quad (3.59)$$

This implies the system of equations

$$\begin{cases} C = -ca_1 + \frac{1}{2}a_1^2 + 2k^2\delta^2a_2, & (3.60) \end{cases}$$

$$\begin{cases} 0 = -ca_2 - 8k^2\delta^2a_2 + a_1a_2, & (3.61) \end{cases}$$

$$\begin{cases} 0 = 6k^2\delta^2a_2 + \frac{1}{2}a_2^2. & (3.62) \end{cases}$$

We are interested in cases where a_2 is nonzero, so Equations (3.60)—(3.62) become

$$\begin{cases} C = -ca_1 + \frac{1}{2}a_1^2 + 2k^2\delta^2a_2, & (3.63) \end{cases}$$

$$\begin{cases} 0 = -c - 8k^2\delta^2 + a_1, & (3.64) \end{cases}$$

$$\begin{cases} 0 = 6k^2\delta^2 + \frac{1}{2}a_2. & (3.65) \end{cases}$$

Notice that Equation (3.65) implies

$$a_2 = -12k^2\delta^2. \quad (3.66)$$

Equation (3.66) is substituted into Equation (3.64) so that

$$a_1 = c + 8k^2\delta^2. \quad (3.67)$$

Now Equations (3.66) and (3.67) are substituted into Equation (3.63) to obtain

$$c^2 = 16k^4\delta^4 - 2C. \quad (3.68)$$

Since C is arbitrary, c is arbitrary. For our purposes, we fix $C = 0$ and, therefore, $c = \pm 4k^2\delta^2$. The solutions of Equations (3.60)—(3.62) are substituted into Equation (3.55), in which two solutions arise:

$$u_1(x, t) = 12k^2\delta^2 - 12k^2\delta^2 \tanh^2(k(x - 4k^2\delta^2t)), \quad (3.69)$$

$$= 12k^2\delta^2 \operatorname{sech}^2(k(x - 4k^2\delta^2t)), \quad (3.70)$$

$$u_2(x, t) = 4k^2\delta^2 - 12k^2\delta^2 \tanh^2(k(x + 4k^2\delta^2t)). \quad (3.71)$$

If we let $k' = \frac{k}{2}$ and $C_0 = -(k')^2\delta^2$, then, after suppressing the apostrophe notation,

$$u_2(x, t) = C_0 + 2\delta^2k^2 - 3\delta^2k^2 \tanh^2\left(\frac{kz}{2}\right), \quad z = x - C_0t, \quad (3.72)$$

as in [19].

3.3.2 KG KdV Equation

We repeat the above Tanh Method for Equation (3.37),

$$0 = u_t + uu_x + 2\delta^2u_xu_{xx} + \delta^2u_{xxx} + \delta^2uu_{xxx} + \frac{2}{5}\delta^4u_{5x}. \quad (3.73)$$

So the transformations,

$$\begin{cases} u(x, t) = v(\xi), \\ \xi = x - ct, \end{cases} \quad (3.74)$$

$$(3.75)$$

imply, after suppressing the apostrophe notation in u' and after integrating the equation in ξ ,

$$C = -cu + \delta^2u_{xx} + \frac{2}{5}\delta^4u_{4x} + \frac{1}{2}u^2 + \frac{1}{2}\delta^2u_x^2 + \delta^2uu_{xx}, \quad (3.76)$$

where $C \in \mathbb{R}$. Let $k \in \mathbb{R}$ and suppose

$$u(k\xi) = a_1 + a_2 \tanh^2(k\xi). \quad (3.77)$$

Recall that Equation (3.77) implies

$$\frac{du}{d\xi} = 2ka_2Y - 2ka_2Y^3, \quad (3.78)$$

$$\frac{d^2u}{d\xi^2} = 2k^2a_2 - 8k^2a_2Y^2 + 6k^2a_2Y^4, \quad (3.79)$$

$$\frac{d^3u}{d\xi^3} = -16k^3a_2Y + 40k^3a_2Y^3 - 24k^3a_2Y^5, \quad (3.80)$$

$$\frac{d^4u}{d\xi^4} = -16k^4a_2 + 136k^4a_2Y^2 - 240k^4a_2Y^4 + 120k^4a_2Y^6, \quad (3.81)$$

where $Y = \tanh(k\xi)$. Now substitute Equations (3.77)—(3.81) with $Y = \tanh(k\xi)$ into Equation (3.76) so that

$$C = c(a_1 + a_2Y^2) + \frac{1}{2}(a_1 + a_2Y^2)^2 + \frac{\delta^2}{2}(2ka_2Y - 2ka_2Y^3)^2 \quad (3.82)$$

$$\begin{aligned} & + \delta^2(2k^2a_2 - 8k^2Y^2a_2 + 6k^2Y^4a_2) + \delta^2(a_1 + Y^2a_2)(2k^2a_2 - 8k^2Y^2a_2 + 6k^2Y^4a_2) \\ & + \frac{2}{5}\delta^4(-16k^4a_2 + 136k^4a_2Y^2 - 240k^4a_2Y^4 + 120k^4a_2Y^6), \\ = & -ca_1 + \frac{1}{2}a_1^2 + 2k^2\delta^2a_2 - \frac{32}{5}k^4\delta^4a_2 + 2k^2\delta^2a_1a_2 \\ & + Y^2(-ca_2 - 8k^2\delta^2a_2 + \frac{272}{5}k^4\delta^4a_2 + a_1a_2 - 8k^2\delta^2a_1a_2 + 4k^2\delta^2a_2^2), \\ & + Y^4(6k^2\delta^2a_2 - 96k^4\delta^4a_2 + 6k^2\delta^2a_1a_2 + \frac{1}{2}a_2^2 - 12k^2\delta^2a_2^2) \\ & + Y^6(48k^4\delta^4a_2 + 8k^2\delta^2a_2^2). \end{aligned} \quad (3.83)$$

This implies the system of equations

$$\begin{cases} C = -ca_1 + \frac{1}{2}a_1^2 + 2k^2\delta^2a_2 - \frac{32}{5}k^4\delta^4a_2 + 2k^2\delta^2a_1a_2, & (3.84) \\ 0 = -ca_2 - 8k^2\delta^2a_2 + \frac{272}{5}k^4\delta^4a_2 + a_1a_2 - 8k^2\delta^2a_1a_2 + 4k^2\delta^2a_2^2, & (3.85) \\ 0 = 6k^2\delta^2a_2 - 96k^4\delta^4a_2 + 6k^2\delta^2a_1a_2 + \frac{1}{2}a_2^2 - 12k^2\delta^2a_2^2, & (3.86) \\ 0 = 48k^4\delta^4a_2 + 8k^2\delta^2a_2^2. & (3.87) \end{cases}$$

We are interested in cases where a_2 is nonzero, so Equations (3.84)—(3.87) become

$$\begin{cases} C = -ca_1 + \frac{1}{2}a_1^2 + 2k^2\delta^2a_2 - \frac{32}{5}k^4\delta^4a_2 + 2k^2\delta^2a_1a_2, & (3.88) \\ 0 = -c - 8k^2\delta^2 + \frac{272}{5}k^4\delta^4 + a_1 - 8k^2\delta^2a_1 + 4k^2\delta^2a_2, & (3.89) \\ 0 = 6k^2\delta^2 - 96k^4\delta^4 + 6k^2\delta^2a_1 + \frac{1}{2}a_2 - 12k^2\delta^2a_2, & (3.90) \\ 0 = 48k^4\delta^4 + 8k^2\delta^2a_2. & (3.91) \end{cases}$$

Notice that Equation (3.91) implies

$$a_2 = -6k^2\delta^2. \quad (3.92)$$

Substitution of Equation (3.92) into Equation (3.90) gives

$$a_1 = 4k^2\delta^2 - \frac{1}{2}. \quad (3.93)$$

Substitution of Equations (3.92) and (3.93) into Equation (3.89) gives

$$c = \frac{-16k^4\delta^4 - 5}{10}. \quad (3.94)$$

Note that c is no longer arbitrary, as was the case for the tanh solution of the KdV equation. Finally, substitution of Equations (3.92)—(3.94) into Equation (3.88) implies

$$C = \frac{2}{5}k^4\delta^4(3 - 8k^2\delta^2) - \frac{1}{8}. \quad (3.95)$$

Since C is arbitrary, Equation (3.95) is satisfied for all k, δ . The solution of Equations (3.88)—(3.91), provided by Equations (3.92)—(3.94), are then substituted into Equation (3.77), in which

$$u(x, t) = 4k^2\delta^2 - \frac{1}{2} - 6k^2\delta^2 \tanh^2 \left(k \left(x + \left(\frac{8}{5}k^4\delta^4 + \frac{1}{2} \right) t \right) \right). \quad (3.96)$$

If we let $k' = \frac{k}{2}$, then, after suppressing the apostrophe notation,

$$u(x, t) = k^2\delta^2 - \frac{1}{2} - \frac{3k^2\delta^2}{2} \tanh^2 \left(\frac{kz}{2} \right), \quad z = x + \left(\frac{\delta^4 k^4}{10} + \frac{1}{2} \right) t, \quad (3.97)$$

as in [19].

3.4 Sech Solutions

Using Equation (3.21), if we let $\nu = x - ct$ and we impose the condition that $u(x, t) = f(\nu)$, our solution will be a traveling wave solution with velocity c . So, noting that

$$u_t = \frac{\partial f}{\partial t} = \frac{\partial f}{\partial \nu} \frac{\partial \nu}{\partial t} = -cf' \quad (3.98)$$

$$u_x = \frac{\partial f}{\partial x} = \frac{\partial f}{\partial \nu} \frac{\partial \nu}{\partial x} = f' \quad (3.99)$$

$$u_{xxx} = \frac{\partial f}{\partial xxx} = \left(\frac{\partial f}{\partial \nu} \frac{\partial \nu}{\partial x} \right)^3 = f''' \quad (3.100)$$

We then have, by substitution, a third order nonlinear ordinary differential equation, which we shall integrate:

$$-cf' + ff' + \delta^2 f''' = 0 \quad (3.101)$$

$$\int (-cf' + ff' + \delta^2 f''') \delta \nu = c_1 \quad (3.102)$$

$$-cf + \frac{1}{2}f^2 + \delta^2 f'' = c_1 \quad (3.103)$$

$$-cff' + \frac{1}{2}f^2 f' + \delta^2 f'' f' - c_1 f' = 0 \quad (3.104)$$

$$\int (-cff' + \frac{1}{2}f^2 f' + \delta^2 f'' f' - c_1 f') \delta \nu = c_0 \quad (3.105)$$

$$-\frac{c}{2}f^2 + \frac{1}{6}f^3 + \frac{\delta^2}{2}(f')^2 - c_1 f = c_0. \quad (3.106)$$

Considering zero integration constants, this relation is reduced to

$$\delta^2 (f')^2 = cf^2 - \frac{1}{3}f^3 \quad (3.107)$$

$$(\delta f')^2 = f^2 \left(c - \frac{1}{3}f \right) \quad (3.108)$$

which implies

$$\delta \frac{df}{d\nu} = f \left(c - \frac{1}{3}f \right)^{\frac{1}{2}} \quad (3.109)$$

$$\delta \int \frac{df}{f \left(c - \frac{1}{3}f \right)^{\frac{1}{2}}} = \int d\nu \quad (3.110)$$

$$-\frac{2\delta}{\sqrt{c}} \tanh^{-1} \left(\sqrt{1 - \frac{f}{3c}} \right) = \nu + K \quad (3.111)$$

$$f = 3c \operatorname{sech}^2 \left(-\frac{\sqrt{c}}{2\delta} (\nu + K) \right). \quad (3.112)$$

And, therefore,

$$u(x, t) = 3c \operatorname{sech}^2 \left(-\frac{\sqrt{c}}{2\delta} (x - ct + K) \right) \quad (3.113)$$

is a solution to Equation (3.21).

CHAPTER 4: ANALYSIS OF GENERALIZED MODIFIED KDV EQUATIONS

4.1 Zabusky and Kruskal's Scheme for the KdV Equation

Recall the KdV equation, Equation (3.21),

$$0 = u_t + uu_x + \delta^2 u_{xxx}. \quad (4.1)$$

In Zabusky and Kruskal's seminal paper [22], the KdV equation was investigated numerically with the finite difference scheme:

$$\begin{cases} u_j^{n+1} = u_j^{n-1} - \frac{k}{3h}(u_{j+1}^n + u_j^n + u_{j-1}^n)(u_{j+1}^n - u_{j-1}^n) & j = 1, \dots, N, n \in \mathbb{N} \\ \quad - \frac{\delta^2 k}{h^3}(u_{j+2}^n - 2u_{j+1}^n + 2u_{j-1}^n - u_{j-2}^n), \\ u_j^n = u_{j+2N}^n, & j = 1, \dots, N, n \in \mathbb{N}. \end{cases} \quad (4.2)$$

$$\quad (4.3)$$

In executing the scheme, $\delta = .022$, initial data was of the form $u(jh, 0) = \cos(\pi jh)$, and the scheme was initialized with lower order schemes for the first two time steps.

4.1.1 Results

In Figure 4.1, the solution of the scheme in Equations (4.2)—(4.3) is plotted for three values of t . Notice that the initial wave form moving to the left is joined by waves traveling in the opposite direction as the initial wave. At a later time, waves traveling in the same direction as the initial wave also appear. By $t = 1.14$, eight such rightward and leftward traveling waves, deemed solitons, have appeared. They are labeled in order of appearance. In Figure 4.2, the surface $u(x, t)$ is provided. Notice that solution becomes unbounded by $t \approx 4.53$, as in [22]. In Figure 4.3, a contour plot of the surface $u(x, t)$ is provided. Level sets are colored according to the gradient of the surface, which gives an alternative perspective on the propagation of the traveling waves. These level sets also illustrate the complicated nonlinear interactions that ensue when the traveling waves collide, as seen in the blue and green-colored contours at $t = 3.5$ and $x = .75$ or $x = 1.4$. In the next section, we develop an alternative scheme using pseudospectral methods.

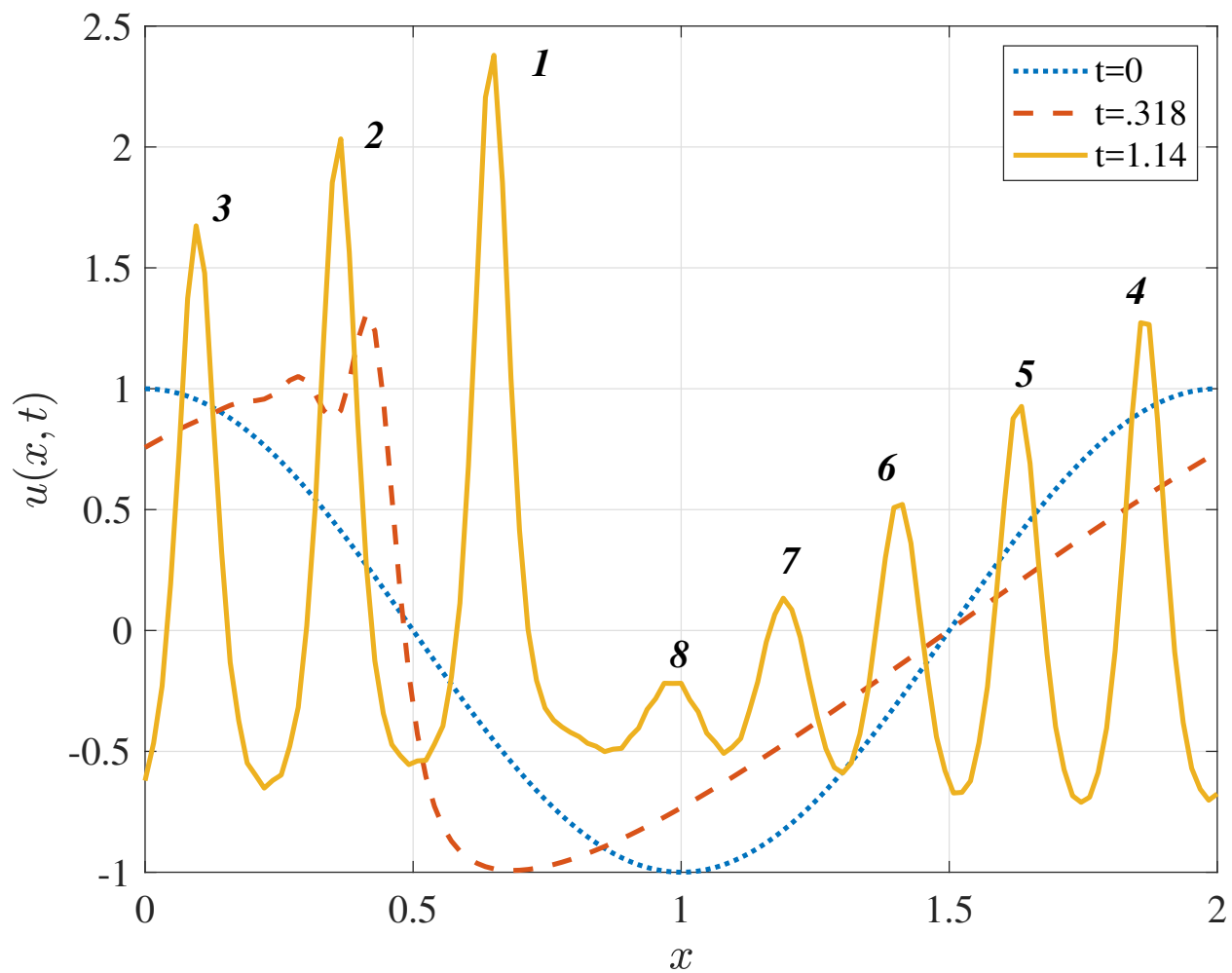


Figure 4.1. Projection of solution of the finite difference scheme, (4.2), with $\delta = .022$, $N = 2^6$, $h = N^{-1}$, $k = N^{-2}$, and $u(jh, 0) = \cos(\pi jh)$. Solitary waves are identified as the eight wave forms all having appeared by $t = 1.14$.

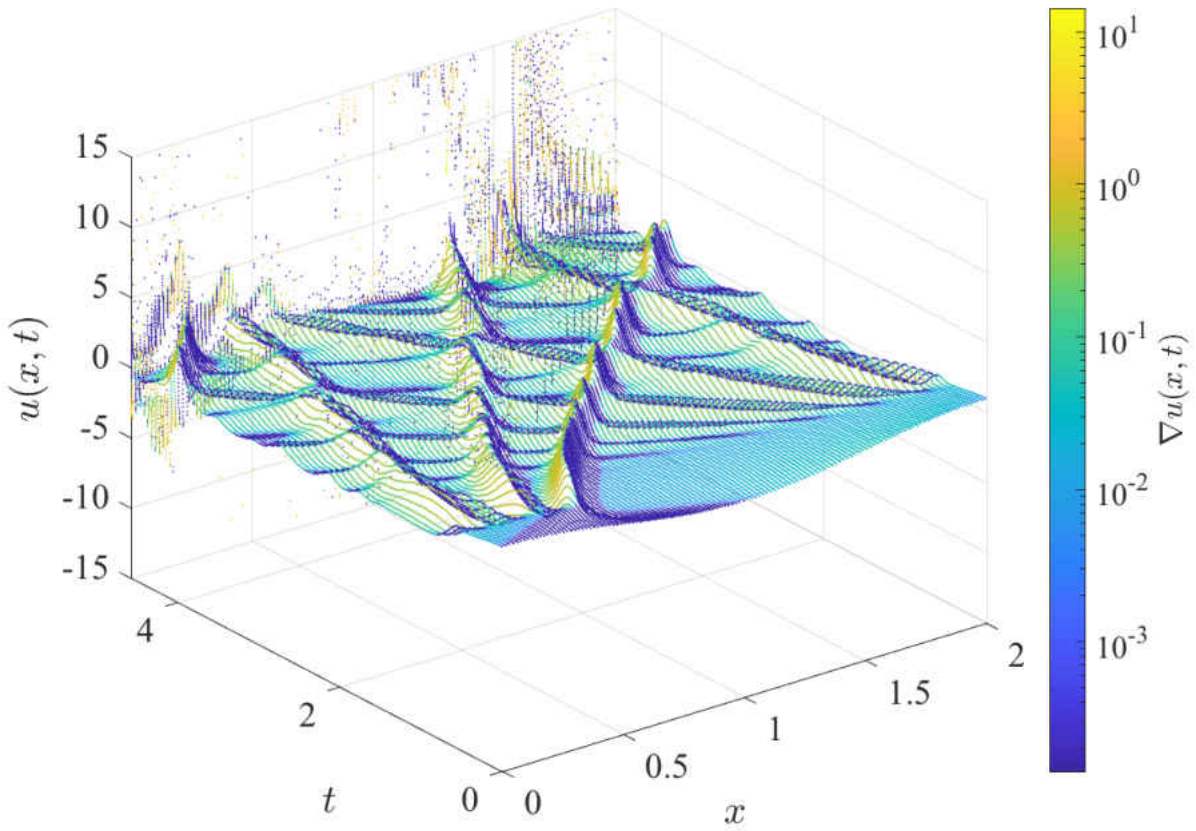


Figure 4.2. Solution of the finite difference scheme, (4.2), with $\delta = .022$, $N = 2^6$, $h = N^{-1}$, $k = N^{-2}$, and $u(jh, 0) = \cos(\pi jh)$. Points, $(x, t, u(x, t))$, are colored corresponding to a logarithmic scaling of ∇u .

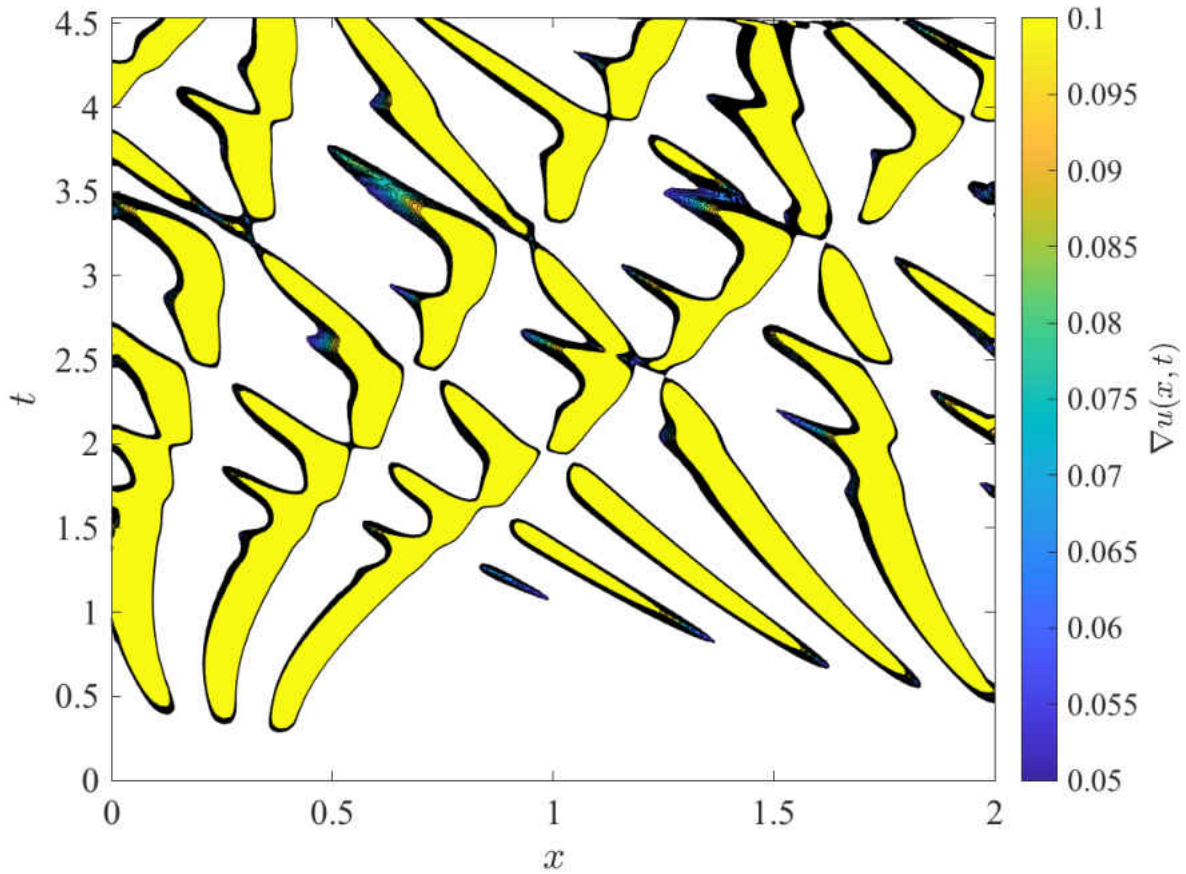


Figure 4.3. Projection of solution of the finite difference scheme, (4.2), with $\delta = .022$, $N = 2^6$, $h = N^{-1}$, and $k = N^{-2}$, and $u(jh, 0) = \cos(\pi jh)$. Neighborhoods where $0 < \nabla u \ll 1$ are colored corresponding to ∇u . Solitons are identified as the nine the wave forms appearing near $t = 1$, each propagating with an approximately constant velocity.

4.2 Numerical Experiments

Recall the Kudryashov-Generalized KdV equation, Equation (4.4), in which

$$0 = u_t + \delta^2 u_{xxx} + \frac{2}{5} \delta^4 u_{xxxxx} + uu_x - 2\delta^2 u_x u_{xx} + \delta^2 uu_{xxx}. \quad (4.4)$$

In the following numerical studies, to better understand the contributions of the higher order nonlinear terms, we consider variants of the Kudryashov-Generalized KdV equation of the form

$$0 = u_t + uu_x + \delta^2 u_{xxx} + s_1 2\delta^2 u_x u_{xx} + s_2 \delta^2 uu_{xxx} + s_3 \frac{2}{5} \delta^4 u_{xxxxx}. \quad (4.5)$$

In the case where $s_1 = s_2 = s_3 = 0$, Equation (4.5) reduces to the KdV equation. In the case where $s_1 = s_2 = s_3 = 1$, Equation (4.5) reduces to the Kudryashov-Generalized KdV (KG KdV) equation. There are two other cases of interest. Namely, KG KdV Variant 1 (KG KdV-1), where $s_1 = s_2 = 0$ and $s_3 = 1$ and KG KdV Variant 2 (KG KdV-2), where $s_1 = 1$ and $s_2 = s_3 = 0$.

4.2.1 Indicators of Equipartition

Assume $u \in (L^2(\mathbb{R}) \cap C^\infty(\mathbb{R})) \times \mathbb{R}$ and suppose $u(x, t_0)$ has compact support for every t_0 . As in [19], consider the Fourier transform of u in the spatial dimension denoted by \hat{u} . Then the Initial Value Problem consisting of Equation (4.4) and an initial condition is of the form

$$\begin{cases} 0 = G(\hat{u}_t, \hat{u}, \omega), & G \in \mathbb{C} \\ \hat{u}(\omega, 0) = \hat{f}(x), & \omega \in \mathbb{C}. \end{cases} \quad (4.6)$$

$$(4.7)$$

The linear part of the resulting problem in Equation (4.6) is stiff. The numerical scheme implemented in [19] involved filtering of modes using the two-thirds rule. Here, we implement a pseudospectral method that handles the stiffness of the equation and uses a 4th order Runge-Kutta method in time, which we will denote PS-RK4 [16]. This method does not filter the modes, which makes it possible to address the question of equipartition. PS-RK4 yields a numerical solution, $U \in \mathcal{M}_{N \times M}(\mathbb{R})$, where U_j^n is the

element in the j th row and n th column of U and where U^n is the n th column vector of U . Let $V^n \in \mathcal{M}_{N \times 1}(\mathbb{C})$ be the discrete Fourier transform of U^n , and let V_j^n be the j th element of V^n . Since solutions, U_j^n , of PS-RK4 are periodic, i.e. $U_j^n = U_{j+N}^n$, U_j^n has $\frac{N}{2}$ independent Fourier modes at every n . To address the energy in the modes, we introduce the function

$$P(j, n) = |V_j^n|^2. \quad (4.8)$$

$P(j, n)$ provides the power of j th Fourier mode at the n th time-step for the data, U . For fixed n_0 , $P(j, n_0)$ is referred to as the power spectrum. The relative normalized power of a nontrivial power spectrum is given by the function

$$\mathfrak{P}(j, n) = \frac{P(j, n)}{\sum_{k=1}^{\frac{N}{2}} P(k, n)}. \quad (4.9)$$

The spectral entropy at the n th time step of the system is defined as

$$S(n) = \sum_{j=1}^{\frac{N}{2}} \mathfrak{P}(j, n) \ln \left(\frac{1}{\mathfrak{P}(j, n)} \right). \quad (4.10)$$

Given \mathfrak{P} at a certain time step, S assigns a weight, $\ln \left(\frac{1}{\mathfrak{P}} \right) \in [0, \infty]$, to \mathfrak{P} . If only a single Fourier mode is excited, i.e. $\exists j_0 : \mathfrak{P}(j_0, n_0) \neq 0, \mathfrak{P}(j, n_0) = 0 \forall j \neq j_0$, then $S(n_0) = 0$.

On the other hand, the maximum of $S(n_0)$, subject to the constraint $\sum_{j=1}^{\frac{N}{2}} \mathfrak{P}(j, n_0) = 1$, can be obtained using Lagrange multipliers and is achieved when $\mathfrak{P}(j, n_0) = \mathfrak{P}(k, n_0) \forall j, k$.

So, $\max S = \sum_{j=1}^{\frac{N}{2}} \frac{2}{N} \ln \left(\frac{N}{2} \right) = \ln \frac{N}{2}$. Indeed, spectral entropy is maximal when there is equipartition of energy among the modes. The functions P , \mathfrak{P} , and S were introduced in [12], and they are designed to provide an indicator of the extent of equipartition.

Since $t = nh$, we will express power and spectral entropy as functions of t by mapping $n \mapsto nh = t$.

4.2.2 Remarks on Error

For the KG KdV equation, the only exact solutions available are the tanh solutions derived in the Section 3.3. We are interested in propagating initial data in the form of a cosine wave, as was done in [22]. With this limitation in mind, we estimate the error in PS-RK4 corresponding to the analytic solutions found in Section 3.3. We choose $\delta = 1$ for these experiments and we vary N . We define maximum relative error as

$$E_{\max}(t) = \max_x \left| \frac{u_{\text{exact}}(x, t) - u_{\text{numerical}}(x, t)}{u_{\text{exact}}(x, t)} \right|. \quad (4.11)$$

Figures 4.4 and 4.5 show the error results for the KdV equation and KG KdV equation, respectively. Notice that $E_{\max}(t)$ decreases as N increases in both cases.

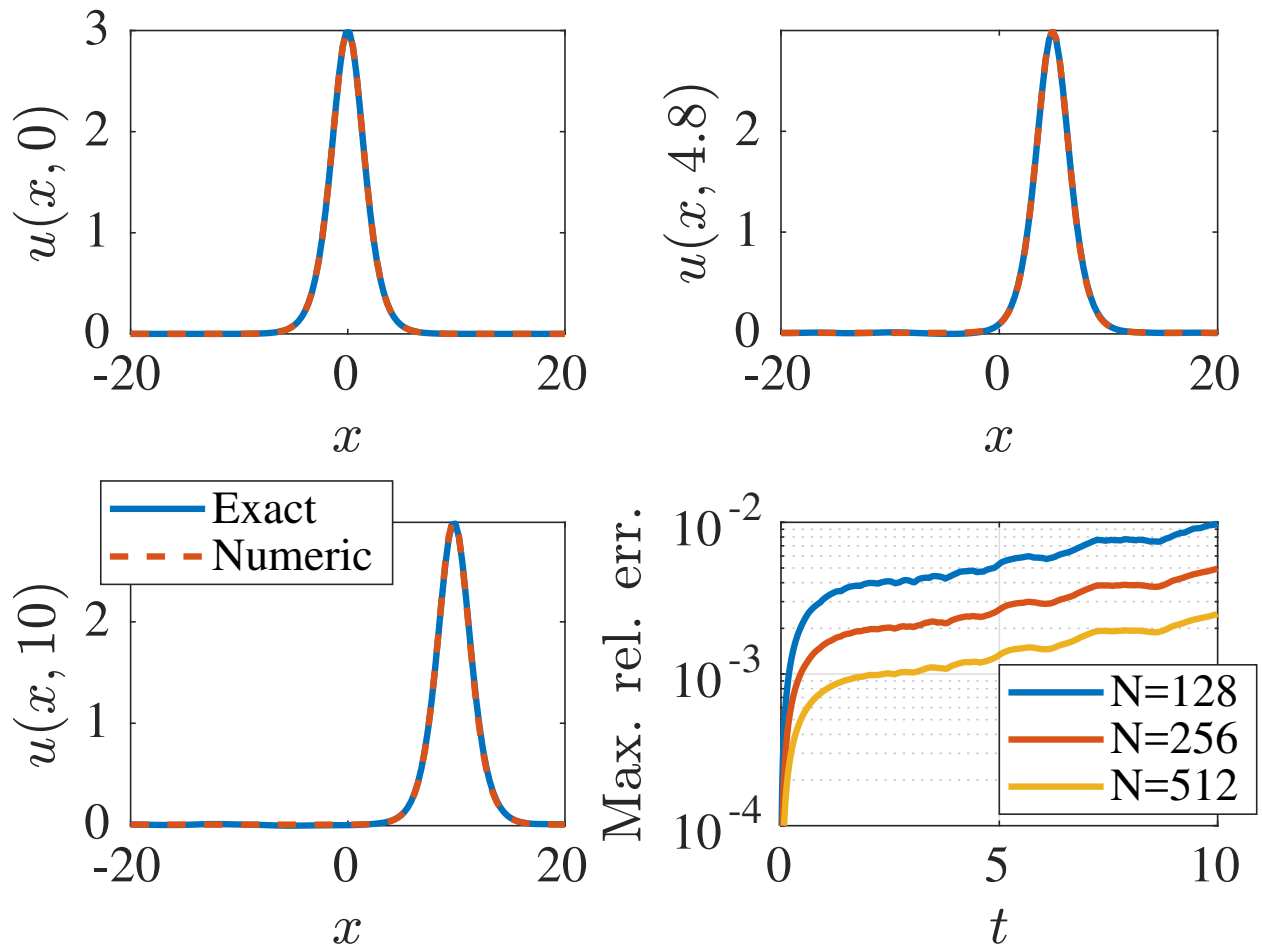


Figure 4.4. KdV equation, $\delta = 1$: Comparison of the exact traveling wave solution, (3.71), and the PS-RK4 solution obtained with $h = .1 \cdot N^{-2}$ and $N = 128$. The lower right graph plots $E_{\max}(t)$.

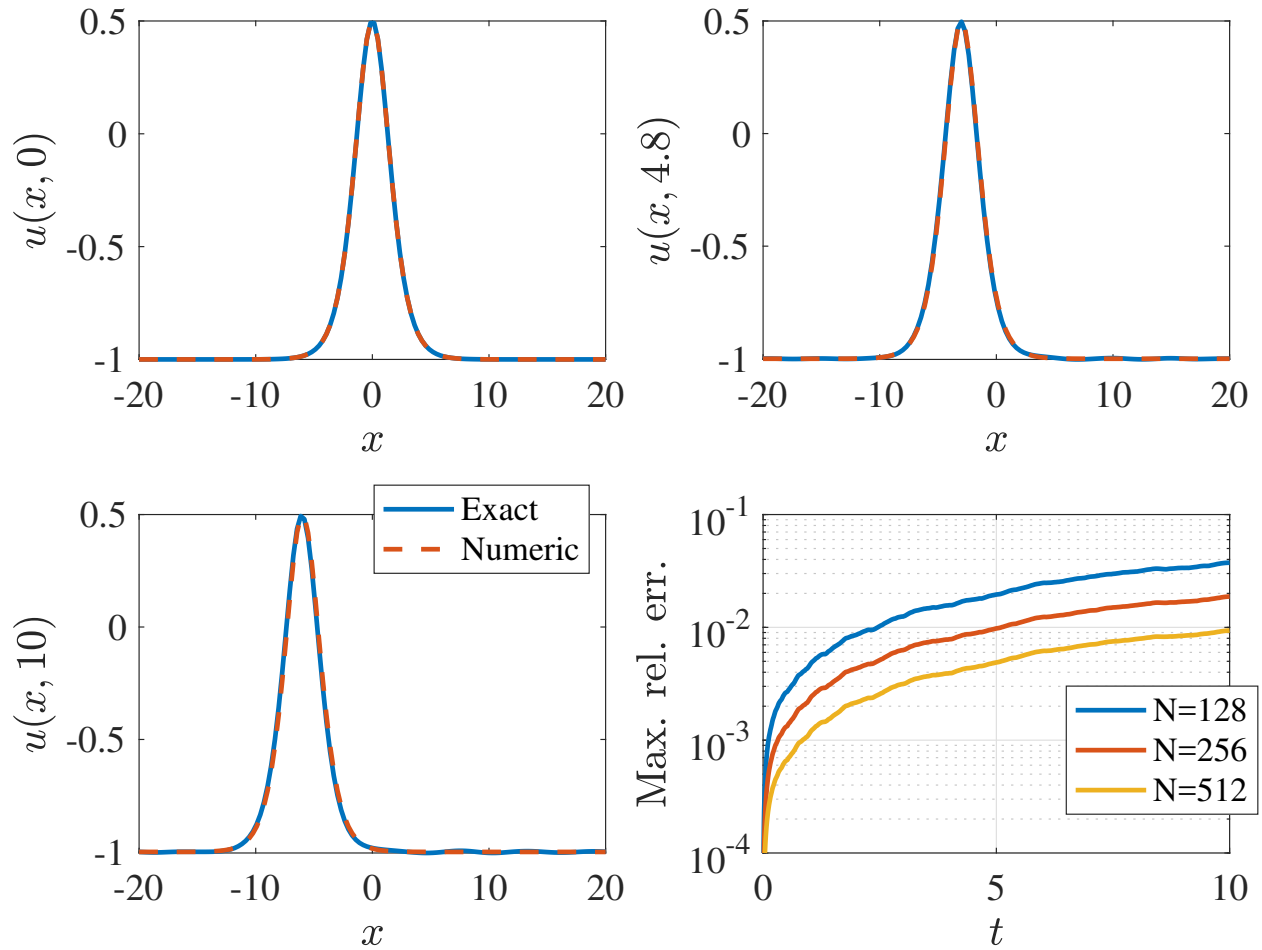


Figure 4.5. KG KdV equation, $\delta = 1$: Comparison of the exact traveling wave solution, (3.71), and the PS-RK4 solution obtained with $h = .1 \cdot N^{-2}$ and $N = 128$. The lower right graph plots $E_{\max}(t)$.

For the experiments with the KG KdV equation, we use small δ . In Figures 4.6 and 4.7, we show the error results for the KdV equation and KG KdV equation with $\delta = 0.022$. Notice that maximum relative error is no worse than $\mathcal{O}(10^{-4})$ at $t = 10$. However, we emphasize that the KdV and KG KdV equations are near Burgers' equation in the regime where δ is small. Solutions to Burgers' equation have large bounded variation in the case of cosine initial data, so the errors observed in Figures 4.4—4.7 are likely liberal estimates.

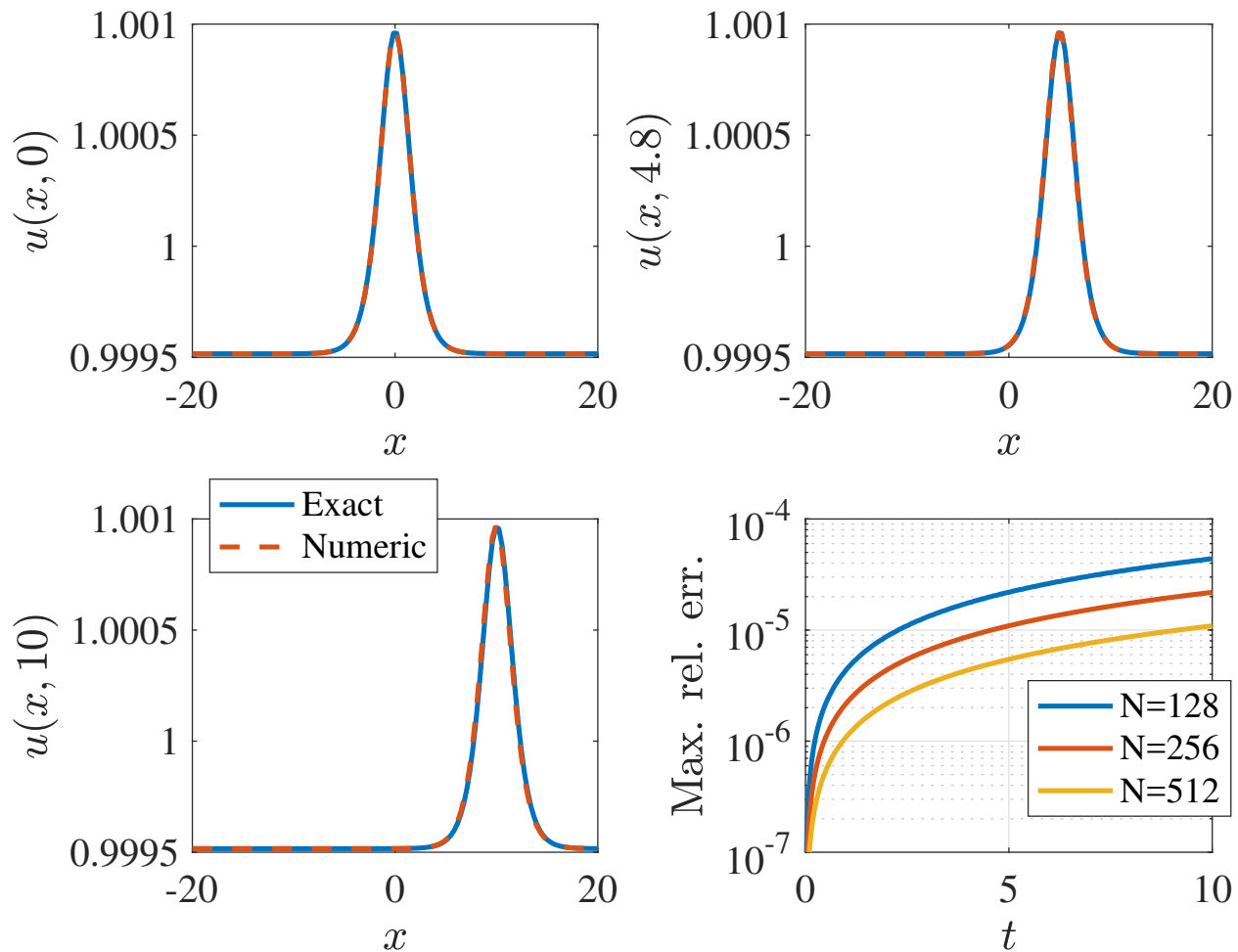


Figure 4.6. KdV equation, $\delta = 0.022$: Comparison of the exact traveling wave solution, (3.71), and the PS-RK4 solution obtained with $h = .1 \cdot N^{-2}$ and $N = 128$. The lower right graph plots $E_{\max}(t)$.

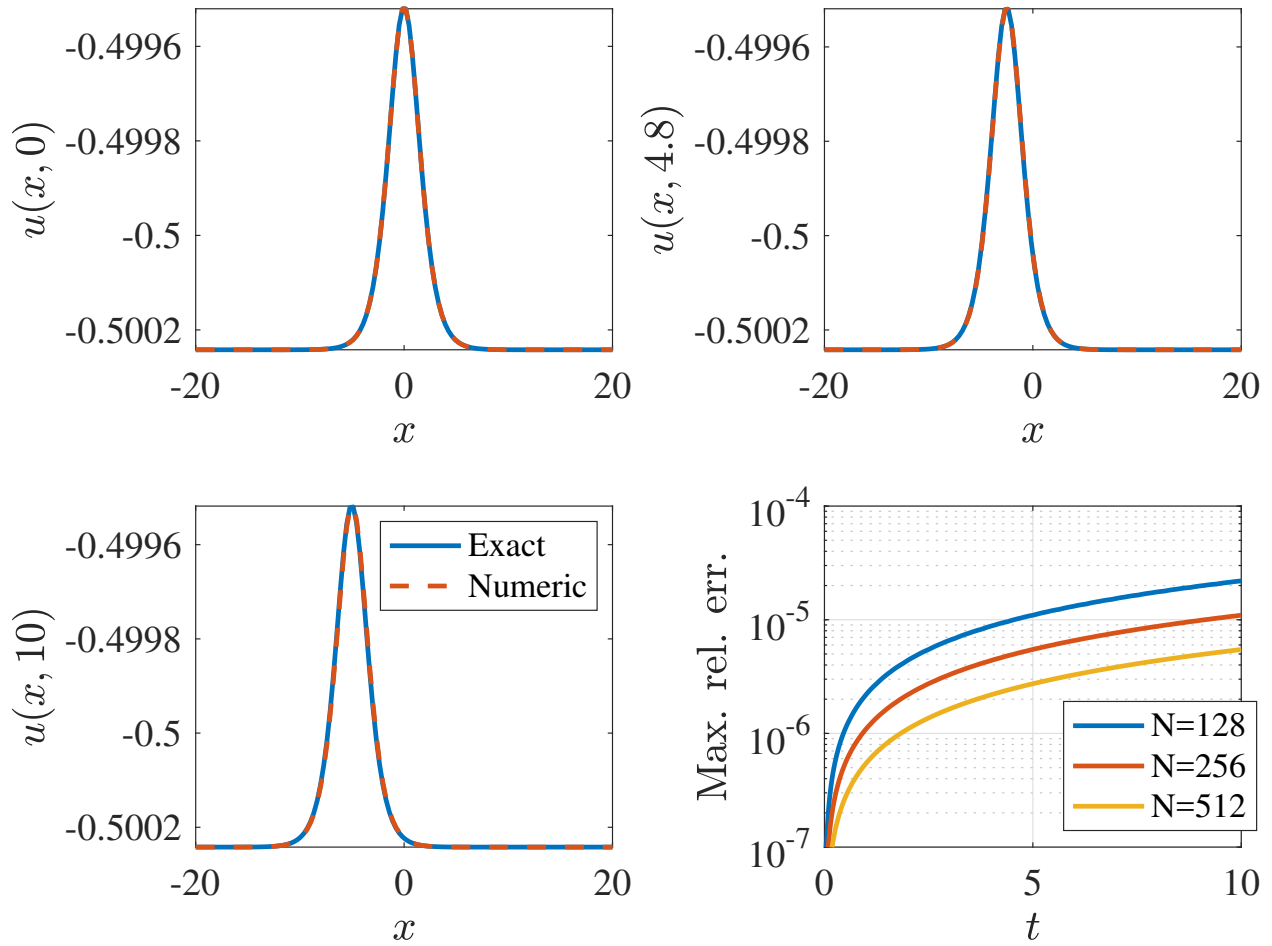


Figure 4.7. KG KdV equation, $\delta = 0.022$: Comparison of the exact traveling wave solution, (3.71), and the PS-RK4 solution obtained with $h = .1 \cdot N^{-2}$ and $N = 128$. The lower right graph plots $E_{\max}(t)$.

4.2.3 Results on Equipartition

For the remaining figures, the data used to initialize PS-RK4 is:

$$\left\{ \begin{array}{l} N = 128, \\ L = 2, \\ l = 0, \\ U_j^0 = \cos(\pi j \Delta x), \quad j = 1, \dots, N. \end{array} \right. \quad \begin{array}{l} (4.12) \\ (4.13) \\ (4.14) \\ (4.15) \end{array}$$

The intent of these experiments is to study the KdV equation, the KG KdV equation, and the individual contributions of the higher order terms. To illustrate these comparisons, we display four graphs per figure. In particular, the upper left graph of each figure corresponds to the KdV equation; the upper right graph, KG KdV-1; the lower left graph, KG KdV-2; and, the lower right graph, KG KdV equation. Moreover, the figure types are repeated four times, each time involving a different δ . For example, in Figure 4.8, $\delta = 0.018$; in Figure 4.9, $\delta = 0.021$; in Figure 4.10, $\delta = 0.022$; and, in Figure 4.11, $\delta = 0.023$.

In Figures 4.8—4.11, we provide a projection of solutions of PS-RK4. See Appendix A for alternative projections of the surfaces in Figures 4.8—4.11. Points, $u(x, t) \in \mathbb{R}$, are colored with a linear mapping of an RGB three-tuple, as in Figure 4.2. Also, note that the yellow lines in each figure are, roughly, the crests of the rightward-traveling waves – their amplitude dominates in the KdV case. The green lines in each figure are, roughly, the crests of the leftward-traveling waves. Complicated nonlinear interactions ensue when these traveling waves collide, as is particularly evident for KG KdV-1 in Figure 4.8, in which there are many high frequency oscillations. Also note that the path of the low frequency modes in this graph wander more than in the other graphs. For KdV, KG KdV-2 and KG KdV in Figure 4.8, the solutions share the same general features, varying primarily in the number of modes present. In fact, as δ is increased in Figures 4.9—4.11, notice that these general features remain intact for KdV, KG KdV-2 and KG KdV. The paths of the rightward traveling waves for KG KdV-1, on the other hand, vary

considerably. Finally, after reviewing Figures 4.8—4.11, it is suggested that the reader revisit KG KdV-1 in Figure 4.8 and make note of the sudden low frequency mode collapse that occurs in *space* near $x = .75$ and $3 < t < 4$. This is soon followed by significant deterioration of all but one low frequency mode, which seemingly jumps in space near $t = 8$.

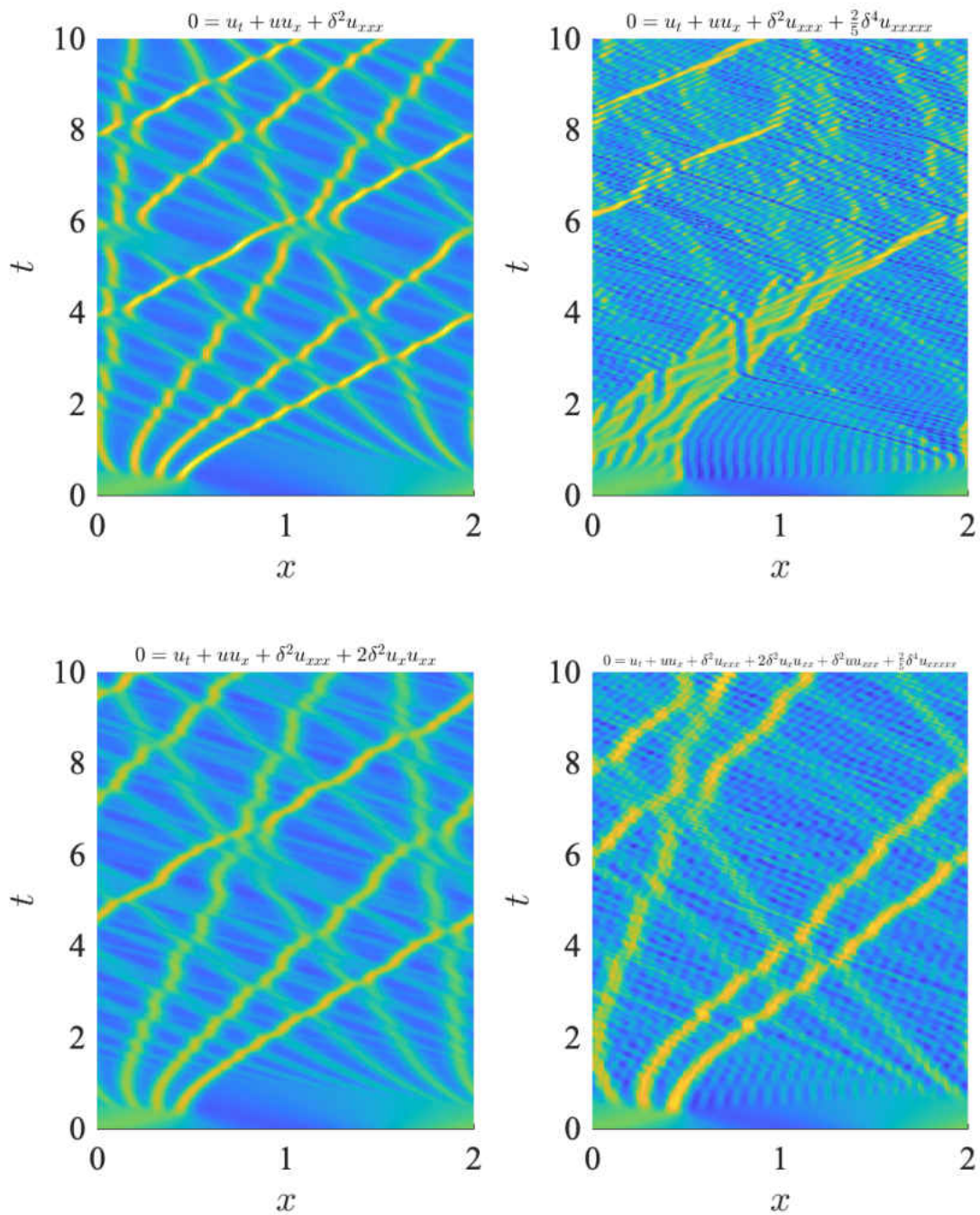


Figure 4.8. Projection of solutions of PS-RK4, with $N = 2^7$, $h = .1 \cdot N^{-2}$, $\delta = 0.018$, $u(x, 0) = \cos(\pi x)$.

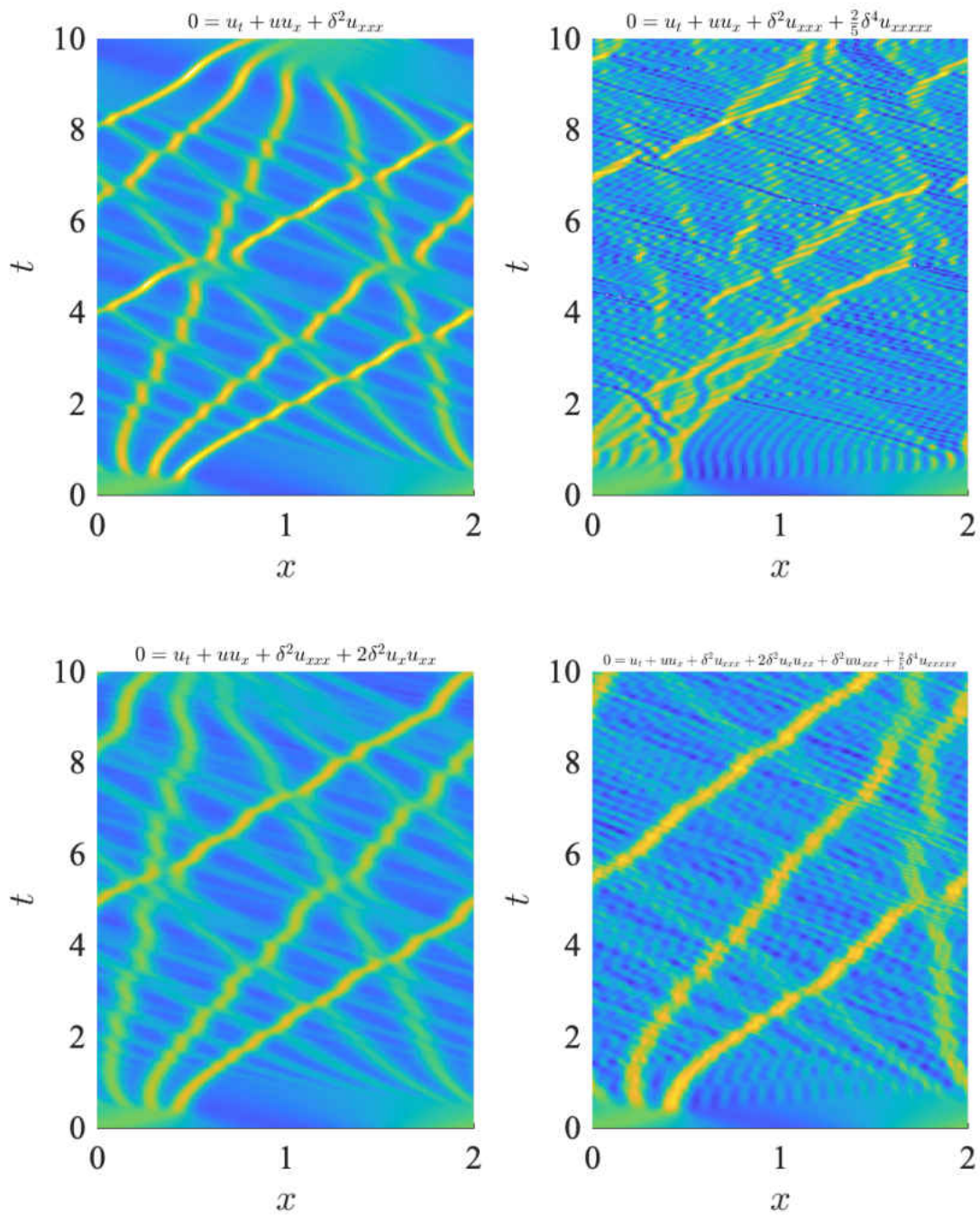


Figure 4.9. Projection of solutions of PS-RK4, with $N = 2^7$, $h = .1 \cdot N^{-2}$, $\delta = 0.021$, $u(x, 0) = \cos(\pi x)$.

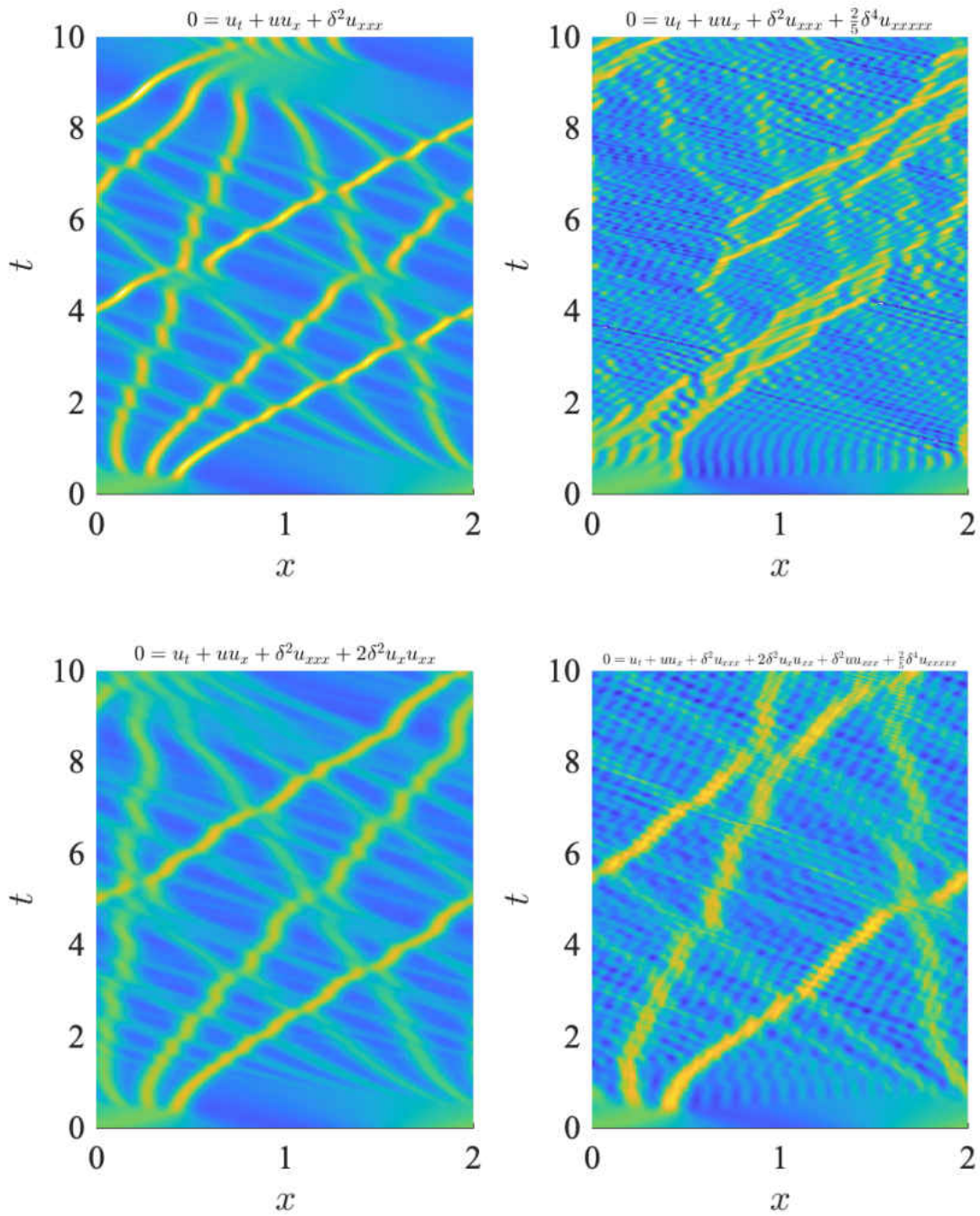


Figure 4.10. Projection of solutions of PS-RK4, with $N = 2^7$, $h = .1 \cdot N^{-2}$, $\delta = 0.022$, $u(x, 0) = \cos(\pi x)$.

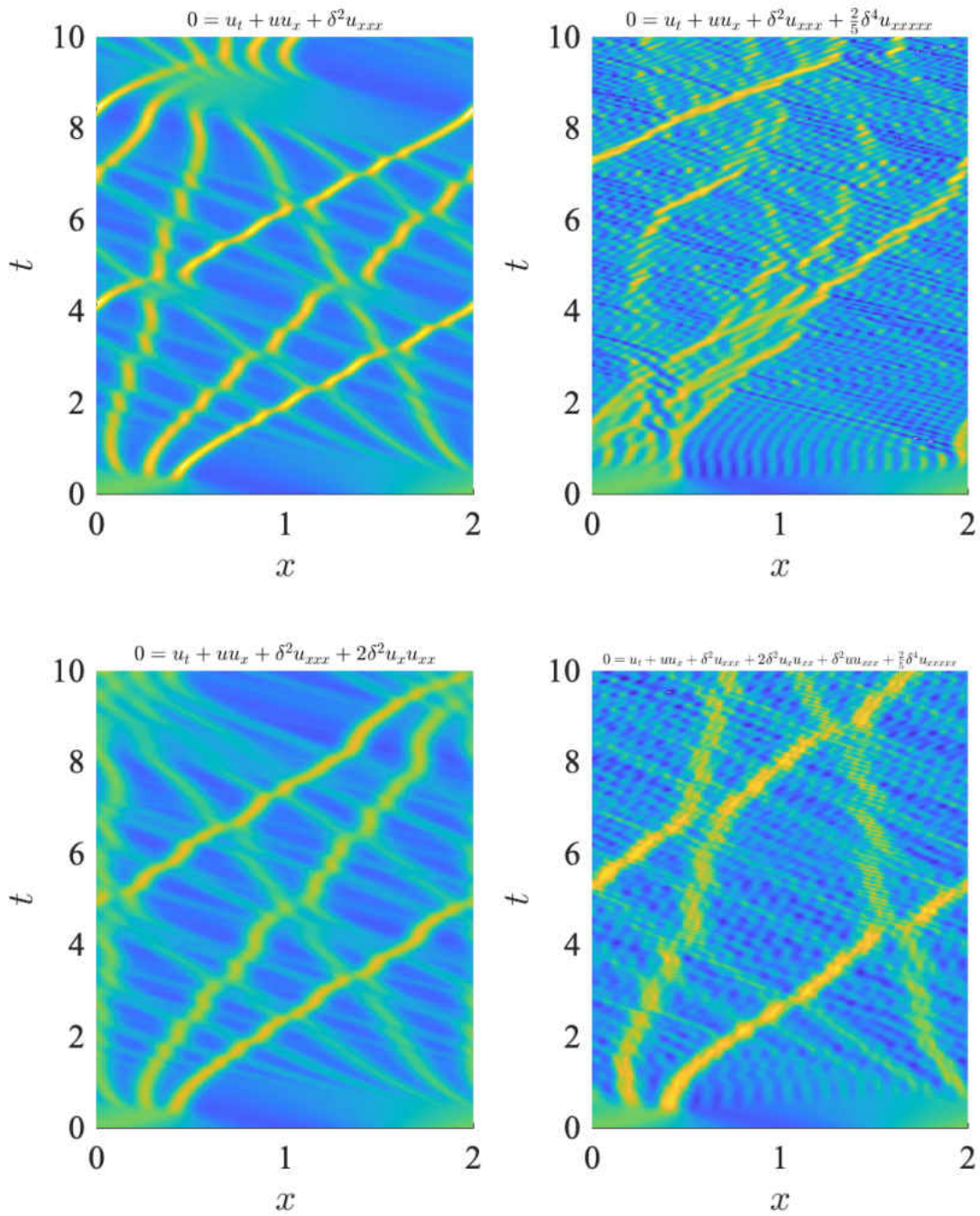


Figure 4.11. Projection of solutions of PS-RK4, with $N = 2^7$, $h = .1 \cdot N^{-2}$, $\delta = 0.023$, $u(x, 0) = \cos(\pi x)$.

In Figures 4.12—4.15, a plot of the power spectrum at $t = t_{\text{final}} = 10$ is provided for $\delta = 0.018, 0.021, 0.022$, and 0.023 , respectively. The configuration of the graphs relative to their equations is the same as in Figures 4.8—4.11. It is evident that equipartition is not achieved to $\mathcal{O}(10^{-4})$ at t_{final} . Notice that this quantity is less than error in the scheme per the experiments in Section 4.2.2.

Unfortunately, the distribution of energy in the power spectrum can change rapidly at times, rendering illustrations of the spectrum at $t_{\text{final}} = 10$ merely instructive. So, in Figures 4.16—4.19, a surface plot of the power spectrum is provided for $\delta = 0.018, 0.021, 0.022$, and 0.023 , respectively. Points, $P(j, t) \in \mathbb{R}$, are colored with a *logarithmic* mapping. The configuration of the graphs relative to their equations is the same as in Figures 4.8—4.11. For all graphs in Figures 4.16—4.19, observe that energy is quickly pumped out of the initial mode (mode two) and distributed to all modes by about $t = \frac{1}{10}$.

Notice, also, that the sharing of energy among the modes with the highest energy can be observed in KdV and KG KdV-2 for all δ . In fact, for KdV in Figure 4.19, notice that the high-energy modes propagate along several arcs in mode-time, starting at $t = \frac{1}{5}$ and ending at $t = 9$. As the energy exits this arc, it flows primarily into mode two – where the energy was initially placed. This is seemingly analogous to the observation of recurrence (say, at $t = 5$) and super-recurrence (say, at $t = 9$) in the FPU- α problem, as illustrated in Figure 2.7. Also notice that, for KG KdV-1 in Figures 4.16—4.19, energy largely plateaus for all t around mode 32. In Figure 4.16, the plateau is nearest mode 32 and the plateau recedes as δ is increased in the following three figures.

Also note that energy for KG KdV in Figures 4.16—4.19 is clearly distributed more so among the higher modes, compared to KG KdV-1. This suggests that KG KdV is closer to equipartition than KG KdV-1. As we shall see in the final set of figures and tables, this is not the case, by way of the spectral entropy function.

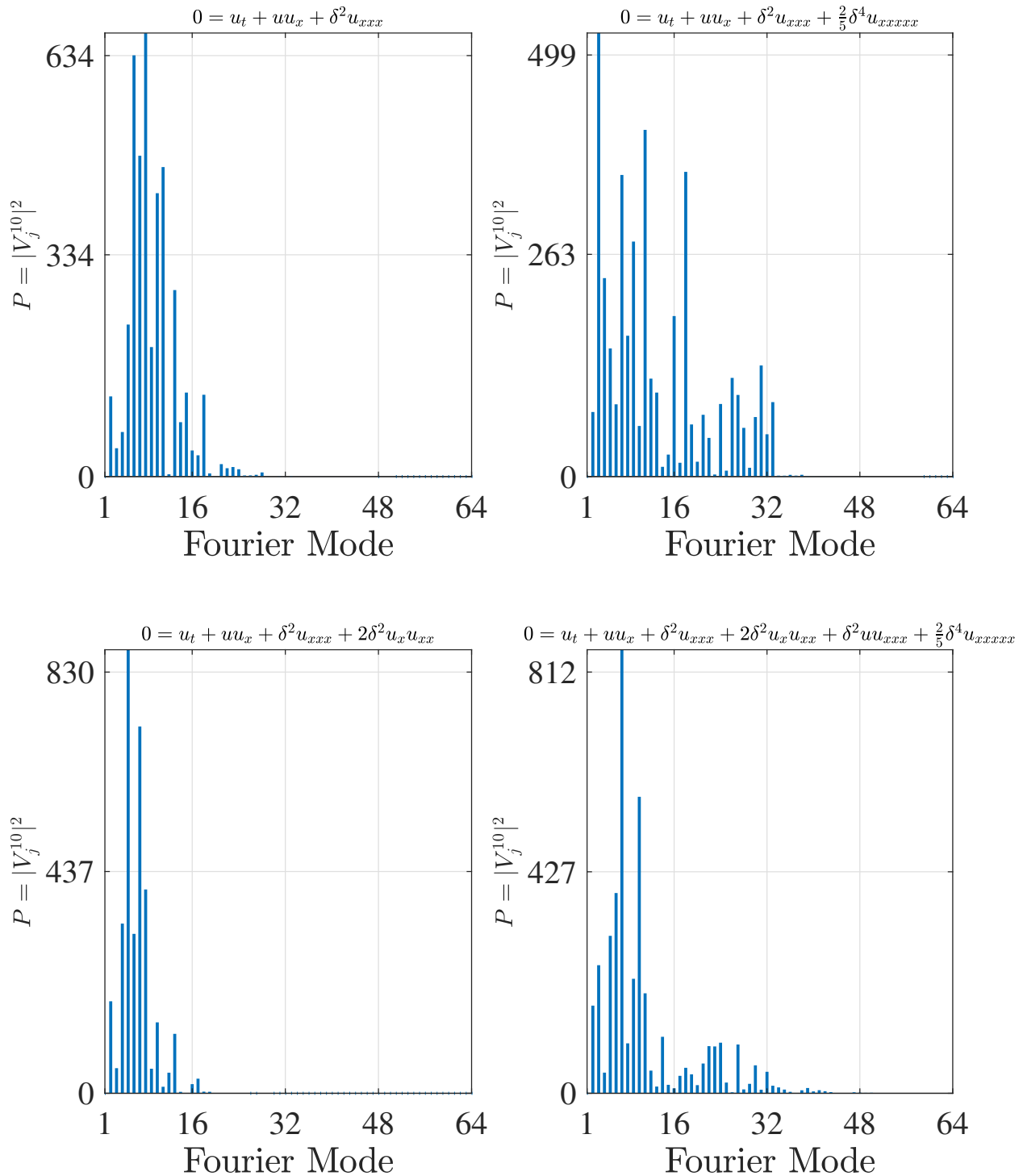


Figure 4.12. Plot of the power, $P(j, 10)$, of the solutions of PS-RK4, with $N = 2^7$, $h = .1 \cdot N^{-2}$, $u(x, 0) = \cos(\pi x)$, and $\delta = 0.018$.

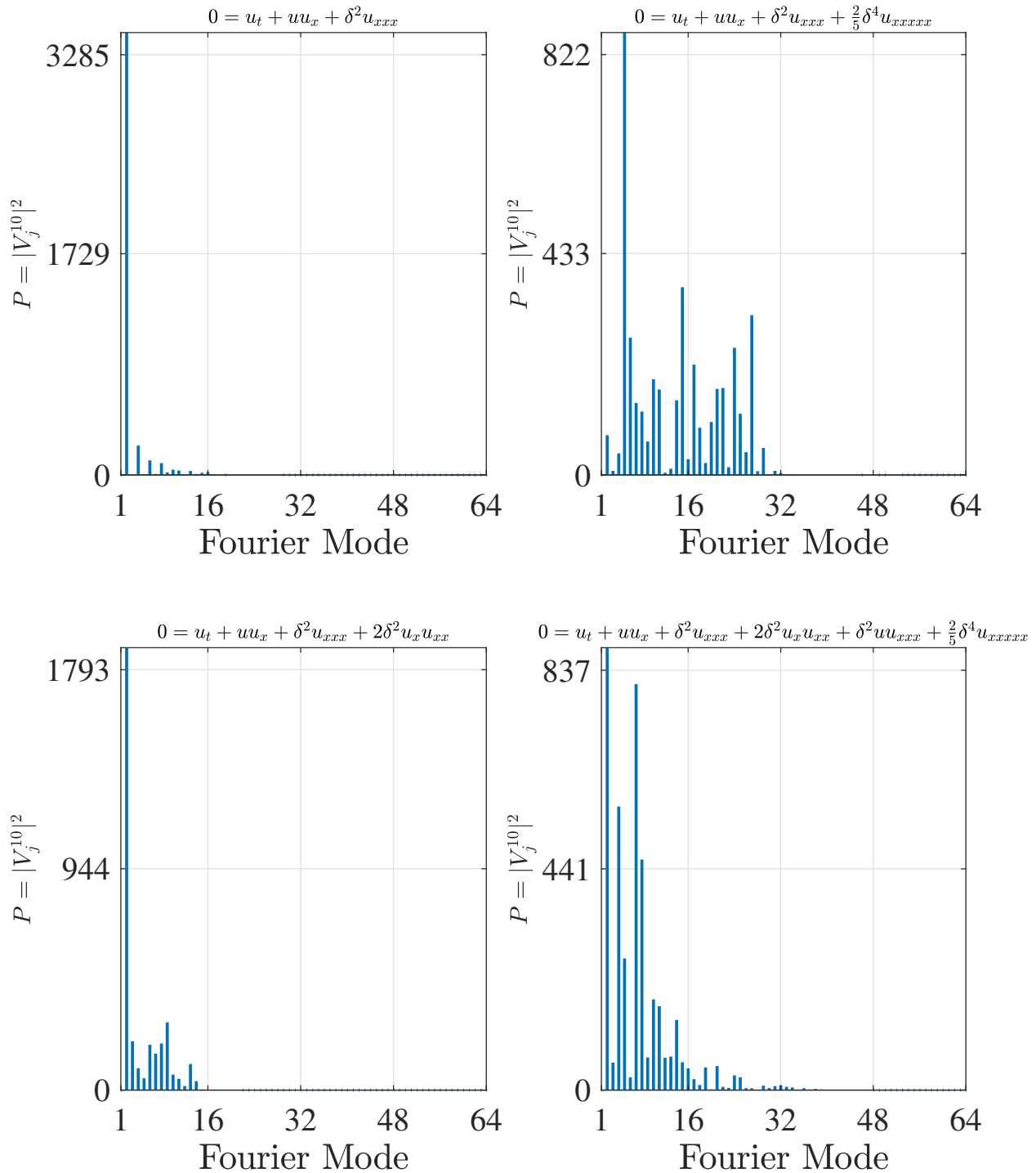


Figure 4.13. Plot of the power, $P(j, 10)$, of the solutions of PS-RK4, with $N = 2^7$, $h = .1 \cdot N^{-2}$, $u(x, 0) = \cos(\pi x)$, and $\delta = 0.021$.

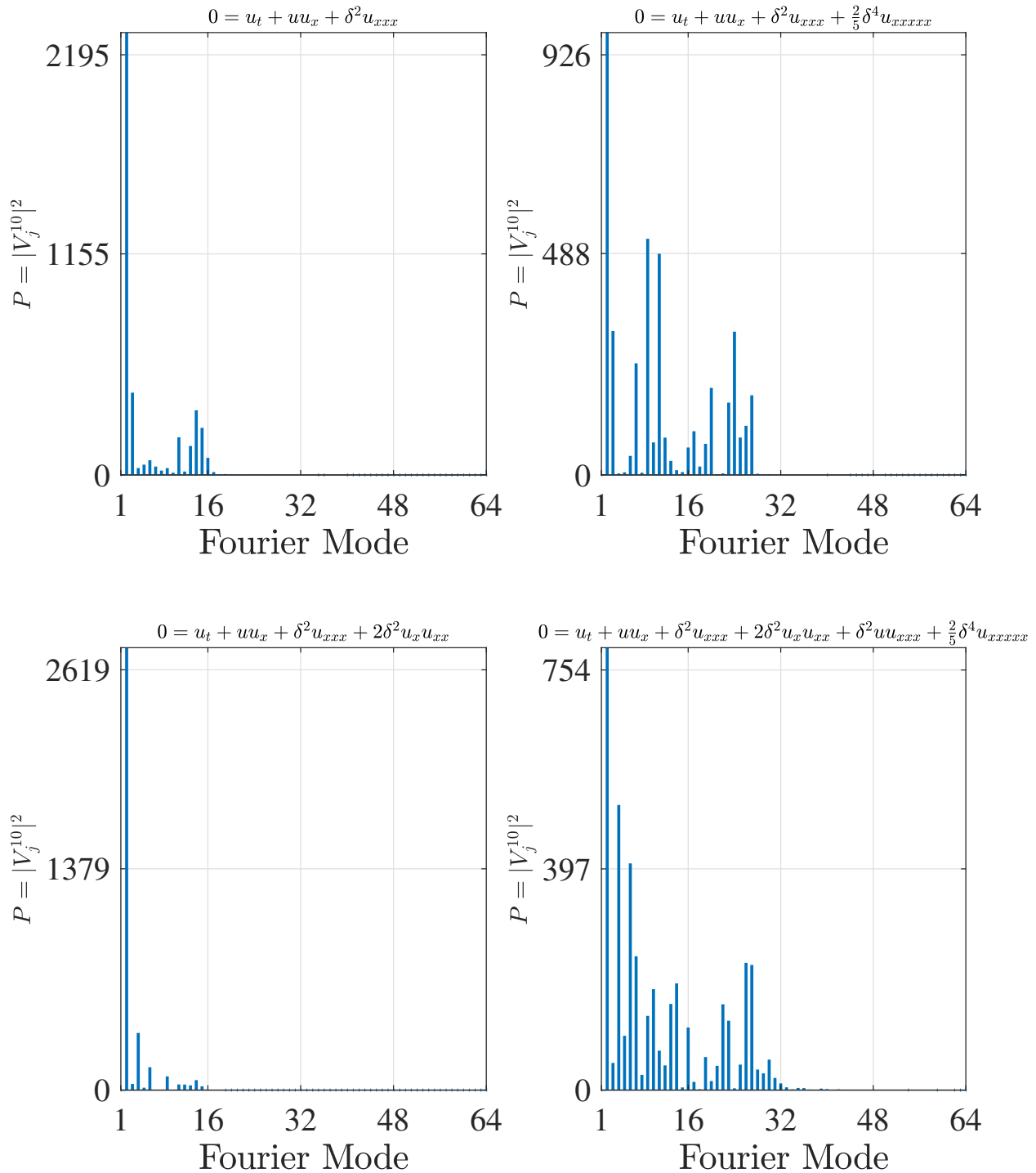


Figure 4.14. Plot of the power, $P(j, 10)$, of the solutions of PS-RK4, with $N = 2^7$, $h = .1 \cdot N^{-2}$, $u(x, 0) = \cos(\pi x)$, and $\delta = 0.022$.

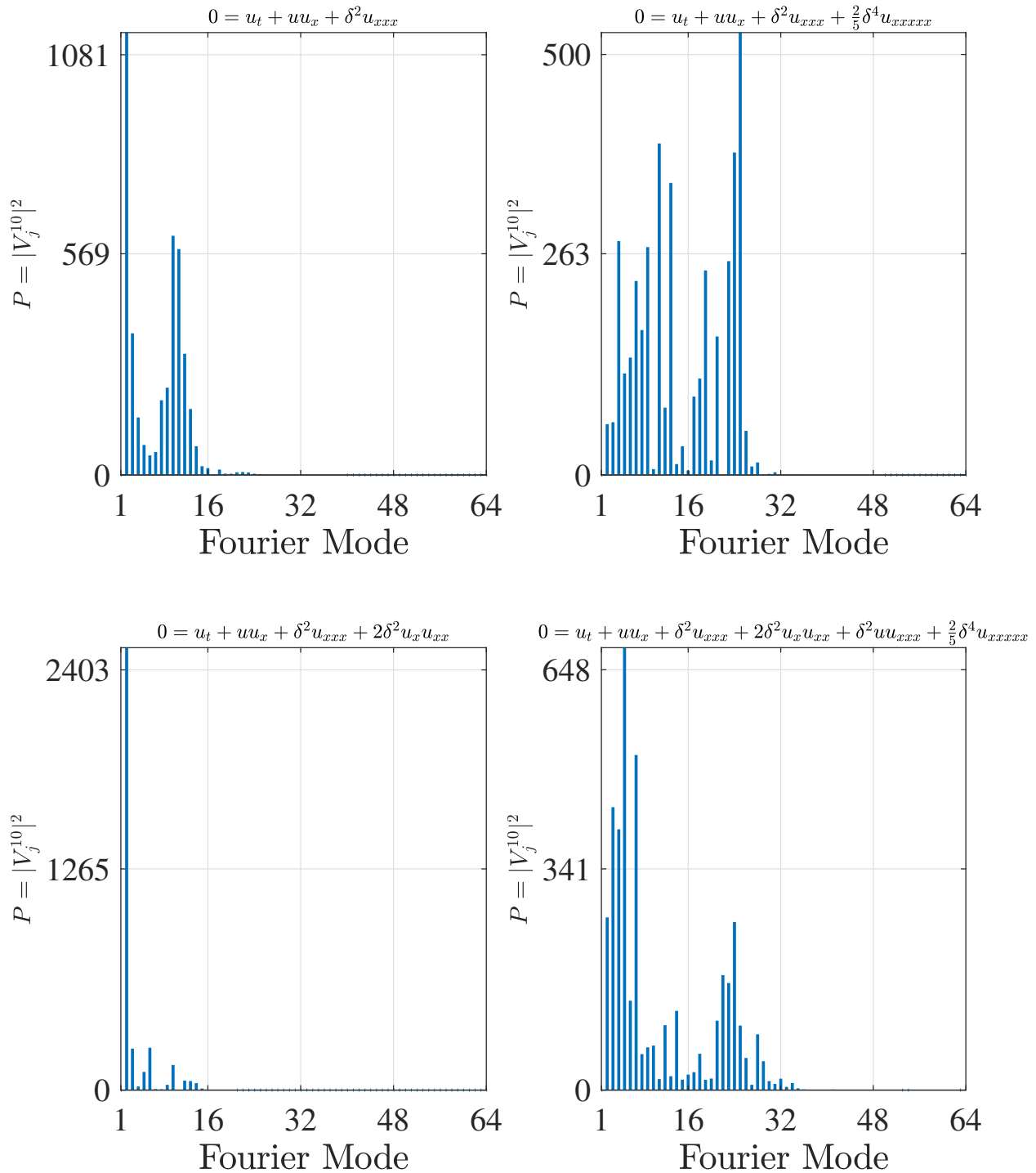


Figure 4.15. Plot of the power, $P(j, 10)$, of the solutions of PS-RK4, with $N = 2^7$, $h = .1 \cdot N^{-2}$, $u(x, 0) = \cos(\pi x)$, and $\delta = 0.023$.

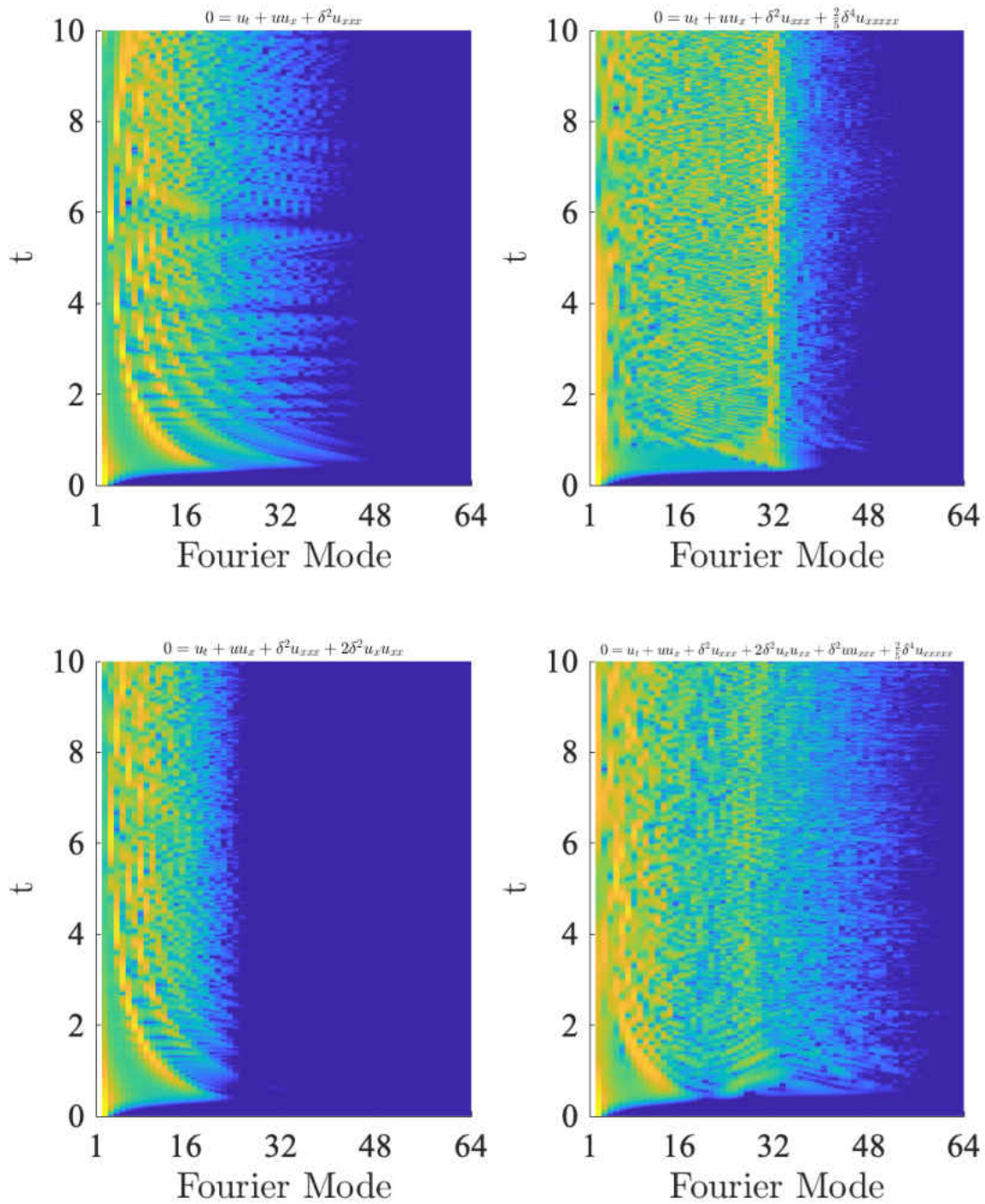


Figure 4.16. Projection of the power, $P(j, t)$, of the solutions of PS-RK4, with $N = 2^7$, $h = .1 \cdot N^{-2}$, $u(x, 0) = \cos(\pi x)$, and $\delta = 0.018$.

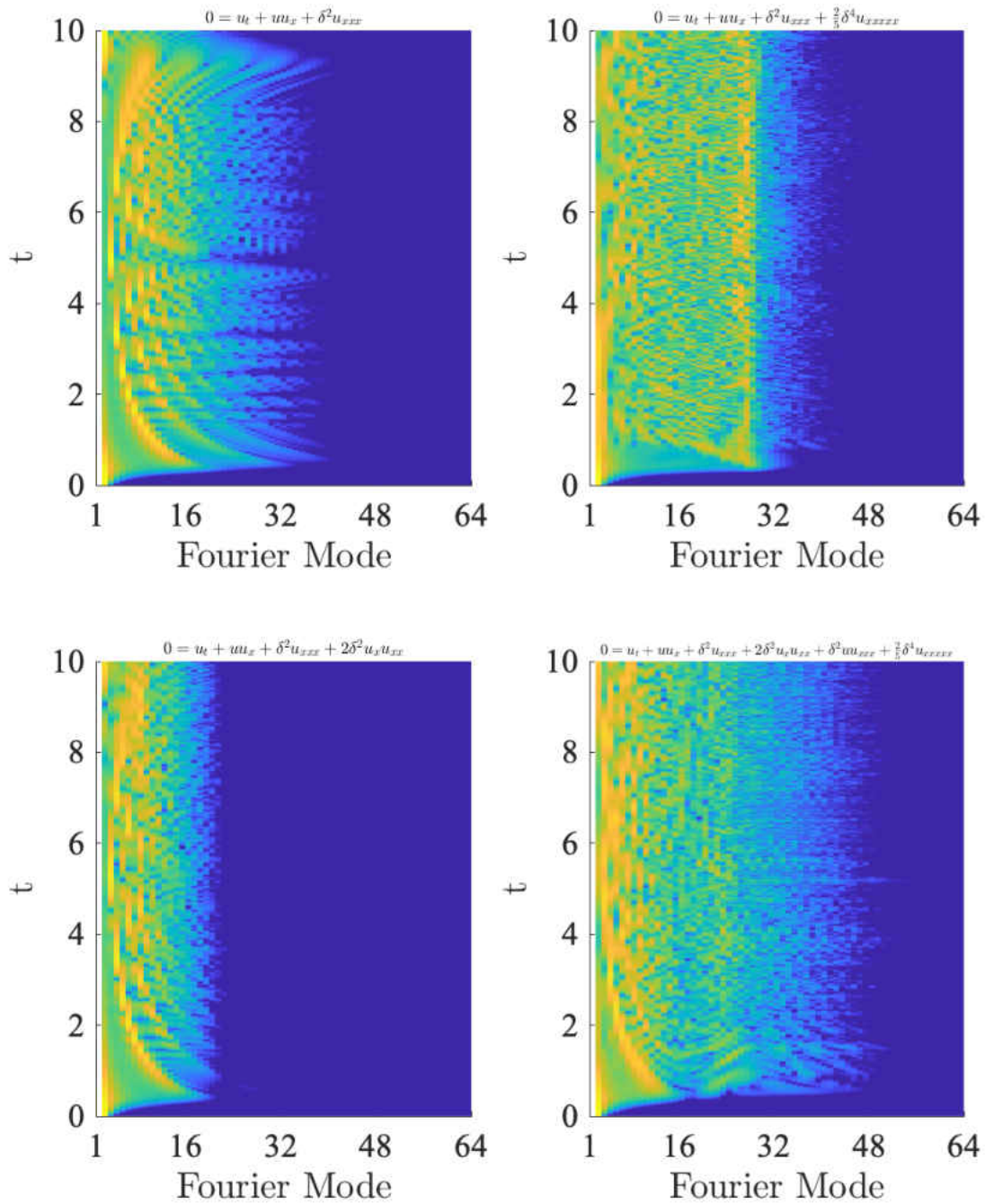


Figure 4.17. Projection of the power, $P(j, t)$, of the solutions of PS-RK4, with $N = 2^7$, $h = .1 \cdot N^{-2}$, $u(x, 0) = \cos(\pi x)$, and $\delta = 0.021$.

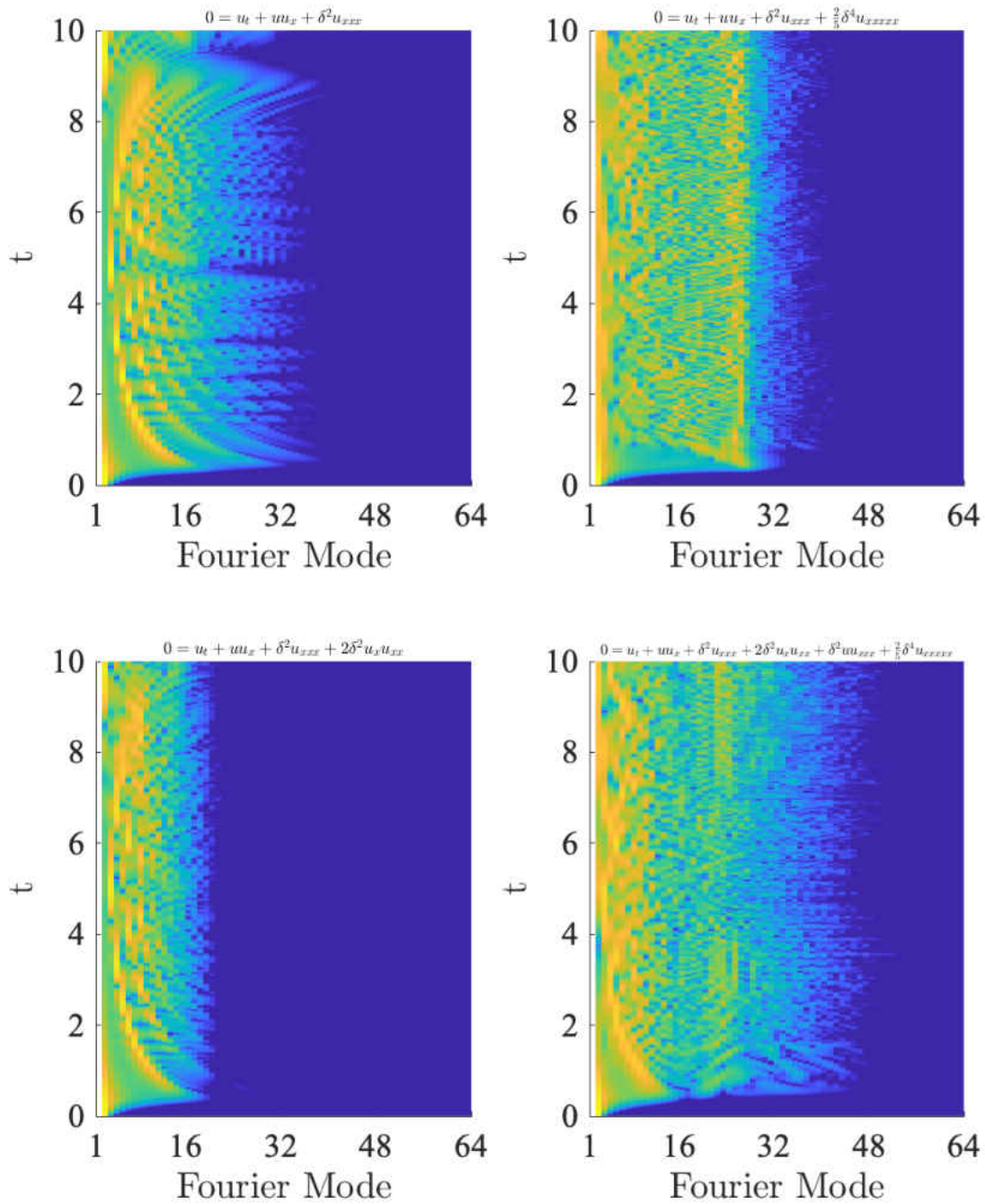


Figure 4.18. Projection of the power, $P(j, t)$, of the solutions of PS-RK4, with $N = 2^7$, $h = .1 \cdot N^{-2}$, $u(x, 0) = \cos(\pi x)$, and $\delta = 0.022$.

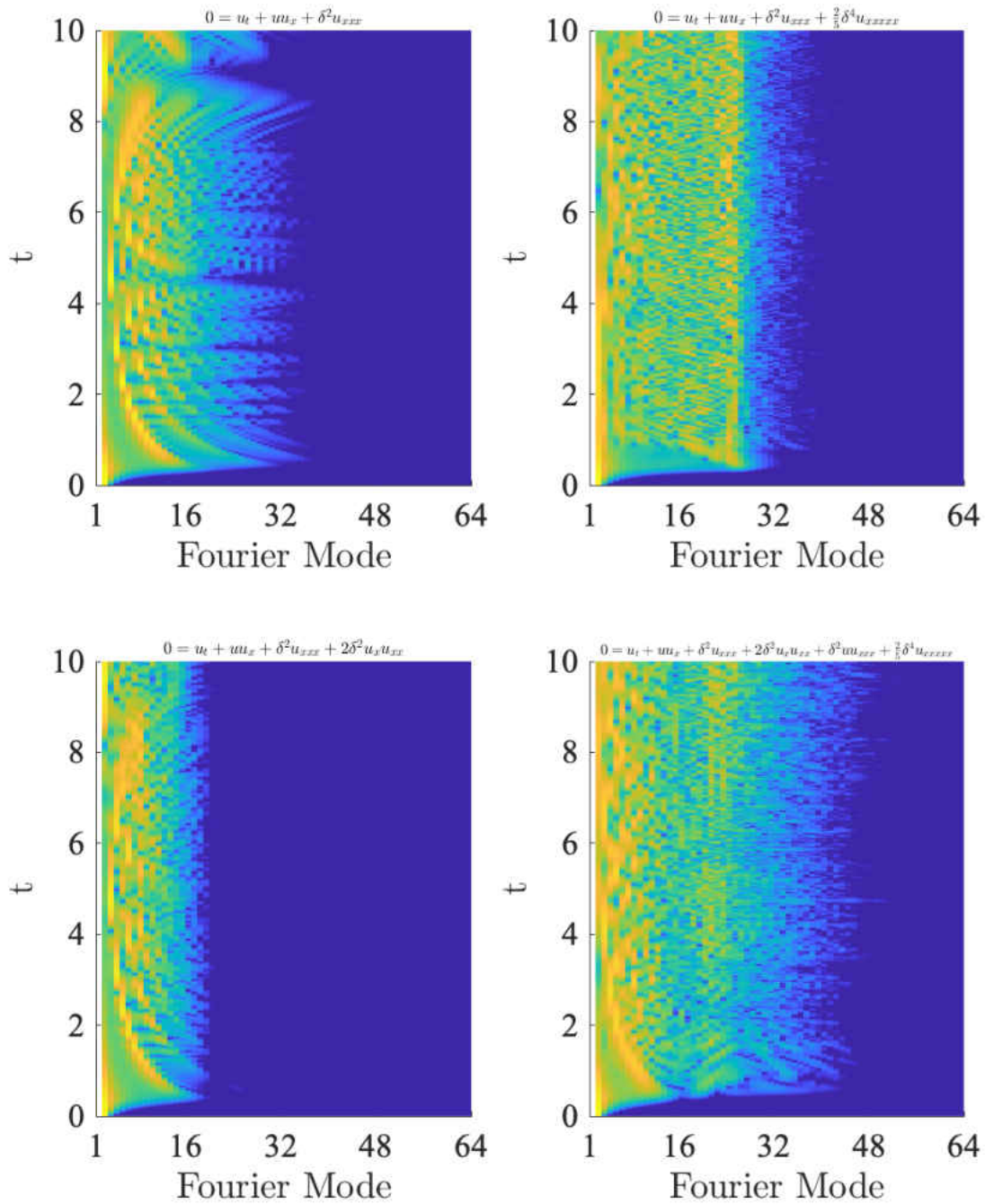


Figure 4.19. Projection of the power, $P(j, t)$, of the solutions of PS-RK4, with $N = 2^7$, $h = .1 \cdot N^{-2}$, $u(x, 0) = \cos(\pi x)$, and $\delta = 0.023$.

In Figure 4.20, we plot the spectral entropy of the systems. The configuration of the graphs relative to their equations is the same as in Figures 4.8—4.11. Note that the maximum of the ordinate axis is set to be $\ln\left(\frac{N}{2}\right) \approx 4.16$. Recall that equipartition is achieved when $S(n)$ reaches this value.

Immediately, we find that none of the dynamical systems considered reach equipartition on the time scale $t \leq 10$. However, there is an approach toward equipartition in some cases. In particular, notice that KdV and KG KdV-2 in Figure 4.20 tend to, on a certain time-average, trend downwards after around $t = 1$ for all δ . This downward trend is less pronounced as δ decreases. On the other hand, KG KdV-2 and KG KdV tend to, on a certain time-average, trend upwards. This upward trend is more pronounced as δ decreases.

Notice that, for KdV and KG KdV-2 in Figure 4.20, $S(n)$ decreases to between a quarter and a third of its maximum value several times. This is indicative of the pumping of energy back into the initial modes, illustrated by the striations in KdV and KG KdV-2 in Figures 4.16—4.19. This phenomenon is absent for the KG KdV-1 and KG KdV equations. Instead, for KG KdV-1, sudden increases in spectral entropy are observed, and they are not followed by decreases of similar magnitude, e.g. at $t = 4.5$ and $\delta = 0.023$. This also occurs for KG KdV at $t = 3$ and $\delta = 0.021$.

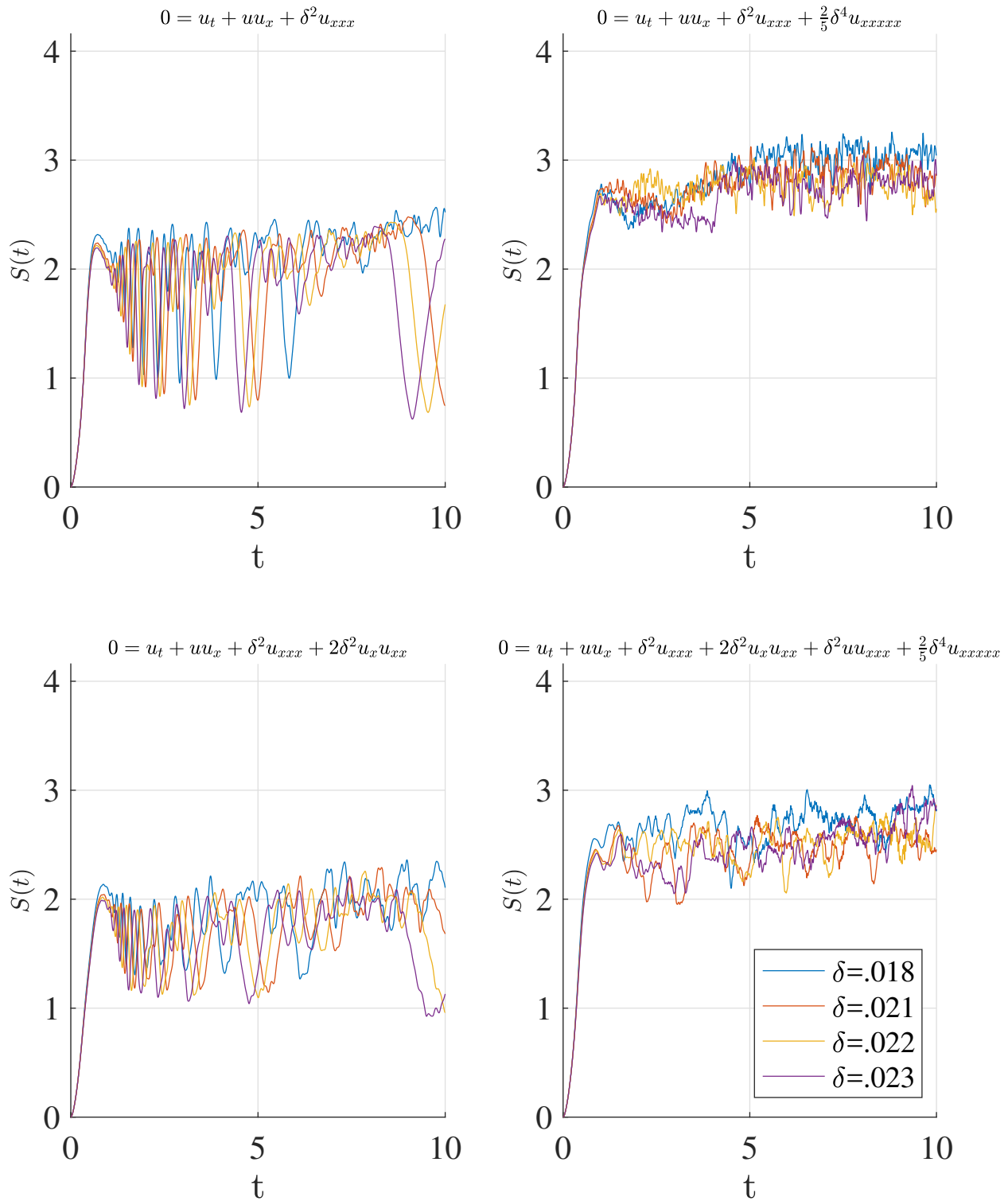


Figure 4.20. Plot of the spectral entropy, $S(t)$, of the solutions of PS-RK4, with $N = 2^7$, $h = .1 \cdot N^{-2}$, $u(x, 0) = \cos(\pi x)$.

In place of a more rigorous diagnostic for time-average spectral entropy, we have provided a means of comparing the total entropy as a proportion of maximum entropy in the IVPs by numerically integrating $S(n)$ on $t : 0 \leq t \leq 10$. In particular, define the total normalized entropy as

$$\tilde{S}_{\text{normal}} = \frac{1}{t_{\text{max}} \ln\left(\frac{N}{2}\right)} \int_0^{t_{\text{max}}} S(t) dt. \quad (4.16)$$

Notice that $\tilde{S}_{\text{normal}} \approx 1$ implies equipartition has been achieved on a given time scale. The results of this computation are provided in Table 4.1. We find that the total normalized entropy in KG KdV-1 is largest overall, followed by KG KdV, KdV, and then KG KdV-2. On the whole, this is consistent with the data in Figures 4.8—4.20.

Table 4.1. The quantity $\tilde{S}_{\text{normal}}$ for the solutions of PS-RK4, with $N = 2^7$, $h = .1 \cdot N^{-2}$, $u(x, 0) = \cos(\pi x)$.

δ	KdV	KG KdV Var. 1	KG KdV Var. 2	KG KdV
0.018	0.492	0.661	0.438	0.619
0.021	0.460	0.646	0.416	0.566
0.022	0.441	0.633	0.403	0.577
0.023	0.434	0.618	0.387	0.572

With these data in mind, we consider a final experiment. PS-RK4 is initialized with $N = 2048$, $L = 2$, $l = 0$, $U_j^0 = \cos(\pi j \Delta x)$ and $\delta = 0.001$. We run the experiment only for the KG KdV-1 equation. Notice that δ is much smaller than previously considered. The results are presented in Figure 4.21. The scheme became unbounded shortly after $t = 6.598$. However, the solution differs from previous cases in subtle, yet significant, ways. In particular, observe the appearance of a group of traveling waves near $x = 1.75$ and $t = 1$. These waves appear to have leftward and rightward-traveling counterparts, the likes of which did not exist in any previous case. Moreover, virtually none of the observed traveling waves remain intact and, near t_{final} , the waves wander significantly. In the power spectrum, notice that between one-half and two-thirds of the modes are excited by t_{final} . The proportion of excited modes for KG KdV-1 with larger δ is notably

smaller, in contrast. Finally, the spectral entropy indicates that, while equipartition is not achieved, there is an obvious second phase of rapid increase in spectral entropy starting around $t = 2$. Interestingly, this second phase in growth appears to, thereafter, grow logarithmically.

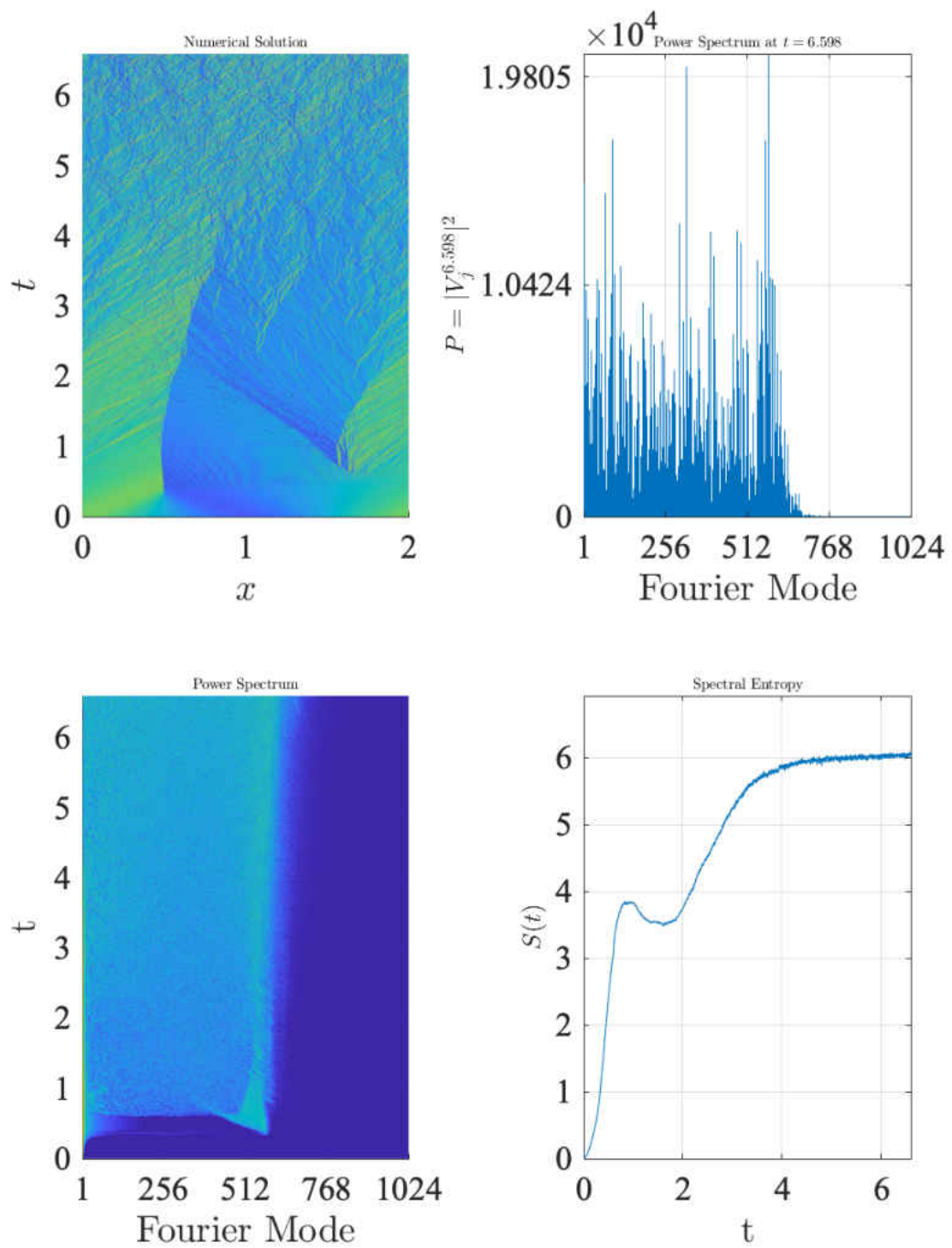


Figure 4.21. KG KdV-1 equation: Plots of the solution, power spectrum, and spectral entropy with $N = 2^{11}$, $h = N^{-2}$, $\delta = 0.001$, $u(x, 0) = \cos(\pi x)$, using PS-RK4.

CHAPTER 5: CONCLUSION

The results obtained in Chapter 2 verify the previous findings. The numerical experiments, by and large, indicate that small perturbations to the linear system corresponding to the FPU problem do not necessarily result in equipartition. Instead, recurrence phenomenon is observed even on very long time scales. In certain special cases, when the initial data and the restoring force are symmetric, recurrence is essentially perfect.

The results obtained in Chapter 3 were undertaken to provide a straightforward derivation of the KdV equation, the KG KdV equations, and some of their traveling wave solutions. It also made clear the manner in which an expansion of arbitrary order for the FPU- α problem could be transformed into a KG KdV equation of arbitrary order, as provided in Appendix B. Unsurprisingly, higher order approximations of the FPU lattice become increasingly stiff. While this presents considerable difficulty for numerical experimentation, analytical investigation of its qualitative features may be of interest.

In Chapter 4, equipartition is not observed on the time scale considered. However, the numerical experiments suggest that spectral entropy, and thus approach toward equipartition of energy, increases as $\delta \rightarrow 0$ in the case of the KG KdV equation and KG KdV-1. For KG KdV-1, this is particularly substantiated by the final experiment, where $\delta = 0.001$. Moreover, KG KdV-1 was found to have higher total normalized spectral entropy than the KG KdV equation.

APPENDIX A: ALTERNATIVE PROJECTIONS OF DISPLACEMENT

The following figures provide alternative projections of the surfaces in Figures 4.8—4.11. The choice of δ proceeds in the same sequence as in Figures 4.8—4.11. The configuration of the graphs relative to their equations is the same as in Figures 4.8—4.11.

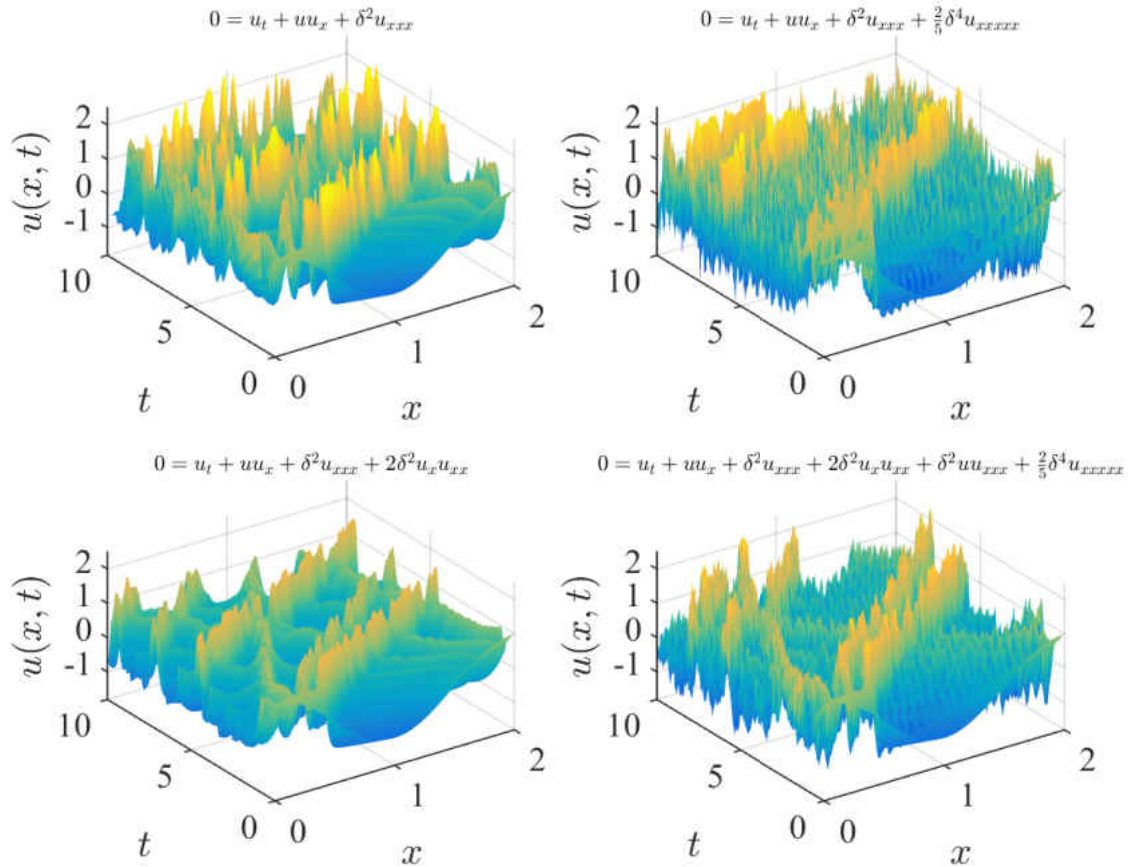


Figure A.1. Projection of solutions of PS-RK4, with $N = 2^7$, $h = .1 \cdot N^{-2}$, $\delta = 0.018$, $u(x, 0) = \cos(\pi x)$. Points, $u(x, t) \in \mathbb{R}$, are colored with a linear mapping.

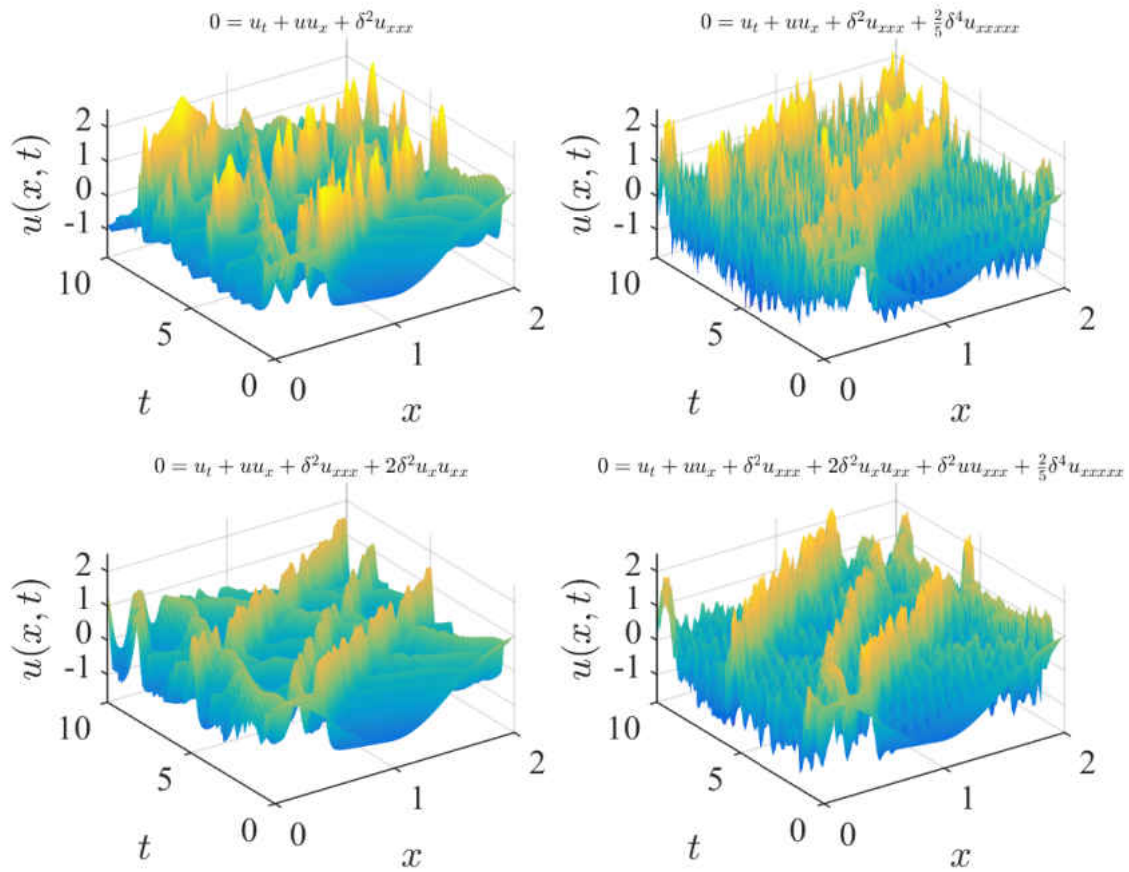


Figure A.2. Projection of solutions of PS-RK4, with $N = 2^7$, $h = .1 \cdot N^{-2}$, $\delta = 0.021$, $u(x, 0) = \cos(\pi x)$. Points, $u(x, t) \in \mathbb{R}$, are colored with a linear mapping.

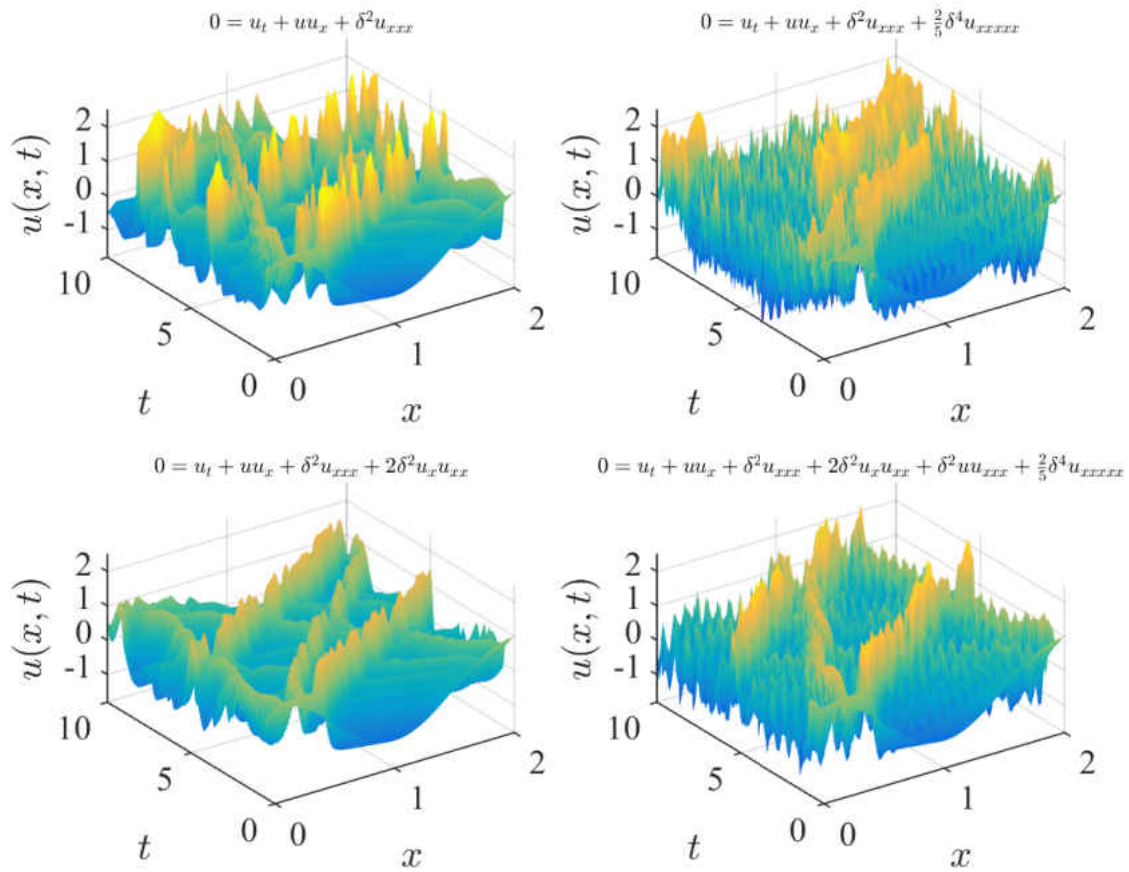


Figure A.3. Projection of solutions of PS-RK4, with $N = 2^7$, $h = .1 \cdot N^{-2}$, $\delta = 0.022$, $u(x, 0) = \cos(\pi x)$. Points, $u(x, t) \in \mathbb{R}$, are colored with a linear mapping.

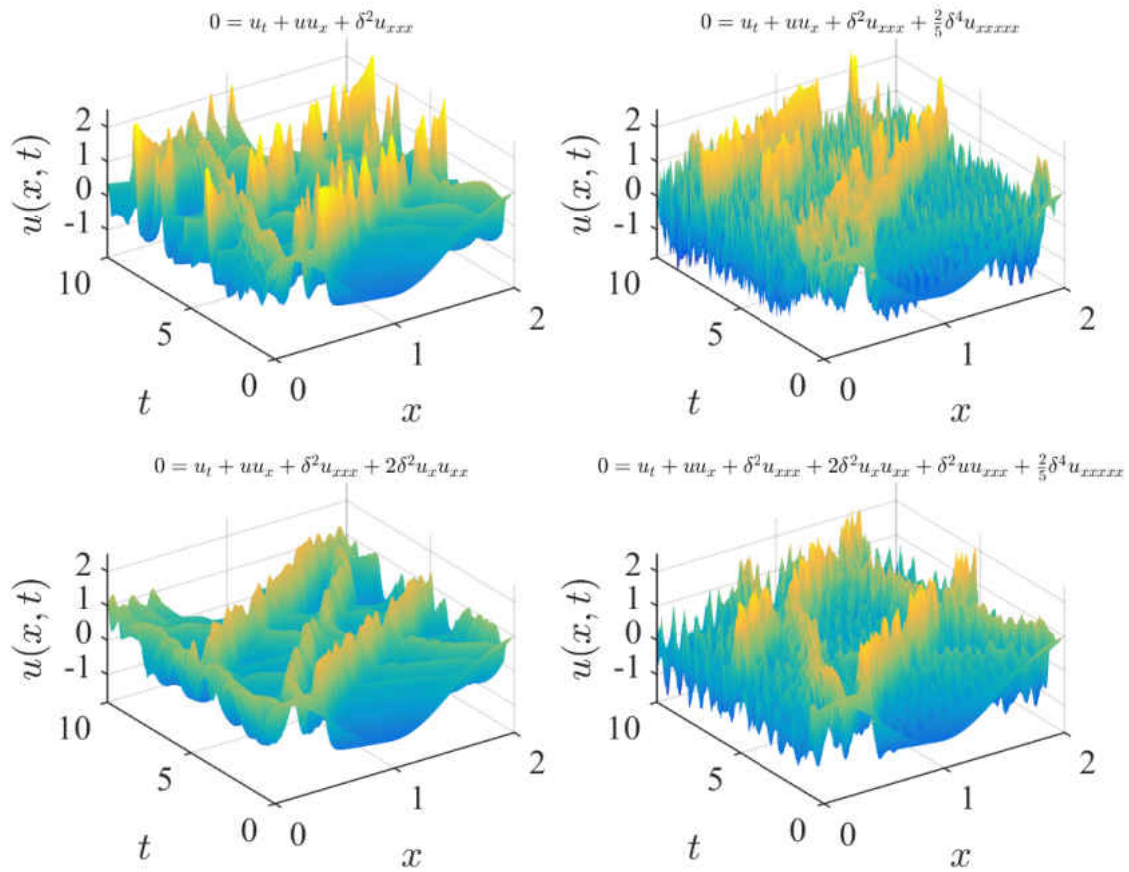


Figure A.4. Projection of solutions of PS-RK4, with $N = 2^7$, $h = .1 \cdot N^{-2}$, $\delta = 0.023$, $u(x, 0) = \cos(\pi x)$. Points, $u(x, t) \in \mathbb{R}$, are colored with a linear mapping.

APPENDIX B: MTH ORDER KUDRYASHOV GENERALIZED KDV EQUATION

Recall the FPU- α case ($\kappa = 1, \beta = 0$) so that Equation (3.1) becomes

$$m\partial_{TT}y = \gamma((y_{i+1} - y_i) + (y_{i-1} - y_i)) + \alpha((y_{i+1} - y_i)^2 - (y_{i-1} - y_i)^2), \quad (\text{B.1})$$

$$= \gamma((y_{i+1} - y_i) + (y_{i-1} - y_i)) + \alpha(y_{i+1}^2 - 2y_i y_{i+1} - y_{i-1}^2 + 2y_i y_{i-1}), \quad (\text{B.2})$$

$$= \gamma((y_{i+1} - y_i) + (y_{i-1} - y_i)) + \alpha((y_{i+1} - y_{i-1})(y_{i+1} + y_{i-1}) - 2y_i(y_{i+1} - y_{i-1})), \quad (\text{B.3})$$

$$= \gamma((y_{i+1} - y_i) + (y_{i-1} - y_i)) + \alpha(y_{i+1} - y_{i-1})(y_{i+1} - y_{i-1} - 2y_i), \quad (\text{B.4})$$

$$= \gamma((y_{i+1} - y_i) + (y_{i-1} - y_i)) + \alpha((y_{i+1} - y_i) + (y_{i-1} - y_i))(y_{i+1} - y_{i-1}). \quad (\text{B.5})$$

Also recall from Section 3.2 the M th order Taylor expansion of $y_{i\pm 1}$ using the continuum interpolant, wherein

$$y_{i\pm 1} - y_i = \sum_{j=1}^M \frac{(\pm h)^j}{j!} \frac{\partial^j}{\partial X^j} y + \mathcal{O}(h^{M+1}). \quad (\text{B.6})$$

Therefore,

$$((y_{i+1} - y_i) + (y_{i-1} - y_i)) = \sum_{j=1}^M \frac{h^j}{j!} \partial_{jX} y + \frac{(-h)^j}{j!} \partial_{jX} y + \mathcal{O}(h^{M+1}), \quad (\text{B.7})$$

$$= \sum_{j=1}^M \frac{h^j}{j!} \partial_{jX} y (1 + (-1)^j) + \mathcal{O}(h^{M+1}), \quad (\text{B.8})$$

$$= 2 \sum_{\substack{j=2 \\ \wedge j \text{ even}}}^M \frac{h^j}{j!} \partial_{jX} y + \mathcal{O}(h^{M+1}), \quad (\text{B.9})$$

and

$$(y_{i+1} - y_{i-1}) = \sum_{j=1}^M \frac{h^j}{j!} \partial_{jX} y - \frac{(-h)^j}{j!} \partial_{jX} y + \mathcal{O}(h^{M+1}), \quad (\text{B.10})$$

$$= \sum_{j=1}^M \frac{h^j}{j!} \partial_{jX} y (1 - (-1)^j) + \mathcal{O}(h^{M+1}), \quad (\text{B.11})$$

$$= 2 \sum_{\substack{j=1 \\ \wedge j \text{ odd}}}^M \frac{h^j}{j!} \partial_{jX} y + \mathcal{O}(h^{M+1}). \quad (\text{B.12})$$

$$(\text{B.13})$$

Consequently, the product

$$((y_{i+1} - y_i) + (y_{i-1} - y_i))(y_{i+1} - y_{i-1}) = 4 \left(\sum_{\substack{i=2 \\ \wedge i \text{ even}}}^M \frac{h^i}{i!} \partial_{jX} y + \mathcal{O}(h^{M+1}) \right) \quad (\text{B.14})$$

$$\cdot \left(\sum_{\substack{l=1 \\ \wedge l \text{ odd}}}^M \frac{h^l}{l!} \partial_{lX} y + \mathcal{O}(h^{M+1}) \right),$$

$$= 4 \sum_{\substack{i=2 \\ \wedge i \text{ even}}}^M \sum_{\substack{l=1 \\ \wedge l \text{ odd}}}^M \frac{h^{i+l}}{i!l!} \partial_{jX} y \partial_{lX} y + \mathcal{O}(h^{M^2+1}), \quad (\text{B.15})$$

$$= 4 \sum_{\substack{i=2 \\ \wedge i \text{ even}}}^M \sum_{\substack{l=1 \\ \wedge l \text{ odd} \\ \wedge i+l \leq M}}^M \frac{h^{i+l}}{i!l!} \partial_{jX} y \partial_{lX} y + \mathcal{O}(h^{M+1}). \quad (\text{B.16})$$

Upon substitution of Equations (B.9) and (B.16) into Equation (B.5), we have

$$m \partial_{TT} y = 2\gamma \sum_{\substack{j=2 \\ \wedge j \text{ even}}}^M \frac{h^j}{j!} \partial_{jX} y + 4\alpha \sum_{\substack{i=2 \\ \wedge i \text{ even}}}^M \sum_{\substack{l=1 \\ \wedge l \text{ odd} \\ \wedge i+l \leq M}}^M \frac{h^{i+l}}{i!l!} \partial_{jX} y \partial_{lX} y + \mathcal{O}(h^{M+1}). \quad (\text{B.17})$$

As in the derivation of the KdV equation in Subsection 3.2.1, we transform the *truncation* of Equation (B.17) according to

$$\begin{cases} y(X, T) = \frac{\gamma}{2\alpha h} v(x, \tau), & \text{(B.18)} \\ x = X - h\sqrt{\frac{\gamma}{m}} T, & \text{(B.19)} \\ \tau = \frac{\epsilon h}{2} \sqrt{\frac{\gamma}{m}} T. & \text{(B.20)} \end{cases}$$

Again, Equations (B.18)—(B.20) have frequently been used to transform interpolations of the FPU lattice into KdV-type equations [9, 11, 14, 17, 20, 22]. To proceed, recall Faa di Bruno's formula,

$$\frac{\partial^n}{\partial \mu^n} f(x, \tau) = \sum_{j=0}^n \frac{n!}{j!(n-j)!} \left(\frac{\partial x}{\partial \mu} \right)^{n-j} \left(\frac{\partial \tau}{\partial \mu} \right)^j \frac{\partial^n f}{\partial x^{n-j} \tau^j}. \quad \text{(B.21)}$$

The transformation in Equations (B.18)—(B.20) implies

$$\frac{\partial x}{\partial X} = 1, \quad \text{(B.22)}$$

$$\frac{\partial x}{\partial T} = -h\sqrt{\frac{\gamma}{m}}, \quad \text{(B.23)}$$

$$\frac{\partial \tau}{\partial X} = 0, \text{ and} \quad \text{(B.24)}$$

$$\frac{\partial \tau}{\partial T} = \frac{\epsilon h}{2} \sqrt{\frac{\gamma}{m}}. \quad \text{(B.25)}$$

So,

$$\frac{\partial^j}{\partial X^j} \left[\frac{\gamma}{2\alpha h} v \right] = \frac{\gamma}{2\alpha h} \partial_{jx} v, \quad \text{(B.26)}$$

$$\begin{aligned} \frac{\partial^j}{\partial T^j} \left[\frac{\gamma}{2\alpha h} v \right] &= m \left(\left(-h\sqrt{\frac{\gamma}{m}} \right)^2 \partial_{xx} \left[\frac{\gamma}{2\alpha h} v \right] + 2 \left(-h\sqrt{\frac{\gamma}{m}} \right) \left(\frac{\epsilon h}{2} \sqrt{\frac{\gamma}{m}} \right) \partial_{x\tau} \left[\frac{\gamma}{2\alpha h} v \right] \right. \\ &\quad \left. + \left(\frac{\epsilon h}{2} \sqrt{\frac{\gamma}{m}} \right)^2 \partial_{\tau\tau} \left[\frac{\gamma}{2\alpha h} v \right] \right), \end{aligned} \quad \text{(B.27)}$$

$$\begin{aligned} &= \frac{h\gamma^2}{2\alpha} \left(\partial_{xx} v - \epsilon \partial_{x\tau} v + \frac{\epsilon^2}{4} \partial_{\tau\tau} v \right). \end{aligned} \quad \text{(B.28)}$$

Using Equations (B.26) and (B.28), the transformation of the truncation of Equation (B.17) is now readily expressed as

$$0 = -\frac{h\gamma^2}{2\alpha} \left(\partial_{xx}v - \epsilon\partial_{x\tau}v + \frac{\epsilon^2}{4}\partial_{\tau\tau}v \right) \quad (\text{B.29})$$

$$+ 2\gamma \sum_{\substack{j=2 \\ \wedge j \text{ even}}}^M \frac{h^j}{j!} \frac{\gamma}{2\alpha h} \partial_{jx}v$$

$$+ 4\alpha \sum_{\substack{i=2 \\ \wedge i \text{ even}}}^M \sum_{\substack{l=1 \\ \wedge l \text{ odd} \\ \wedge i+l \leq M}}^M \frac{h^{i+l}}{i!l!} \left(\frac{\gamma}{2\alpha h} \right)^2 \partial_{ix}v \partial_{lx}v,$$

$$= -\frac{h\gamma^2}{2\alpha} \left(\partial_{xx}v - \epsilon\partial_{x\tau}v + \frac{\epsilon^2}{4}\partial_{\tau\tau}v \right) \quad (\text{B.30})$$

$$+ \frac{h\gamma^2}{\alpha} \sum_{\substack{j=2 \\ \wedge j \text{ even}}}^M \frac{h^{j-2}}{j!} \partial_{jx}v$$

$$+ \frac{h\gamma^2}{\alpha} \sum_{\substack{i=2 \\ \wedge i \text{ even}}}^M \sum_{\substack{l=1 \\ \wedge l \text{ odd} \\ \wedge i+l \leq M}}^M \frac{h^{i+l-3}}{i!l!} \partial_{ix}v \partial_{lx}v.$$

After multiplying Equation (B.31) by $\frac{2\alpha}{h\gamma^2}$,

$$0 = - \left(\partial_{xx}v - \epsilon\partial_{x\tau}v + \frac{\epsilon^2}{4}\partial_{\tau\tau}v \right) \quad (\text{B.31})$$

$$+ 2 \sum_{\substack{j=2 \\ \wedge j \text{ even}}}^M \frac{h^{j-2}}{j!} \partial_{jx}v$$

$$+ 2 \sum_{\substack{i=2 \\ \wedge i \text{ even}}}^M \sum_{\substack{l=1 \\ \wedge l \text{ odd} \\ \wedge i+l \leq M}}^M \frac{h^{i+l-3}}{i!l!} \partial_{ix}v \partial_{lx}v,$$

$$= \epsilon\partial_{x\tau}v - \frac{\epsilon^2}{4}\partial_{\tau\tau}v \quad (\text{B.32})$$

$$+ 2 \sum_{\substack{j=4 \\ \wedge j \text{ even}}}^M \frac{h^{j-2}}{j!} \partial_{jx}v$$

$$+ 2 \sum_{\substack{i=2 \\ \wedge i \text{ even}}}^M \sum_{\substack{l=1 \\ \wedge l \text{ odd} \\ \wedge i+l \leq M}}^M \frac{h^{i+l-3}}{i!l!} \partial_{ix}v \partial_{lx}v.$$

Thus,

$$0 = \epsilon \partial_{x\tau} v + 2 \sum_{\substack{j=4 \\ \wedge j \text{ even}}}^M \frac{h^{j-2}}{j!} \partial_{jx} v + 2 \sum_{\substack{i=2 \\ \wedge i \text{ even}}}^M \sum_{\substack{l=1 \\ \wedge l \text{ odd} \\ \wedge i+l \leq M}}^M \frac{h^{i+l-3}}{i!l!} \partial_{ix} v \partial_{lx} v + \mathcal{O}(\epsilon^2). \quad (\text{B.33})$$

Using the assumption that $0 < \epsilon \ll 1$, Equation (B.33) is truncated, as in [9, 11, 14, 20, 22].

This yields,

$$0 = \epsilon \partial_{x\tau} v + 2 \sum_{\substack{j=4 \\ \wedge j \text{ even}}}^M \frac{h^{j-2}}{j!} \partial_{jx} v + 2 \sum_{\substack{i=2 \\ \wedge i \text{ even}}}^M \sum_{\substack{l=1 \\ \wedge l \text{ odd} \\ \wedge i+l \leq M}}^M \frac{h^{i+l-3}}{i!l!} \partial_{ix} v \partial_{lx} v. \quad (\text{B.34})$$

Equation (B.34) is now transformed according to

$$\begin{cases} \partial_x v(x, \tau) = u(x, t), & (\text{B.35}) \\ t = \frac{\tau}{\epsilon}. & (\text{B.36}) \end{cases}$$

Again, it is critical to note that truncation of Equation (B.33) and subsequent transformation according to Equations (B.35) and (B.36) have the effect of imposing a long-wavelength assumption of the form $\|v_{\tau\tau}\| \ll 1$ on the continuum limit model. So, we have

$$0 = u_t + 2 \sum_{\substack{j=4 \\ \wedge j \text{ even}}}^M \frac{h^{j-2}}{j!} u_{(j-1)x} + 2 \sum_{\substack{i=2 \\ \wedge i \text{ even}}}^M \sum_{\substack{l=1 \\ \wedge l \text{ odd} \\ \wedge i+l \leq M}}^M \frac{h^{i+l-3}}{i!l!} u_{(i-1)x} u_{(l-1)x}. \quad (\text{B.37})$$

Now define $\delta = \frac{h}{\sqrt{12}}$. Then Equation (B.37) becomes

$$0 = u_t + 2 \sum_{\substack{j=4 \\ \wedge j \text{ even}}}^M \frac{12^{\frac{j-2}{2}} \delta^{j-2}}{j!} u_{(j-1)x} + 2 \sum_{\substack{i=2 \\ \wedge i \text{ even}}}^M \sum_{\substack{l=1 \\ \wedge l \text{ odd} \\ \wedge i+l \leq M}}^M \frac{12^{\frac{i+l-3}{2}} \delta^{i+l-3}}{i!l!} u_{(i-1)x} u_{(l-1)x}, \quad (\text{B.38})$$

$$= u_t + 2 \sum_{\substack{j=4 \\ \wedge j \text{ even}}}^M \frac{12^{\frac{j-2}{2}} \delta^{j-2}}{j!} u_{(j-1)x} + 2 \sum_{\substack{i=2 \\ \wedge i \text{ even}}}^M \sum_{\substack{l=1 \\ \wedge l \text{ odd} \\ \wedge i+l \leq M}}^M \frac{12^{\frac{i+l-3}{2}} \delta^{i+l-3}}{i!l!} u_{(i-1)x} u_{(l-1)x}, \quad (\text{B.39})$$

$$= u_t + \sum_{j=2}^{\lfloor \frac{M}{2} \rfloor} \frac{2^{2j-1} 3^{j-1} \delta^{2j-2}}{(2j)!} u_{(2j-1)x} + \sum_{i=1}^{\lfloor \frac{M}{2} \rfloor} \sum_{\substack{l=1 \\ \wedge l \text{ odd}}}^{s(M,i)} \frac{2^{2i+l-2} 3^{\frac{2i+l-3}{2}} \delta^{2i+l-3}}{(2i)!l!} u_{(2i-1)x} u_{(l-1)x}, \quad (\text{B.40})$$

where $s(M, i) = \lfloor \frac{M}{2} \rfloor - 1 - \lfloor |2i - \lfloor \frac{M}{2} \rfloor - \frac{1}{2}| \rfloor$. The case where $M = 2$ was considered in [17, 22]. The case where $M = 2$ and $\beta \neq 0$ was provided in [20]. The case where $M = 3$ was studied in [9, 19] and, with $\beta \neq 0$, in [11]. Dissipative modifications have also been investigated [10].

INDEX

- bandwidth, 5
- characteristic polynomial, 5
- ergodic, 1
- Fourier
 - modes, 5
 - transformation, 6
- FPU paradox, 1
- FPU problem, 16
- Hamiltonian, 3
- lattice, 16
- matrix
 - symmetric, 5
 - Topelitz, 5
- perturbation, 16
- recurrence, 1
- solitary wave, 16
- soliton, 16
- traveling wave, 28
- unbounded, 30

REFERENCES

- [1] Khristo N Boyadzhiev, *Derivative polynomials for tanh, tan, sech and sec in explicit form*, arXiv preprint arXiv:0903.0117 (2009).
- [2] E. Fermi, J. Pasta, S. Ulam, and M. Tsingou, *Studies of Nonlinear Problems. I*, 1955.
- [3] G. Friesecke and R. L. Pego, *Solitary waves on FPU lattices: I. Qualitative properties, renormalization and continuum limit*, *Nonlinearity* **12** (1999), no. 6, 1601–1627.
- [4] ———, *Solitary waves on FPU lattices: II. Linear implies nonlinear stability*, *Nonlinearity* **15** (2002), no. 4, 1343–1359.
- [5] ———, *Solitary waves on Fermi-Pasta-Ulam lattices: III. Howland-type Floquet theory*, *Nonlinearity* **17** (2004), no. 1, 207–227.
- [6] ———, *Solitary waves on Fermi-Pasta-Ulam lattices: IV. Proof of stability at low energy*, *Nonlinearity* **17** (2004), no. 1, 229–251.
- [7] F Fucito, F Marchesoni, E Marinari, G Parisi, L Peliti, S Ruffo, and A Vulpiani, *Approach to equilibrium in a chain of nonlinear oscillators*, *Journal de Physique* **43** (1982), no. 5, 707–713.
- [8] F.M. Izrailev and B.V. Chirikov, *Statistical properties of a nonlinear string*, *Proceedings of the USSR Academy of Sciences* (1966).
- [9] Nikolay A. Kudryashov, *Refinement of the Korteweg-de Vries equation from the Fermi-Pasta-Ulam model*, *Physics Letters, Section A: General, Atomic and Solid State Physics* **379** (2015), no. 40-41, 2610–2614.
- [10] ———, *On solutions of generalized modified Korteweg-de Vries equation of the fifth order with dissipation*, *Applied Mathematics and Computation* **280** (2016), 39–45.
- [11] Nikolay A. Kudryashov and Alexandr K. Volkov, *The fifth-order partial differential equation for the description of the $\alpha+\beta$ Fermi-Pasta-Ulam model*, *Communications in Nonlinear Science and Numerical Simulation* **42** (2017), 491–501.

- [12] Roberto Livi, Marco Pettini, Stefano Ruffo, Massimo Sparpaglione, and Angelo Vulpiani, *Equipartition threshold in nonlinear large hamiltonian systems: The fermi-pasta-ulam model*, Physical Review A **31** (1985), no. 2, 1039.
- [13] Willy Malfliet and Willy Hereman, *The tanh method: I. exact solutions of nonlinear evolution and wave equations*, Physica Scripta **54** (1996), no. 6, 563.
- [14] L. Martina, *Continuum Approximation of the Fermi-Pasta-Ulam Lattice*, Lettere al Nuovo Cimento della Societa Italiana di Fisica **25** (1979), no. 9, 277–282.
- [15] P. Poggi and S. Ruffo, *Exact solutions in the FPU oscillator chain*, Physica D: Nonlinear Phenomena **103** (1997), no. 1-4, 251–272.
- [16] Constance Schober and Alvaro Islas, *Private communication*, 2018.
- [17] C. H. Su and C. S. Gardner, *Korteweg-de Vries equation and generalizations. III. Derivation of the Korteweg-de Vries equation and Burgers equation*, Journal of Mathematical Physics **10** (1969), no. 3, 536–539.
- [18] J.L Tuck and M.T Menzel, *The superperiod of the nonlinear weighted string (FPU) problem*, Advances in Mathematics **9** (1972), no. 3, 399–407.
- [19] A. K. Volkov and N. A. Kudryashov, *Nonlinear waves described by a fifth-order equation derived from the FermiPastaUlam system*, Computational Mathematics and Mathematical Physics **56** (2016), no. 4, 680–687.
- [20] Miki Wadati, *Wave Propagation in Nonlinear Lattice. I*, Journal of the Physical Society of Japan **38** (1975), no. 3, 673–680.
- [21] Abdul-Majid Wazwaz, *The extended tanh method for new solitons solutions for many forms of the fifth-order kdv equations*, Applied Mathematics and Computation **184** (2007), no. 2, 1002 –1014.
- [22] N. J. Zabusky and M. D. Kruskal, *Interaction of "solitons" in a collisionless plasma and the recurrence of initial states*, Physical Review Letters **15** (1965), no. 6, 240–243.